

T-3892

A BOUNDARY ELEMENT DIRECT CURRENT RESISTIVITY MODEL TO
AID IN THE INTERPRETATION OF AN UNDERGROUND
DC RESISTIVITY MULTICOMPONENT SURVEY

by
Earle M. Williams

ARTHUR LAKES LIBRARY
COLORADO SCHOOL of MINES
GOLDEN, COLORADO 80401

ProQuest Number: 10783606

All rights reserved

INFORMATION TO ALL USERS

The quality of this reproduction is dependent upon the quality of the copy submitted.

In the unlikely event that the author did not send a complete manuscript and there are missing pages, these will be noted. Also, if material had to be removed, a note will indicate the deletion.



ProQuest 10783606

Published by ProQuest LLC (2018). Copyright of the Dissertation is held by the Author.

All rights reserved.

This work is protected against unauthorized copying under Title 17, United States Code
Microform Edition © ProQuest LLC.

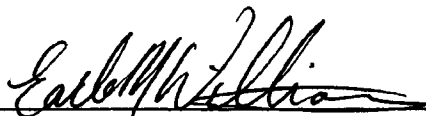
ProQuest LLC.
789 East Eisenhower Parkway
P.O. Box 1346
Ann Arbor, MI 48106 – 1346

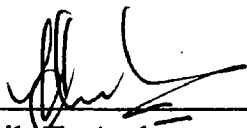
T-3892

A thesis submitted to the Faculty and Board of Trustees of the Colorado School of Mines in partial fulfillment of the requirements for the degree of Master of Science (Geophysical Engineering).

Golden, Colorado

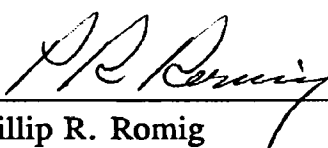
Date 7 April, 1991

Signed: 
Earle M. Williams

Approved: 
Henrik T. Andersen
Thesis Advisor

Golden, Colorado

Date 9 April 1991


Phillip R. Romig
Head, Department of Geophysics

ABSTRACT

Boundary element modeling of the direct current resistivity response is an alternative to the computation-intensive finite-element and finite-difference modeling methods. The solution is found by treating the potential due to a closed body as the potential due to a static charge distributed on the surface of the body. The result is a system of linear equations, and an approximate solution can be solved for using the Gauss-Seidel iterative method.

A FORTRAN program was written to calculate the forward solution of a closed body. The results of the surface charge method compare favorably with the analytical solution for a sphere, verifying the validity of the method.

The forward model was used to aid in the interpretation of multicomponent underground DC resistivity data. A multicomponent underground resistivity survey was conducted within the bedded salt formation of the Waste Isolation Pilot Plant, an underground waste storage facility in Carlsbad, New Mexico. A geoelectric model of the site is made based on previous borehole and underground resistivity data. Model results are found to correlate with large-scale trends in the field data.

Lens-shaped bodies are used to model conductive fracture zones in order to identify such zones in the field data and locate them azimuthally. Problems inherent in the data prevent fitting a quantitative model, yet the method provides a qualitative means of determining how the electric field interacts with bodies of contrasting resistivity.

TABLE OF CONTENTS

ABSTRACT	iii
TABLE OF CONTENTS	iv
LIST OF ILLUSTRATIONS	v
LIST OF TABLES	vii
ACKNOWLEDGEMENTS	ix
Chapter 1	
1.1 Objective of DC Resistivity Modeling	1
1.2 Overview of DC Resistivity Modeling	3
1.3 Field Area Background.	4
Chapter 2	
2.1 Surface Charge Boundary Element Method	12
2.2 Surface Charge Distribution.	14
2.3 Gauss-Seidel Iterative Solution.	23
2.3 Boundary Element Modeling Code.	25
2.4 Modeling Accuracy.	28
2.5 Summary of Surface Charge Boundary Element Method	36
Chapter 3	
3.1 Geometry of the Test Site	37
3.2 Modeling of Current Sources.	38
3.3 Modeling of Underground Features.	44
Chapter 4	
4.1 Survey Locations	50
4.2 Room G Access	52
4.3 Room 7	54
4.4 Room Q Access	56
4.5 N300 Drift	58
Chapter 5	
5.1 Modeling Results	61
5.2 Interpretation of Field Data.	68
Chapter 6	
6.1 Success of Boundary Element Method	71
6.2 Limits of Boundary Element Method	71
6.3 Interpretation of Field Data	72
6.4 Future Work	73

REFERENCES74

APPENDIX A

 A-1 DCMODEL.FOR PROGRAM CODE76

 A-2 SPHLENS.FOR PROGRAM CODE92

 A-3 VSWING.C PROGRAM CODE97

APPENDIX B Multicomponent Resistivity Data 111

APPENDIX C Data Acquisition System 118

LIST OF ILLUSTRATIONS

Figure 1 Location of WIPP site. 5

Figure 2 Plot of Archie's Law for halite (after Kessels, et al, 1985). Parameters for the calculation of bulk resistivity are as follows: $a = 0.9$, $\rho_w = 0.1$ ohm-meters. 7

Figure 3 Geologic section of the Delaware Basin in the vicinity of the WIPP site. 9

Figure 4 Illustration of WIPP underground facility. 10

Figure 5 Electric field for a) a spherical body of resistivity $\rho_2 \gg \rho_1$, b) media with a resistivity of ρ_1 , and c) a charge distribution representing spherical body of resistivity ρ_2 13

Figure 6 Element ds of the surface A and element ds' of the surface A' 18

Figure 7 Letting p_1 and p_2 approach the point p on the surface element ds . . . 21

Figure 8 Schematic diagram of DCMODEL.FOR. 27

Figure 9 Spherical body generated using SPHLENS.FOR. The sphere is divided into 10 latitudinal bands and 20 longitudinal bands. 29

Figure 10 Analytical response and model response of sphere. DCMODEL calls IMAGE subroutine. 30

Figure 11 Analytical and model responses for sphere without IMAGE subroutine. 31

Figure 12 Effect of calling IMAGE subroutine in DCMODEL code. When IMAGE subroutine is not called the error function approaches zero. 32

Figure 13 Apparent resistivity for a faceted resistive sphere with different facet densities 34

Figure 14 Apparent resistivity for a faceted sphere with varying iteration values 35

Figure 15 WIPP-22 cumulative conductance from laterolog digitized at ten foot intervals and numerically integrated 39

Figure 16	Location of WIPP-22 and WIPP-12 boreholes	40
Figure 17	WIPP-22 conductance segments representing an eleven-layered earth model	42
Figure 18	Colinear point sources representing a line source of current at WIPP-22, with a single point source at WIPP-12.	43
Figure 19	Lens shaped faceted body created using SPHLENS. (200 facets, scale factor $L = 0.2, 1, 1$)	45
Figure 20	Electric field response of a lens shaped body located fifteen meters north of profile (Radius = 10 m, $L = .2, 1, 1$ and $k = -0.8$).	46
Figure 21	Electric field response of a lens shaped body located fifteen meters north of profile (Radius = 10 m, $L = 1, .2, 1$ and $k = -0.8$).	47
Figure 22	Electric field response of a lens shaped body located fifteen meters north of profile (Radius = 10 m, $L = 1, 1, .2$ and $k = -0.8$).	48
Figure 23	Locations of multicomponent resistivity surveys at WIPP underground facility.	51
Figure 24	Station locations and electric field data from Room G Access multicomponent survey.	53
Figure 25	Station locations and electric field data from Room 7	55
Figure 26	Station locations and electric field data from Room Q Access.	57
Figure 27	Station locations and electric field data from N300 drift.	59
Figure 28	Electric field response of a conductive sphere ($\rho_1 = 10 \Omega\text{-m}$, $\rho_2 = 0.01 \Omega\text{-m}$, radius=7 meters, depth=10 meters) generated using DCMODEL.	60
Figure 29	Disturbing potential curves of drift model (Dimensions: 100,10,10; Location: -55,100,645; grid: 10,5,5; $k=.999$).	62
Figure 30	Disturbing potential curves for a conductive lens located 15 meters north of drift.	63
Figure 31	Disturbing potential curves for a conductive lens located 15 meters above drift	65
Figure 32	Disturbing potential curves for a conductive lens located 15 meters south of drift	66

Figure 33 Disturbing potential curves for a conductive lens located 15 meters below drift67

Figure 34 Drift 300N Model: Conductive lens below and to the south of the drift69

Figure 35 Drift 300N model: Conductive lens located below the drift. 70

LIST OF TABLES

Table I Well and Base Station locations.37

Table II Eleven layer model earth conductance and current scaling factors . . 41

ACKNOWLEDGEMENTS

My sincerest gratitude is due to those who provided the assistance and encouragement that carried me through this thesis. For his aid and insight, I thank my advisor, Dr. Andy Andersen. For providing funding on this project I am thankful to Sandia National Laboratory, and specifically Dr. David Borns. Credit for this work coming into being is also due to Dr. Dan Hawkins for showing me the many opportunities that lie beyond that first exposure to science we know as undergraduate education.

I doubt I would have had the strength to complete my studies were it not for the belief in my abilities and constant encouragement supplied by Beverley Rutledge. With her understanding and patience, I have completed my master of science degree with sanity intact, spirit serene, and the great fortune to make this collaboration permanent.

Chapter 1

INTRODUCTION

1.1 Objective of DC Resistivity Modeling

The boundary element method of modeling the electrical response of a body enclosed in a half-space has been in existence for years, and has been used to successfully model the induced polarization (IP) response of arbitrarily shaped bodies (Keller and Frischknecht, 1966; Barnett, 1972). Effectively modeling the direct current (DC) response of a three-dimensional body has required using finite element or finite difference modeling, which require a grid defining the volume of the body as well as the surrounding space. By treating the problem as a boundary value problem, the surface integral method needs only to define surfaces where a contrast in resistivity exists, ie. the surface of a closed body. The problem can then be modelled by treating changes in the electric field due to the resistivity contrast of the body as the electric field of an accumulation of charge along the body boundary. This allows for the geoelectric model to be defined using fewer elements, thus decreasing the computation time required to calculate the model response. The problem at hand was to determine if a computer implementation of the surface charge boundary element method can accurately model the resistivity response of closed bodies, and, if so, to use the method to interpret field data.

Historically, the surface charge concept for modeling the DC response has not been widely accepted. This may be due in part to an inconsistency in the units used by Keller and Frischknecht in the original derivation. Retracing their steps and following the conventions of mks units resulted in a method that is efficient and

accurate when compared to the analytical calculation for a sphere enclosed in a half-space.

The surface-charge boundary-element method was used to aid in the interpretation of multicomponent DC resistivity data obtained from the WIPP site near Carlsbad, New Mexico. The objective was to locate and characterize conductive brine-filled fracture zones.

1.2 Overview of DC Resistivity Modeling.

In DC resistivity mapping, an electrical current is driven through the earth and the electric potential is measured at a point some distance from the source. The potential measured can be thought of as the sum of two potentials: a normal potential due to current flowing through a homogeneous half-space and a disturbing potential due to current encountering the resistivity contrast of features within the medium. The analytical solution for an arbitrary model is given by a solution to Poisson's equation for the potential field applied to the boundary conditions as defined by the geometry of the model chosen (Alfano, 1959).

Since an analytical solution can be found for only the simplest of geometries, a common approach to calculate a resistivity response is to seek a numerical approximation. Finite difference and finite-element methods have been used to find a two-dimensional approximation, but require extensive computing time when the complexity of the model increases, as when extended to three dimensions (Scriba, 1981; Dey and Morrison, 1979).

In the solution to Poisson's equation, the integral over the volume can be replaced with an integral over the surface enclosing that volume. Approximating the surface integration as a sum over discrete surface elements results in an efficient numerical method for approximating the potential field for a three-dimensional body.

The surface element method for resistivity modeling was first suggested by Alfano (1959). The method was further developed by Keller and Frischknecht (1966) and Dieter, et al (1969). Computer programs employing the boundary element method for modeling the IP and resistivity response of three dimensional bodies were developed by Barnett (1972), Daniels (1977), and was also developed for two-

dimensional bodies (Snyder, 1976). More recent work includes a study of the arbitrary inhomogeneities problem by Okabe (1981).

1.3 Field Area Background.

The U.S. Department of Energy has developed the Waste Isolation Pilot Plant (WIPP), 25 miles east of Carlsbad, New Mexico, to study the feasibility of storing low-level transuranic radioactive waste in a bedded salt formation (Figure 1). A key factor in the study is the effectiveness of the salt formation to serve as a barrier, isolating any radioactive waste stored at the facility from the groundwater. Structural features in the salt formation that are permeable could provide pathways for the movement of water into or out of the storage area, thus compromising the isolation capabilities of the salt rock.

The presence of permeable zones could affect the design and construction of the testing facility, so it would be desirable to locate permeable zones during the early phases of construction, and prior to the storage of waste. Since the facility is designed as a storage area for radioactive waste, it is essential to perform all testing in a non-invasive manner in order to minimize damage to the host rock. To this end efforts have been made using electrical geophysics methods to locate and characterize brine-saturated fracture zones within the experimental mine.

The halite of the Salado Formation is generally resistive, having a resistivity in the range of 500 to 700 ohm-meters (Pfeifer, 1987; Elliot, 1977). The presence of water in halite creates a very conductive brine having a resistivity on the order of 0.1

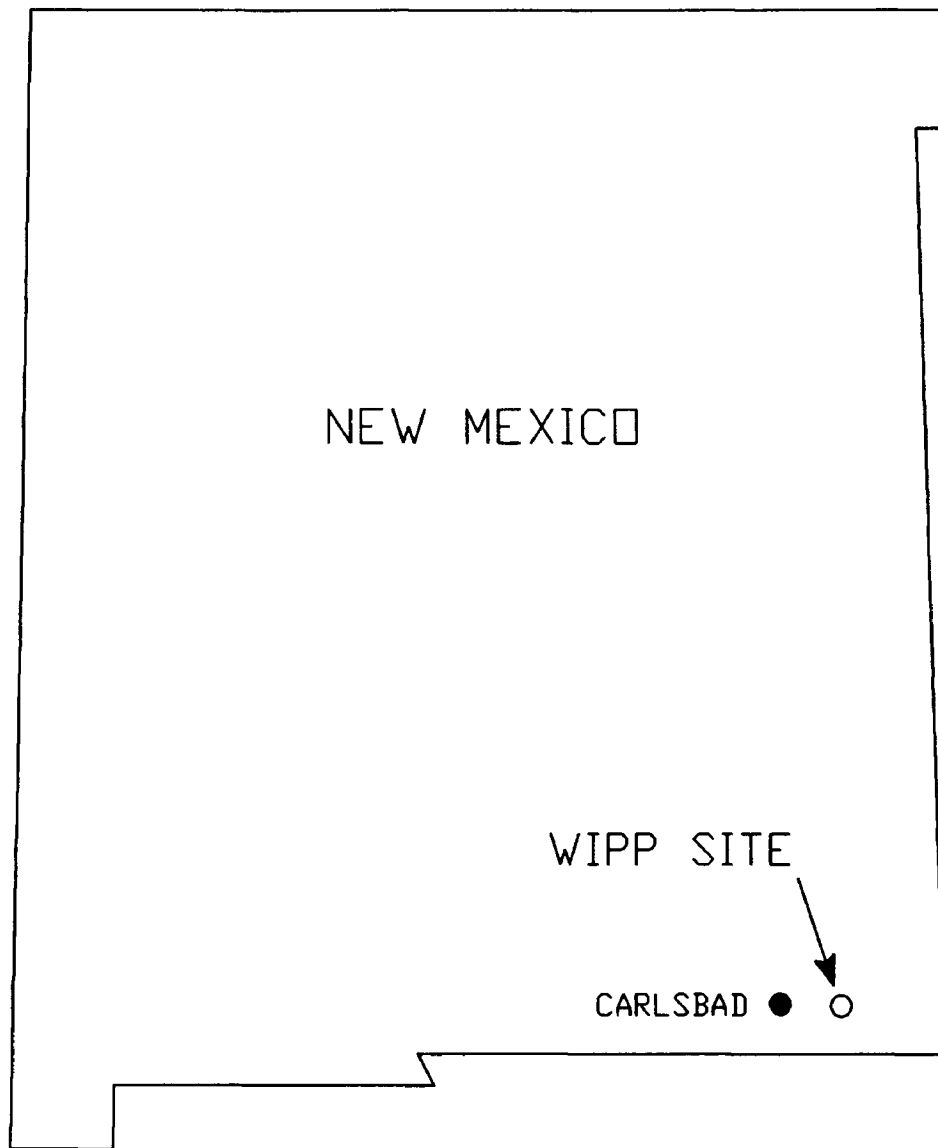


Figure 1 Location of WIPP site.

ohm-meters (Keller and Frischknecht, 1966). Even a small amount of brine in the rock yields a low bulk resistivity, contrasting sharply with the dry halite. Previous studies on the resistivity of dry and saturated halite have confirmed the applicability of Archie's Law in the estimation of water content based on the bulk resistivity, as shown in Figure 2.

Because of the strong resistivity contrast, electrical methods can be employed to map regions of low resistivity, indicating the presence of brine. Once a body of brine has been identified, hydrological testing can determine if it is an isolated pocket or part of a larger fracture zone. The target zones of the survey are ideally suited to the modeling as closed bodies of highly contrasting resistivity to the surrounding half-space.

Three orthogonal components were observed in order to determine the electric field vector. Using this vector information, it is possible to locate a body of contrasting resistivity within three dimensions by use of the multicomponent modeling method developed within this study.

The WIPP site is located in the Delaware Basin, a Permian age basin extending from southeastern New Mexico into western Texas. A characterization of the basin stratigraphy and structure was documented by Barrows and Fett (1985). The Delaware Mountain Group, mainly fine-grained clastics, is considered to be the stratigraphic basement. It is overlain by the Castile formation, composed of anhydrite and calcite interbedded with halite. Above the Castile lies the Salado formation, a thick halite unit interbedded with anhydrite, polyhalite and clayey clastic seams. The Salado is conformably overlain by the Rustler formation, an interbedded halite, anhydrite, and siltstone unit, which is overlain by the gypsiferous Dewey Lake

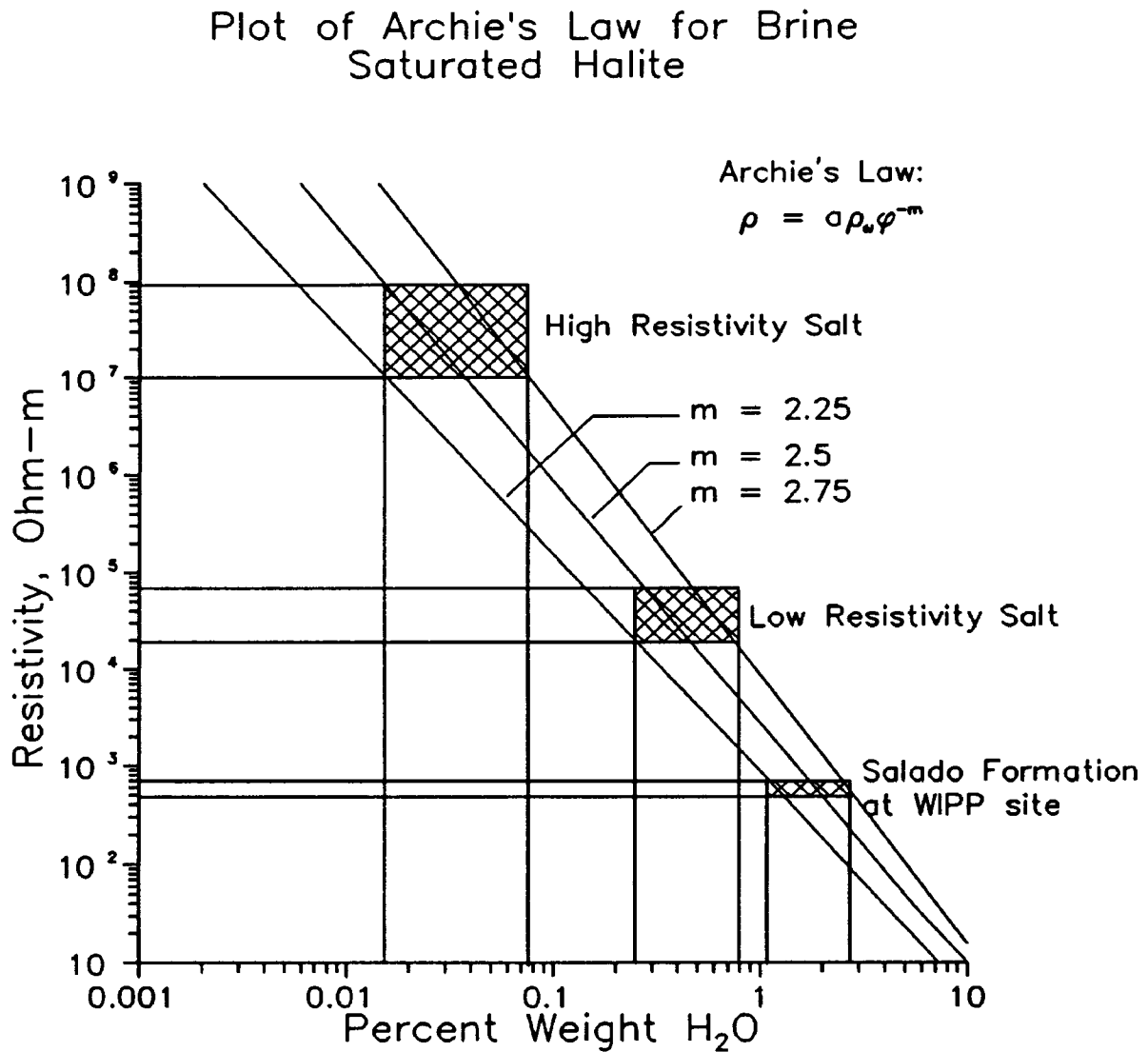


Figure 2 Plot of Archie's Law for halite (after Pfeifer, 1987). Parameters for the calculation of bulk resistivity are as follows:
 $a = 0.9$, $\rho_w = 0.1$ ohm-meters.

redbeds. The remainder of the stratigraphic section is often incomplete. The Dewey Lake redbeds are unconformably overlain by the Triassic Dockum Group and the Quaternary Gatuna formation. The Dockum Group is composed of cross-bedded, medium to coarse grained sandstones while the Gatuna formation consists of unconsolidated blanket and dune sands, lag gravels, and channel sands (Figure 3).

The WIPP facility has been excavated as a room and pillar mine within the Salado formation at a depth of approximately 650 meters, in the middle of the formation (Figure 4). Regional karst features due to the dissolution of evaporites and carbonates are present throughout the section, and have been described by Morgan(1941), Olive(1957), and Bachman(1980). Such processes can form dissolution zones and fluid conduits, as well as extend fracture zones. The presence of any of these deformation features could provide a pathway for either the transportation of radionuclides out of a storage chamber or the leakage of brine into a storage chamber. In order to ensure maximum integrity of the storage facility, it is necessary to locate and map these zones of increased permeability.

Prior to excavation of the WIPP site, a regional gravity survey was performed by Barrows and Fett (1985) to delineate structural features. During the initial excavation, the Colorado School of Mines (CSM) completed work on a surface transient electromagnetic survey in an attempt to map the brine saturated fracture zone intersected by drill hole WIPP-12 (Andersen, 1987; Pfeifer, 1987).

The second CSM project was an underground profiling survey using frequency domain electromagnetic and direct current (DC) resistivity methods. The DC resistivity acquisition system was the prototype of the system used by the author, measuring the voltage difference between two receiver electrodes due to a surface

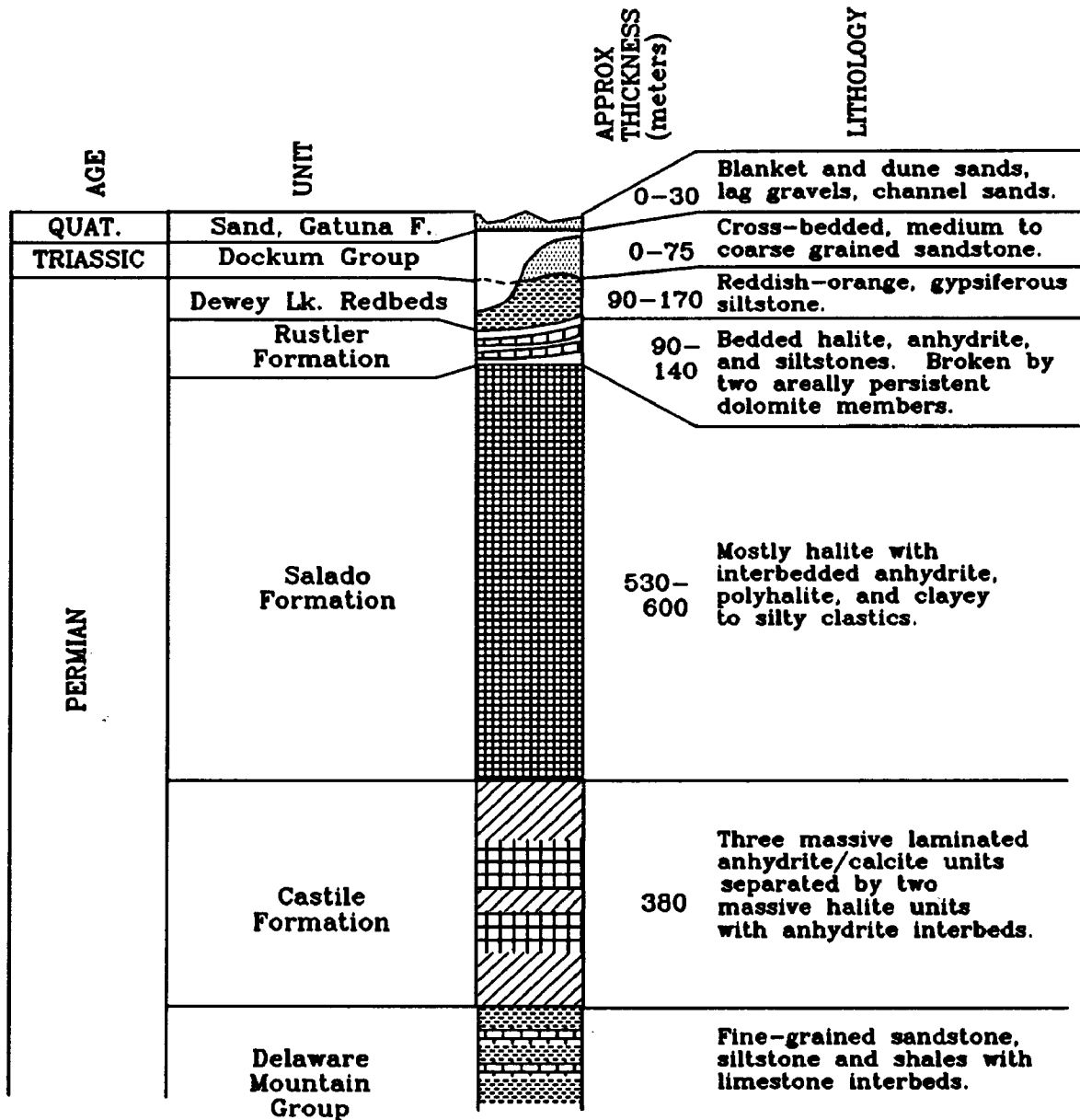


Figure 3 Geologic section of the Delaware Basin in the vicinity of the WIPP site (After Barrows and Fett, 1985)

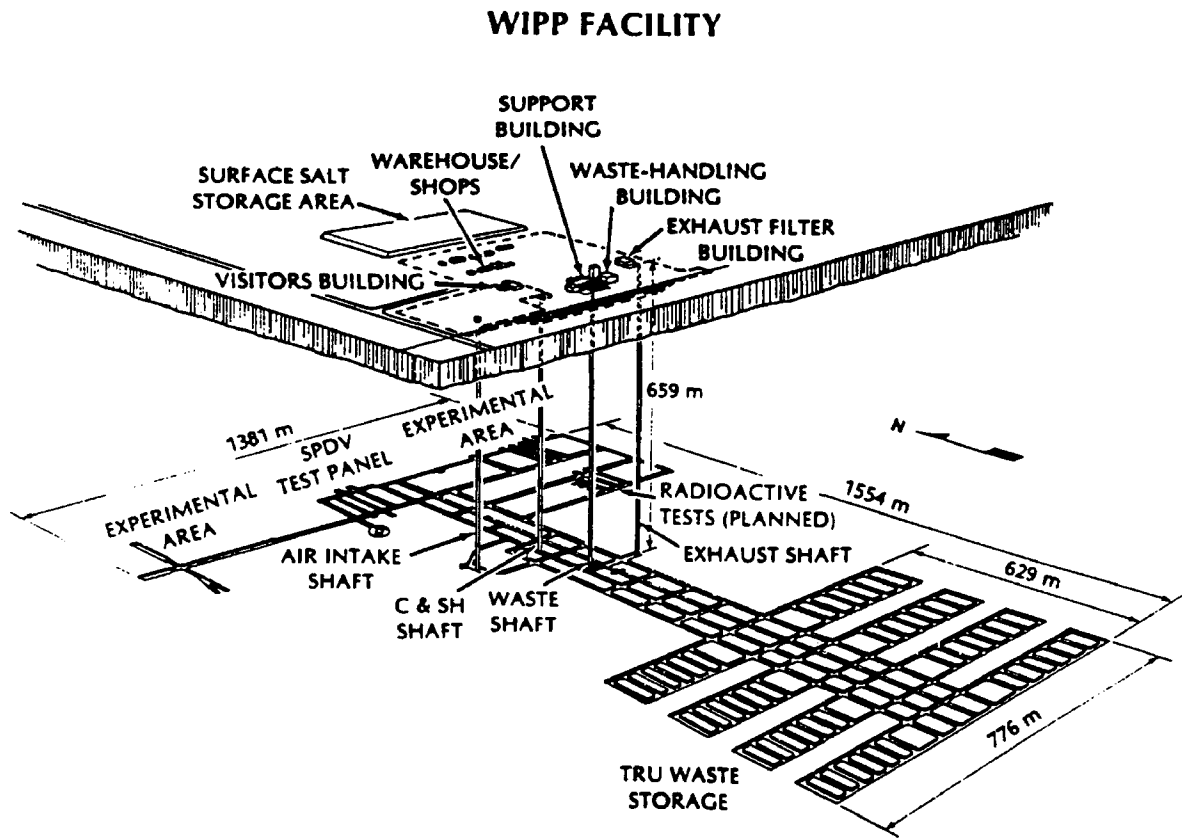


Figure 4 Illustration of WIPP underground facility (From Borns and Stormont, 1987).

bipole source. The method gained momentum when it was used to successfully locate a wet zone in Room D in the northeast region of the underground facility between drifts 1100N and 1420N (H.T. Andersen, personal communication).

Current work at the WIPP site includes development of a permanent DC grid for monitoring temporal variations in resistivity associated with exfoliation of the salt rock (Pfeifer, et al, 1990). In situ testing at the site is being performed by Sandia National Laboratory regarding the long term feasibility of the facility (Matalucci, 1987).

Chapter 2

DC RESISTIVITY MODELING

2.1 Surface Charge Boundary Element Method.

The boundary element method of approximating the direct current response of a body at depth assumes that the potential due to a resistive feature can be represented as a potential due to a distribution of static charge over the surface of the body (Keller and Frischknecht, 1966). The total potential is then a sum of two potentials: a normal potential due to current flowing through the earth and a disturbing potential due to the accumulation of charge along boundaries of media with contrasting resistivities (Figure 5).

The solution for the static charge distribution can be derived by applying conservation of current to Ohm's Law relation. Using a body whose boundary is represented by n discrete surface elements, the charge distribution over the body is approximated as a system of linear equations. These equations form an $n \times n$ matrix with coefficients in every cell. With all the elements being non-zero, a direct solution can not be found efficiently. An approximation of the charge distribution can be reached by using an iterative approach using the Gauss-Seidel method (Kolman, 1984). The surface charge densities of the body elements are assigned an initial value and introduced into the system of equations to calculate a new value. With the Gauss-Seidel method, new values for each element charge density are used in the equation for successive elements. Once the solution for the charge distribution converges, the potential due to the static charge is calculated.

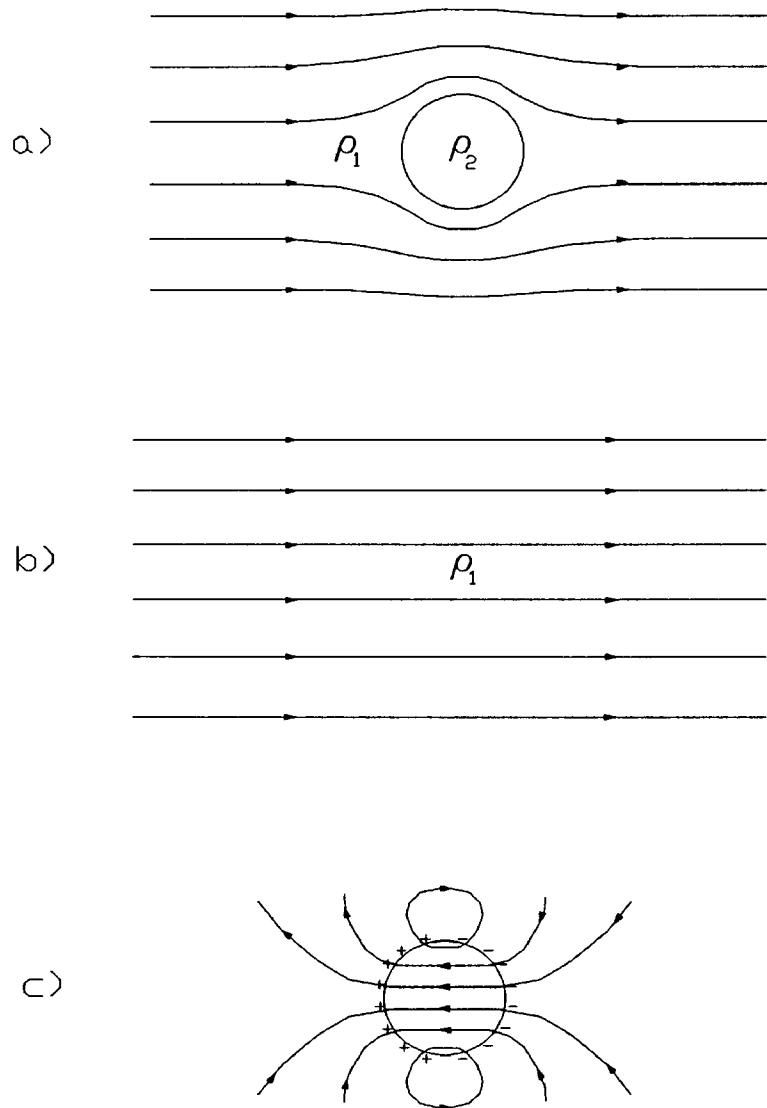


Figure 5 Electric field for a) a sphere of resistivity $\rho_2 \gg \rho_1$, b) media with a resistivity of ρ_1 , and c) a spherical charge distribution.

2.2 Surface Charge Distribution.

The current density is related to the electric field intensity by Ohm's law,

$$\bar{E} = \rho \bar{j}. \quad (1)$$

Taking the divergence of the current density results in

$$\bar{\nabla} \cdot \bar{j} = \frac{1}{\rho} (\bar{\nabla} \cdot \bar{E}) + \bar{E} \cdot \nabla \frac{1}{\rho}. \quad (2)$$

The electric potential is related to the electric field by

$$\bar{E} = -\nabla U \quad (3)$$

Substituting (3) into (2) yields

$$\bar{\nabla} \cdot \bar{j} = \frac{1}{\rho} (-\bar{\nabla} \cdot \nabla U) + (\nabla U \cdot \nabla \frac{1}{\rho}). \quad (4)$$

Rearranging the terms,

$$\bar{\nabla} \cdot \nabla U = -\rho (\bar{\nabla} \cdot \bar{j} + \nabla u \cdot \nabla \frac{1}{\rho}). \quad (5)$$

The term on the left is the Laplacian of U,

$$\nabla^2 U = -\rho (\bar{\nabla} \cdot \bar{j} + \nabla u \cdot \nabla \frac{1}{\rho}). \quad (6)$$

This is Poisson's equation for the electric potential. The solution is given by the integral

$$U = \frac{1}{4\pi} \int_v \rho (\bar{\nabla} \cdot \bar{j} + \nabla U \cdot \nabla \frac{1}{\rho}) dv. \quad (7)$$

The potential solution can be separated into two terms; the first integral term represents the potential due to the current source or normal potential U_o , and the second integral term represents the potential due to variations in resistivity, or disturbing potential U_d ,

$$U = \frac{1}{4\pi} \int_v \rho \frac{\bar{\nabla} \cdot \bar{j}}{r} dv + \frac{1}{4\pi} \int_v \rho \frac{\bar{\nabla} u \cdot \bar{\nabla} \frac{1}{\rho}}{r} dv. \quad (8)$$

This formulation assumes a homogeneous space surrounding a similarly formed three-dimensional body of contrasting resistivity. The gradient of the inverse resistivity will be zero everywhere but across the boundaries of the body. The integrand of the disturbing potential term will then be zero everywhere but at the surface of the body. The term for the disturbing potential can then be calculated as a surface integral,

$$U_d = \frac{1}{4\pi} \int_A \frac{\rho \nabla U \cdot \nabla \frac{1}{\rho}}{r} ds. \quad (9)$$

Equation (9) looks very similar to the Poisson integral to calculate the potential due to a surface charge distribution, which in mks units is given by

$$U = \frac{1}{4\pi} \int_A \frac{\sigma}{\epsilon_o} \frac{1}{r} ds. \quad (10)$$

where σ = surface charge density in coulomb/m²,
 ϵ_o = permittivity constant in coulomb²/N-m², and
 A = surface of the body in m².

The fundamental concept of this method is that the portion within the integrand

in equation (9),

$$\rho \nabla U \cdot \nabla \frac{1}{\rho}, \quad (11)$$

can be manipulated so as to resemble a distribution of electric charge σ over the surface of the body. This equivalent charge distribution then can be used in (10) to calculate the disturbing potential in (8).

Applying conservation of current to the boundary of an element ds requires the normal current densities at points p_1 and p_2 near the surface element ds to be equal,

$$\bar{j}_{\perp p_1} = \bar{j}_{\perp p_2} \quad (12)$$

Relating (12) in terms of Ohm's law,

$$\frac{1}{\rho_1} \frac{\partial U}{\partial n} \Big|_{p_1} = \frac{1}{\rho_2} \frac{\partial U}{\partial n} \Big|_{p_2}. \quad (13)$$

Substituting in the relation $U = U_o + U_a$ into equation (12) and representing U_a by the integral in equation (10) yields

$$\frac{1}{\rho_1} \frac{\partial U}{\partial n} \Big|_{p_1} = \frac{1}{\rho_1} \frac{\partial U_o}{\partial n} \Big|_{p_1} + \frac{1}{\rho_1 4\pi} \int_A \frac{\sigma}{\epsilon_o} \frac{\partial}{\partial n} \frac{1}{r_1} ds' \quad (14)$$

and

$$\frac{1}{\rho_2} \frac{\partial U}{\partial n} \Big|_{p_2} = \frac{1}{\rho_2} \frac{\partial U_o}{\partial n} \Big|_{p_2} + \frac{1}{\rho_2 4\pi} \int_A \frac{\sigma}{\epsilon_o} \frac{\partial}{\partial n} \frac{1}{r_2} ds'. \quad (15)$$

Substituting equations (14) and (15) into equation (13) yields

$$\begin{aligned} & \frac{1}{\rho_1} \frac{\partial U}{\partial n} \Big|_{p_1} + \frac{1}{\rho_2} \frac{\partial U}{\partial n} \Big|_{p_2} \\ & + \frac{1}{4\pi} \int_A \frac{\sigma}{\epsilon_o} \left[\frac{1}{\rho_1} \frac{\partial}{\partial n} \frac{1}{r_1} - \frac{1}{\rho_2} \frac{\partial}{\partial n} \frac{1}{r_2} \right] ds' = 0. \end{aligned} \quad (16)$$

As p_1 and p_2 approach s , the term involving U_o simplifies so that

$$\frac{\rho_2 - \rho_1}{\rho_1 \rho_2} \frac{\partial U}{\partial n} \Big|_{ds} + \frac{1}{4\pi} \int_A \frac{\sigma}{\epsilon_o} \left[\frac{1}{\rho_1} \frac{\partial}{\partial n} \frac{1}{r_1} - \frac{1}{\rho_2} \frac{\partial}{\partial n} \frac{1}{r_2} \right] ds' = 0. \quad (17)$$

The remaining integral term can be divided into two parts: the portion of the surface A that is very near to p_1 and p_2 , and the remaining surface of the body, called A' (Figure 6),

$$\begin{aligned} & \frac{\rho_2 - \rho_1}{\rho_1 \rho_2} \frac{\partial U}{\partial n} \Big|_{ds} \\ & + \frac{1}{4\pi} \int_A \frac{\sigma}{\epsilon_o} \left[\frac{1}{\rho_1} \frac{\partial}{\partial n} \frac{1}{r_1} - \frac{1}{\rho_2} \frac{\partial}{\partial n} \frac{1}{r_2} \right] ds' \\ & + \frac{1}{4\pi} \int_{A'} \frac{\sigma}{\epsilon_o} \left[\frac{1}{\rho_1} \frac{\partial}{\partial n} \frac{1}{r_1'} - \frac{1}{\rho_2} \frac{\partial}{\partial n} \frac{1}{r_2'} \right] ds' = 0. \end{aligned} \quad (18)$$

Near the surface s , the normal component of the electric field can be approximated as that of an infinite thin sheet, $2/\epsilon_o$,

$$\begin{aligned} E_{\perp_1} &= \frac{\sigma}{2\epsilon_o} = \frac{\partial U}{\partial n} \Big|_{p_1} = \frac{\partial}{\partial n} \left[\frac{1}{4\pi} \int_A \frac{\sigma}{\epsilon_o} \frac{1}{r_1} ds' \right] \\ E_{\perp_2} &= -\frac{\sigma}{2\epsilon_o} = \frac{\partial U}{\partial n} \Big|_{p_2} = \frac{\partial}{\partial n} \left[\frac{1}{4\pi} \int_A \frac{\sigma}{\epsilon_o} \frac{1}{r_2} ds' \right] \end{aligned} \quad (19)$$

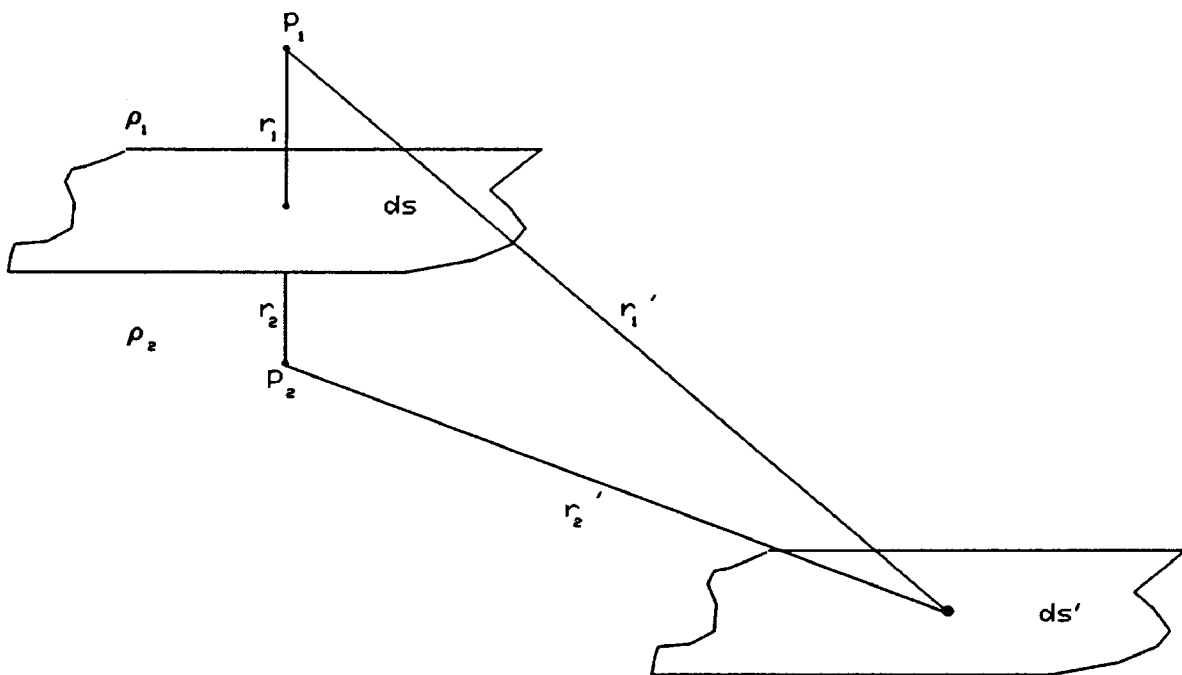


Figure 6 Element ds of the surface portion A and element ds' of the surface portion A'.

Equation (18) then becomes

$$\begin{aligned} \frac{\rho_2 - \rho_1}{\rho_1 \rho_2} \frac{\partial U}{\partial n} \Big|_{ds} + \left(\frac{1}{\rho_1} + \frac{1}{\rho_2} \right) \frac{\sigma}{2\epsilon_0} + \\ \frac{1}{4\pi} \int_{A'} \frac{\sigma}{\epsilon_0} \left[\frac{1}{\rho_1} \frac{\partial}{\partial n} \frac{1}{r_1} - \frac{1}{\rho_2} \frac{\partial}{\partial n} \frac{1}{r_2} \right] ds' = 0. \end{aligned} \quad (20)$$

As p_1 and p_2 become infinitely close to ds (Figure 7),

$$\lim_{p_1 \rightarrow ds} \left(\frac{1}{r_1} \right) = \lim_{p_2 \rightarrow ds} \left(\frac{1}{r_2} \right) = \frac{1}{r}. \quad (21)$$

Equation (20) then simplifies to

$$\begin{aligned} \frac{\rho_2 - \rho_1}{\rho_2 \rho_1} \frac{\partial U}{\partial n} \Big|_{ds} + \left(\frac{1}{\rho_1} + \frac{1}{\rho_2} \right) \frac{\sigma}{2\epsilon_0} \\ + \frac{1}{4\pi} \int_{A'} \frac{\sigma}{\epsilon_0} \left[\frac{1}{\rho_1} \frac{\partial}{\partial n} \frac{1}{r_1} - \frac{1}{\rho_2} \frac{\partial}{\partial n} \frac{1}{r_2} \right] ds' = 0. \end{aligned} \quad (22)$$

Leaving the σ/ϵ_0 term on the left and bringing the others to the right and multiplying through by

$$2 \frac{\rho_1 \rho_2}{\rho_1 + \rho_2} \quad (23)$$

leads to the equation for the surface charge distribution

$$\frac{\sigma}{\epsilon_0} = -2k \left[\frac{\partial U_o}{\partial n} \Big|_{ds} + \frac{1}{4\pi} \int_{A'} \frac{\sigma}{\epsilon_0} \frac{\partial}{\partial n} \frac{1}{r'} ds' \right], \quad (24)$$

where k is the reflection coefficient for the resistivity contrast between ρ_1 and ρ_2 ,

$$k = \frac{\rho_2 - \rho_1}{\rho_2 + \rho_1}. \quad (25)$$

The permittivity constant is absorbed into a scaled charge distribution Q ,

$$Q = \frac{\sigma}{\epsilon_0}, \quad (26)$$

with units of N/coulomb. In order to approximate equation (24) numerically, it needs to be written in discrete form. The surface A is divided into N elements ds_i , and the surface charge distribution Q_i is constant over each surface element. The integral is changed to a sum of Q_i over the surface elements,

$$Q_i = -2K \left[\frac{\partial U_o}{\partial n} \Big|_i + \frac{1}{4\pi} \sum_{\substack{j=1 \\ j \neq i}}^N Q_j \frac{\partial}{\partial n} \left(\frac{1}{r_{ij}} \right) ds_j \right]. \quad (27)$$

This is the linear system of equations that needs to be solved for the distribution of charge over the body surface. Using the final charge distribution, the disturbing potential is given by

$$U_{appx} = U_o + \frac{1}{4\pi} \sum_{i=1}^N \frac{Q_i}{r_i} ds_i. \quad (28)$$

With the normal potential defined as

$$U = \frac{\rho I}{4\pi r}, \quad (29)$$

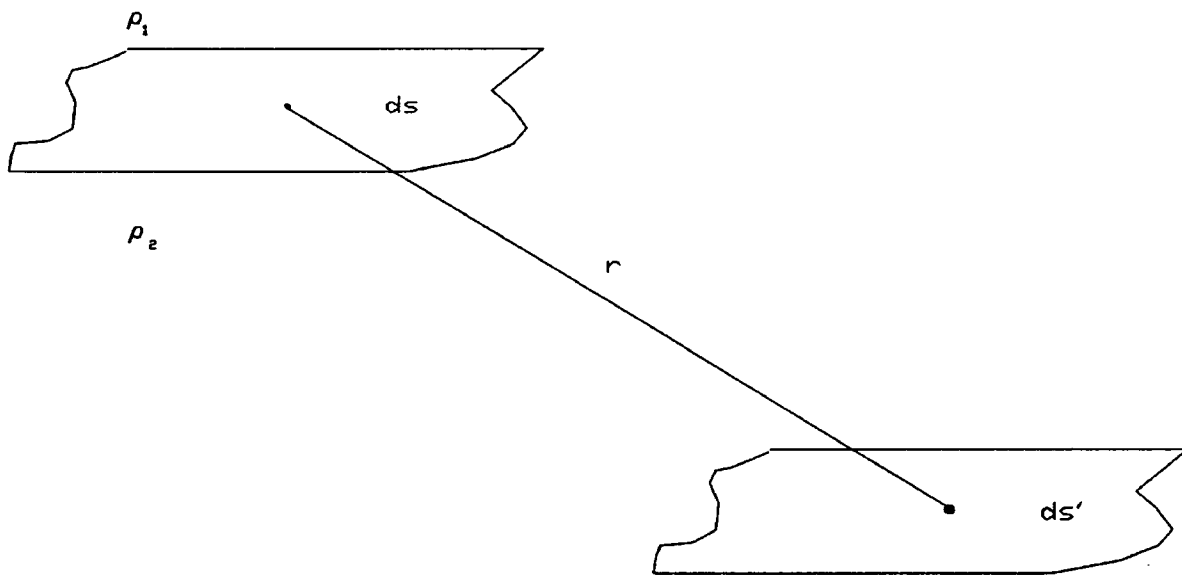


Figure 7 Letting p_1 and p_2 approach the point p on the surface element ds .

the total potential is given by

$$U_{appx} = \frac{\rho I}{4\pi r} + \frac{1}{4\pi} \sum_{i=1}^N \frac{Q_i}{r_i} ds_i . \quad (30)$$

2.3 Gauss-Seidel Iterative Solution.

The Gauss-Seidel method of solving a system of linear equations uses an initial approximation for the solution and attempts to improve the approximation by substituting it into the system of equations. Consider the simple system of equations,

$$\begin{aligned}x_1 &= c_1 + a_1x_2 + b_1x_3 \\x_2 &= c_2 + a_2x_1 + b_2x_3 \\x_3 &= c_3 + a_3x_1 + b_3x_3\end{aligned}\tag{31}$$

The steps involved to perform the Gauss-Seidel approximation are as follows:

- 1) The first order approximation would be to set

$$x_1 = c_1, \quad x_2 = c_2, \quad x_3 = c_3.\tag{32}$$

- 2) The values for x_2 and x_3 are used in the calculation for x_1 ,

$$x_{1_{new}} = c_1 + a_1x_{2_{old}} + b_1x_{3_{old}}.\tag{33}$$

- 3) This new value for x_1 is used with the old value of x_3 to calculate x_2 ,

$$x_{2_{new}} = c_2 + a_2x_{1_{new}} + b_2x_{3_{old}}.\tag{34}$$

- 4) Then the new value for x_2 is used with x_1 to calculate x_3 ,

$$x_{3_{new}} = c_3 + a_3x_{1_{new}} + b_3x_{2_{new}}.\tag{35}$$

- 5) If the solution has converged, then the calculation is complete. Otherwise, return to step 2.

With the linear system defined in equation (26), the first order approximation would

be to set to

$$Q_i = -2K \left. \frac{\partial U_o}{\partial n} \right|_i . \quad (36)$$

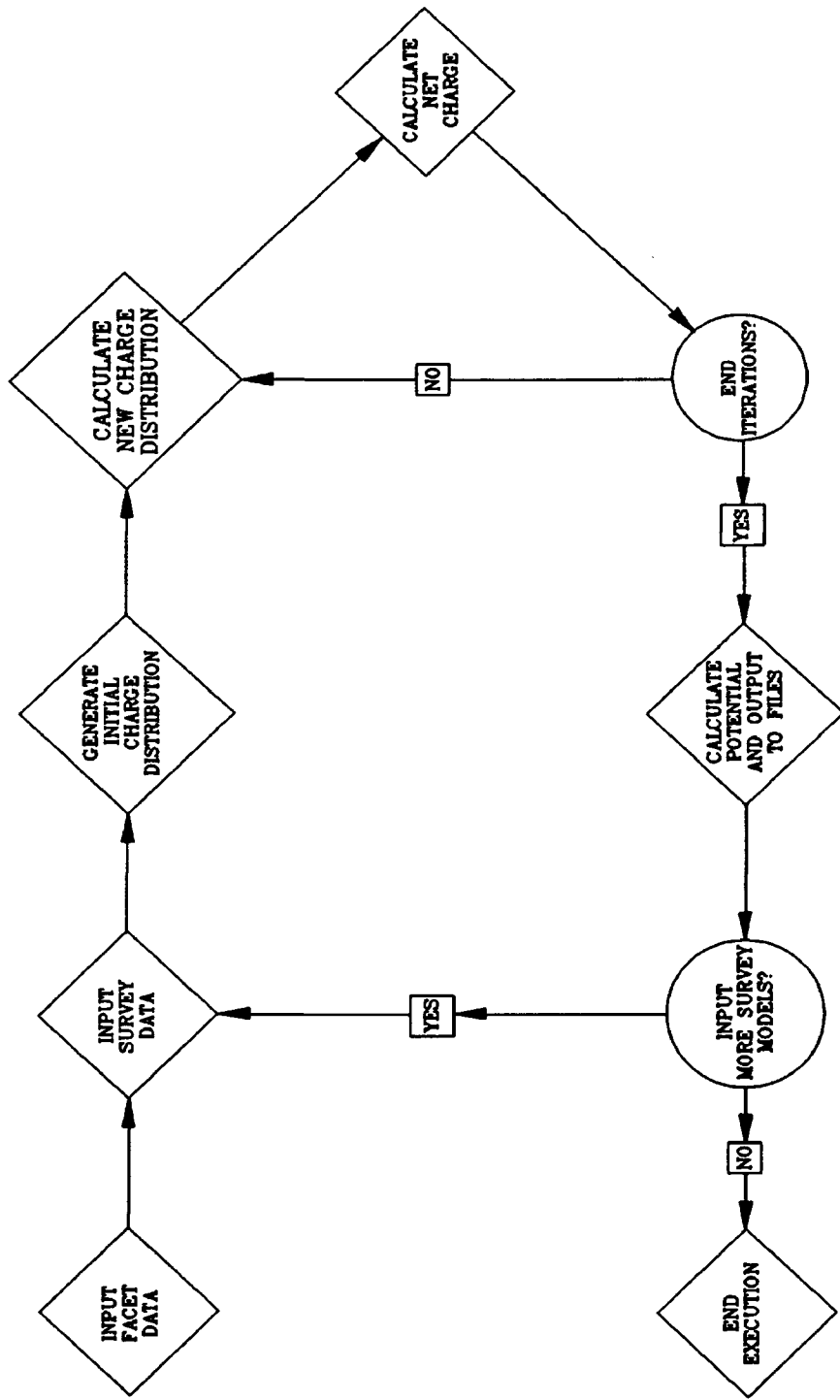
The new values of Q_i are substituted into equation (26) and the process is repeated until the solution converges. Convergence is reached when successive changes in the approximation with each iteration are within tolerable error limits.

2.3 Boundary Element Modeling Code.

The FORTRAN program DCMODEL.FOR (Appendix A-1) was written using the boundary element method to calculate the DC response of a closed faceted body at depth. The program is composed of several subroutines designed to perform just one or two operations. The program starts by reading in a data file containing information on a body or bodies, one facet at a time. Once the geoelectric model has been put in, the program reads information regarding the survey parameters. With a fixed current source, it is only necessary to calculate the charge distribution on the body once. The program then calculates the potential for various receiver locations.

The faceted surface of the body is assigned a first order charge distribution approximation by the subroutine FIRST. A second order approximation is made by including the interactive effects of the charges on the facets using the SECOND subroutine. Since image theory requires image sources, it was considered to include an imaged body reflected above the earth-air interface when solving for the charge distribution, as in subroutine IMAGE. Once the interactive terms are accounted for, the program checks to see if the charge distribution has stabilized or if the number of iterations exceeds the user-defined maximum. If the answer is no, the program returns to the SECOND and IMAGE subroutines again until the charge density solution proves to be converging or diverging. The solution is converging if the net charge on the body stabilizes with successive iterations, indicated by a change in the net charge of less than 0.1 percent. If the solution does not meet the criteria within the user-specified maximum number of iterations, twenty-five was adequate for the modeling performed, the solution is said to be divergent and the program ceases

operations. Otherwise, the program proceeds to calculate the potential values for each of the three components at each receiver location. Geometric factors are calculated for each receiver position and all source positions. The electric field components are then written to a file. A schematic diagram of the program is shown in Figure 8.



Schematic Diagram of DCMODEL.FOR Program Execution

Figure 8 Schematic diagram of DCMODEL.FOR.

2.4 Modeling Accuracy.

A comparison was made between the results of the boundary element model and the analytical response for a sphere. A FORTRAN subroutine developed by Merkel and Alexander (1971) was used to calculate the electric field of a resistive sphere buried in a homogeneous half-space and a fixed bipole current source. The model used to approximate the electric field using the boundary element method was based on a faceted spherical body with identical dimensions and resistivity.

The FORTRAN program SPHLENS.FOR was used to create a faceted body (Figure 9, Appendix A-2). Using a surface bipole source with current electrodes located at -500 meters and +500 meters, a surface dipole with a one meter separation was used to calculate the boundary element model response for a resistive sphere buried 10 meters below the surface. The analytical response and the boundary element approximation of the sphere with the imaged body included are shown in Figure 10. This model has a root mean square (RMS) error of 0.144 percent. At this point the image effects were removed and the response calculated, as shown in Figure 11. This model has an RMS error of 0.024 percent. It would seem that including a reflected body in the iterative charge distribution calculation is not justified. This conclusion is verified by noting the error value of the final solutions for both cases. The error of each solution is calculated by noting the net scaled charge of all the surface elements. Implicit in the solution is conservation of charge, which requires the net charge on the body to be zero. As can be seen in Figure 12, when the IMAGE subroutine is included in the program, the solution converges in three iterations with an error of 5.0×10^{-8} N-m²/coulomb. However, when the IMAGE

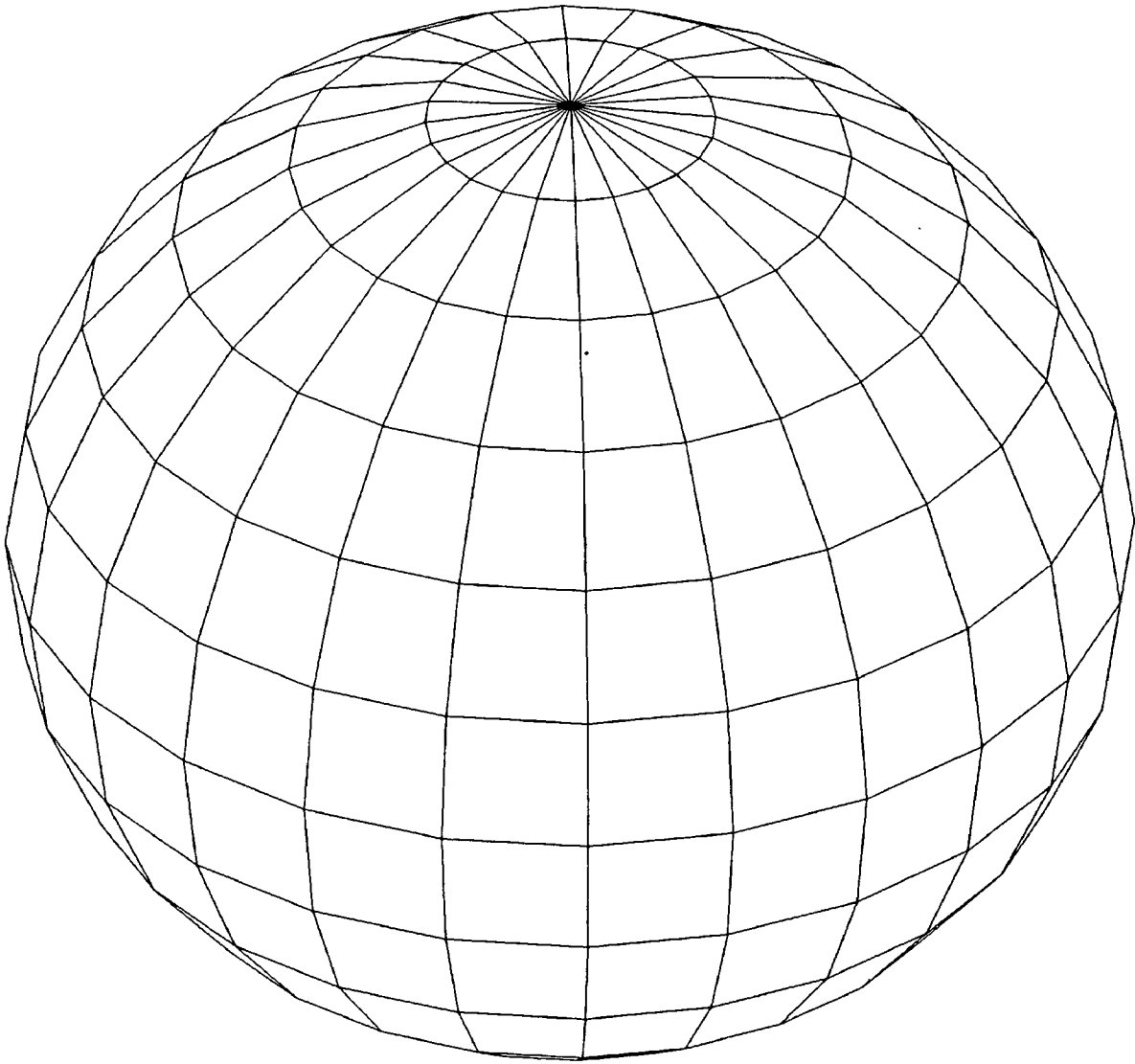
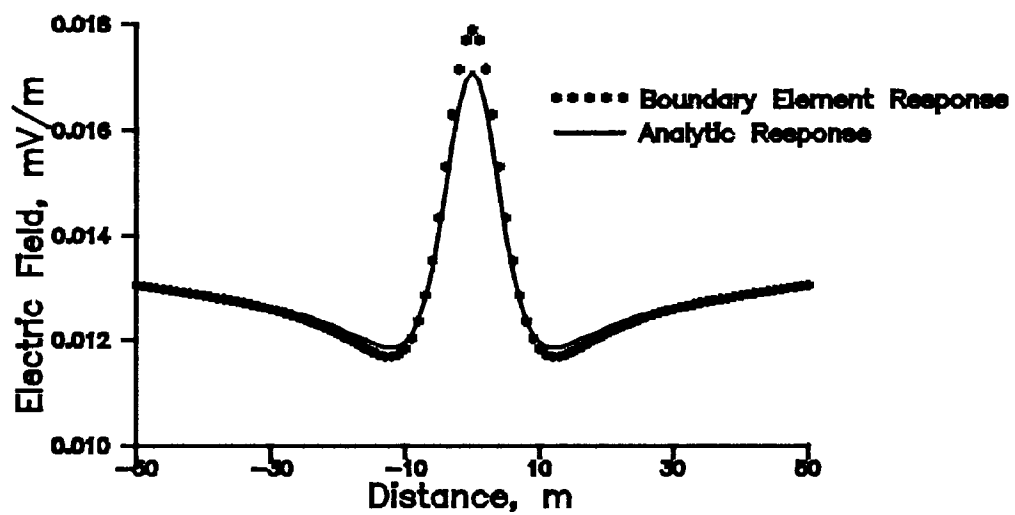


Figure 9 Spherical body generated using SPH.FOR. The sphere is divided into 12 latitudinal bands and 24 longitudinal bands, resulting in 288 surface elements.

Analytic vs. Boundary Element Response for a Resistive Sphere

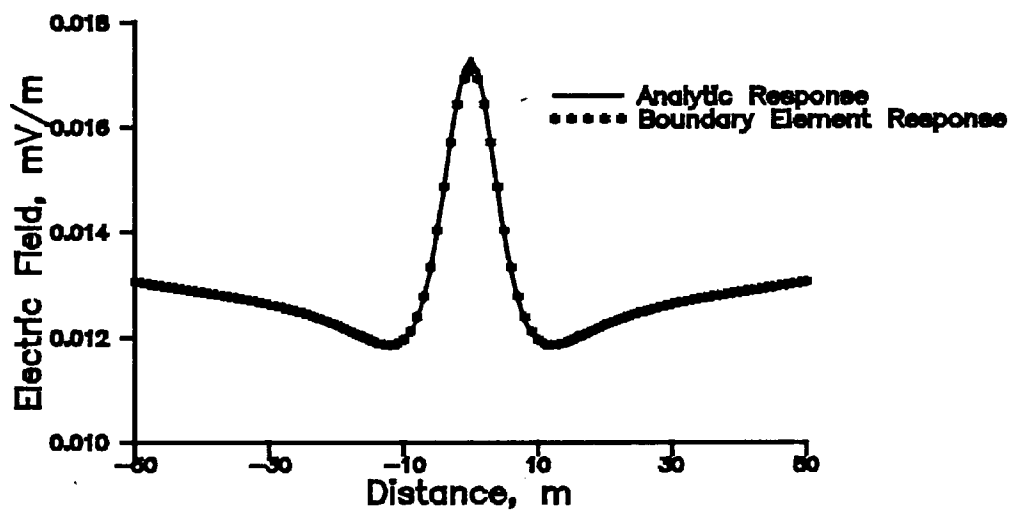


$\rho_1 = 10 \ \Omega\text{-m}$


 $\rho_2 = 1000 \ \Omega\text{-m}$

Figure 10 Analytical response and boundary element model response of sphere. DCMODEL calls IMAGE subroutine. Resulting root mean square error is 1.38 percent.

Analytic vs. Boundary Element Response for a Relative Sphere



$$\rho_i = 10 \quad \Omega\text{-m}$$



$$\rho_e = 1000 \quad \Omega\text{-m}$$

Figure 11 Analytical and model response for sphere. DCMODEL program does not call IMAGE subroutine. Resulting root mean square error is 0.48 percent.

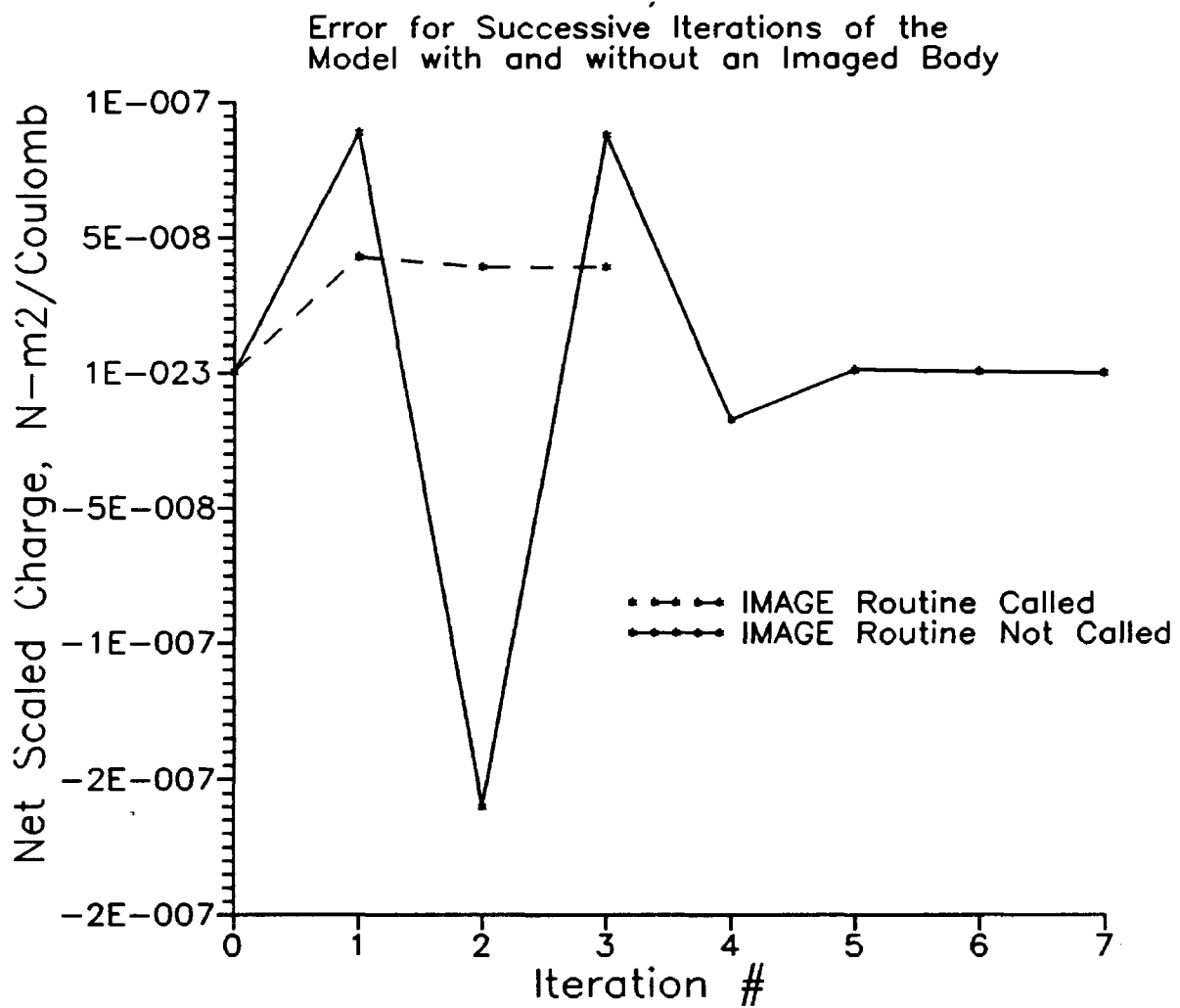


Figure 12 Effect of calling IMAGE subroutine in DCMODEL code. When the IMAGE subroutine is not called, the error function approaches zero.

subroutine is not included, the solution converges with an error of zero. Although the number of iterations is greater, the solution satisfies the conservation of charge restriction. Accordingly, the IMAGE subroutine was removed from the FORTRAN program in all subsequent modeling.

Two factors effecting the accuracy of the modeling program are the facet density and the number of iterations allowed when calculating the surface charge redistribution. Figure 13 illustrates the relationship between the surface element density on the body and the accuracy of the model response. However, there is a trade-off in increasing the surface element density. The computing time is proportional to n^2 where n is the number of surface elements. The number of iterations, however, has a linear effect on the computing time. For a quickly converging body, the total charge on the body can stabilize within a few iterations (Figure 14). For a configuration that converges slowly, the number of iterations can exceed ten or twenty before the error is reduced to acceptable limits.

It was noticed in the course of generating several models that for resistive bodies, those with a positive reflection coefficient k as defined in Chapter 2, the solution converged very rapidly, whereas for an identical body with a negative reflection coefficient it would usually converge so slowly that it would reach the maximum of twenty-five iterations without converging.

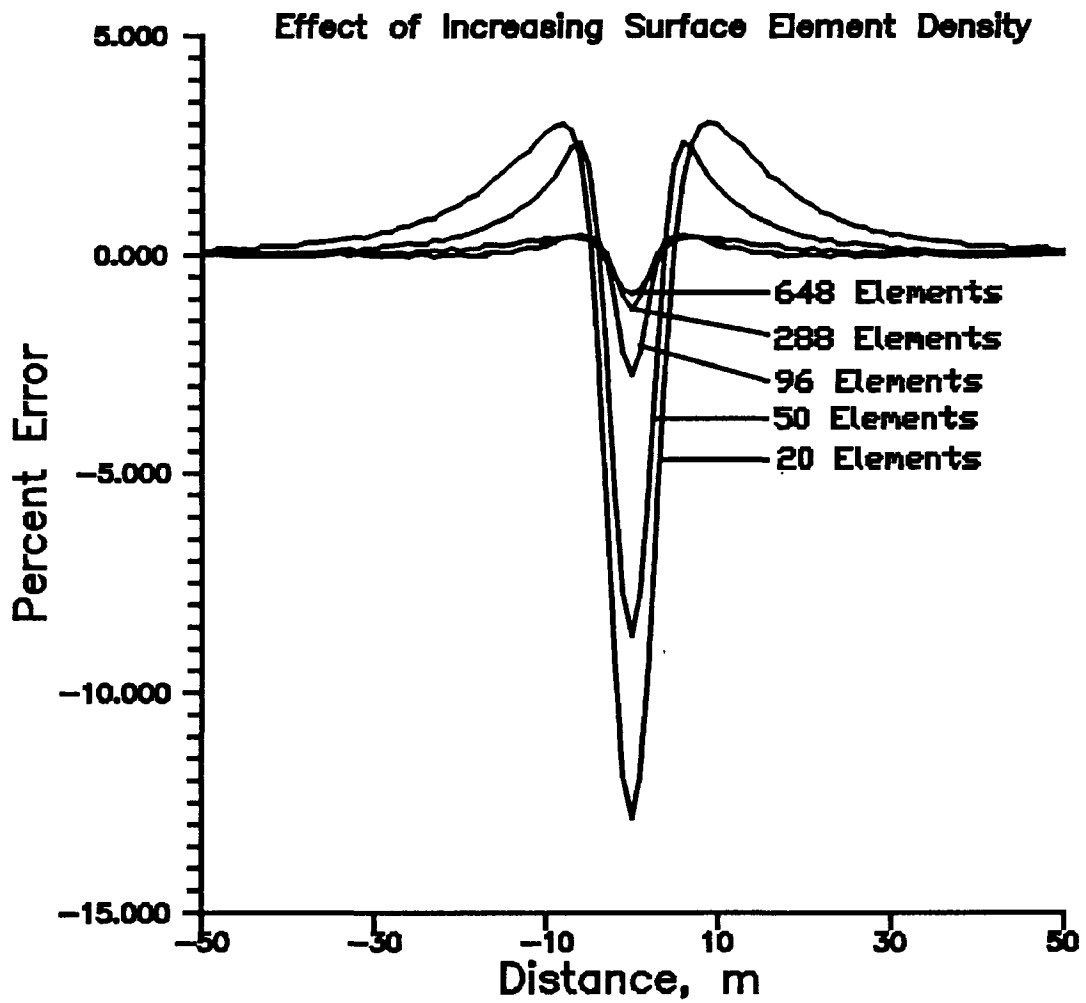


Figure 13 Accuracy of modeled resistive sphere ($\rho_1=10 \Omega\text{-m}$, $\rho_2=1000 \Omega\text{-m}$) with different facet densities. Error is deviation from analytic solution.

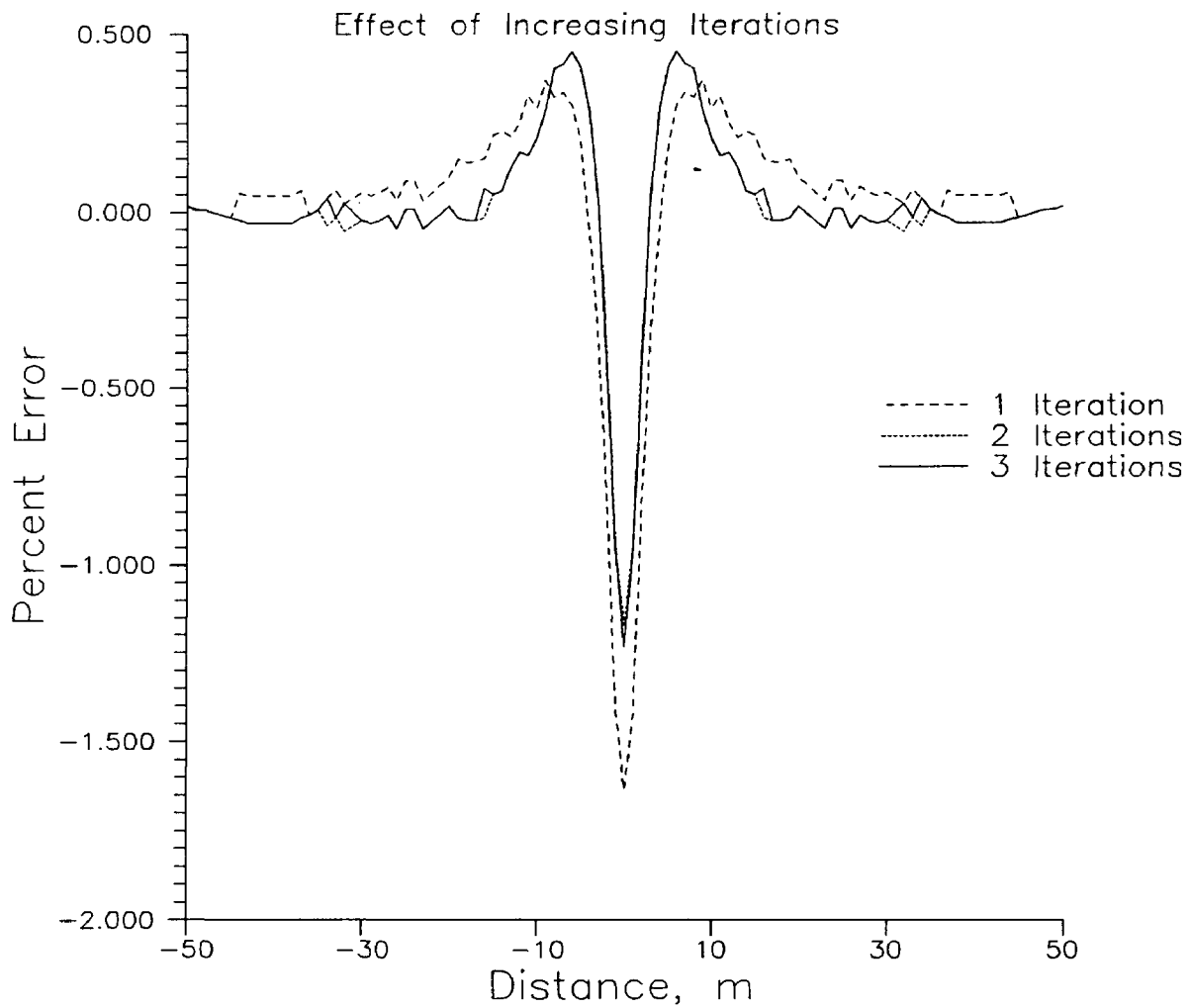


Figure 14 Accuracy of modeled resistive sphere ($\rho_1=10 \Omega\text{-m}$, $\rho_2=1000 \Omega\text{-m}$, 288 surface elements) with different iteration numbers. Error is deviation from analytic solution.

2.5 Summary of Surface Charge Boundary Element Method

The computer implementation of the surface charge method is a fast and accurate means of approximating the DC response of a closed faceted body. It should be noted that the method is derived for a whole space, and the half space interface is accounted for using the method of images for current sources. Extending the method to problems involving uneven topography or open bodies (ie, layers extending laterally to infinity) will produce unsatisfactory results, as the conservation of charge restriction may not always be satisfied. Under those circumstances, the use of finite difference or finite element modeling is recommended.

Chapter 3

MODELING OF TEST SITE

3.1 Geometry of the Test Site.

In order to create a geoelectric model of the WIPP site, station and well locations had to be converted to a common scale and reference. Well and shaft locations were obtained from Gonzales (1989), while underground survey base station locations were digitized from a map of the facility. The C&SH shaft was chosen as the origin, with all distances converted to meters (Table I). The model coordinate system is aligned with the x-axis as east, the y-axis as north, and the z-axis as downward vertical.

Table I Well and Base Station locations.

Station	Easting ft	Northing ft	WIPP X ft	WIPP Y ft	WIPP X m	WIPP Y m
Surface						
C&SH	666894.9	499687.2	0	0	0	0
AIS	666270	499687.1	-624.9	-0.1	-190.5	0
EXHAUST	667370.4	499287.2	475.5	-400	144.9	-121.9
WASTE	666919.9	499287.2	25	-400	7.6	-121.9
WIPP-22	667453	501165	558.1	1477.8	170.1	450.4
WIPP-12	667371	504068	476.1	4380.8	145.1	1335.3
Underground						
N300			-15	318	-4.5	96.9
Q ACC			-890.8333	-87.16666	-271.5	-26.6
G ACC			-646.5833	1119.75	-197.1	341.3
ROOM 7			1304.3333	-1933.083	397.6	-589.2

3.2 Modeling of Current Sources.

Two cased boreholes were used as current source electrodes (Figure 15). Pfeifer (1987) dealt with a linear source of current along an infinitely conductive line in a layered medium by representing it as several point sources. A laterolog was performed down the WIPP-22 borehole (Seward, 1982). The log was digitized at ten foot intervals, and the cumulative conductance curve calculated by integrating the conductivity with depth, as shown in Figure 16. Several line segments can be fit to the curve, representing the cumulative conductance of a layered earth model. It was assumed that the amount of current flowing into each layer is proportional to the total conductance of that layer. Pfeifer assumed that at great distances from the well the difference between treating the current source as a line source versus a point source was negligible, as the current flow approaches that of a bipole. In the vicinity of the well, the current source can be represented as a collection of colinear point sources. Each point source is located in the center of each layer, and the amount of current flowing from each point source is weighted by the conductance of the layer. Image sources were created by reflecting each point source across the earth-air interface.

Improving on the method used by Pfeifer to account for a line source in layered media, an eleven-layer model was fit to the cumulative conductance plot (Figure 17). Table II lists the weight that each layer is given and the depth to each point source. Since the WIPP-12 borehole is a kilometer north of the northernmost portion of the underground facility, a single point source was used to represent that current source. Current sources and image sources are shown in Figure 18.

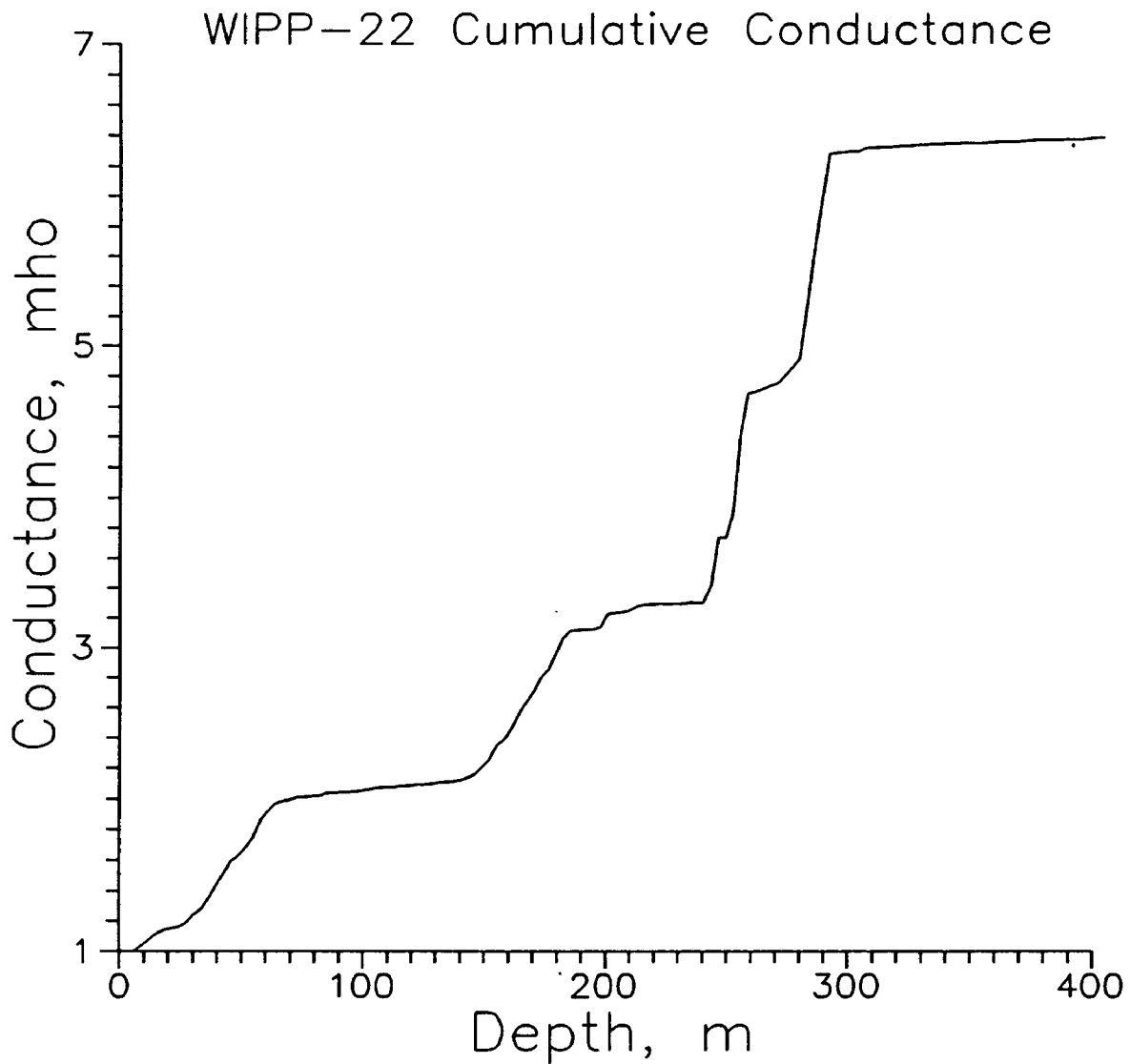


Figure 15 WIPP-22 cumulative conductance, from laterolog digitized at ten-foot intervals and numerically integrated (After Pfeifer, 1987).

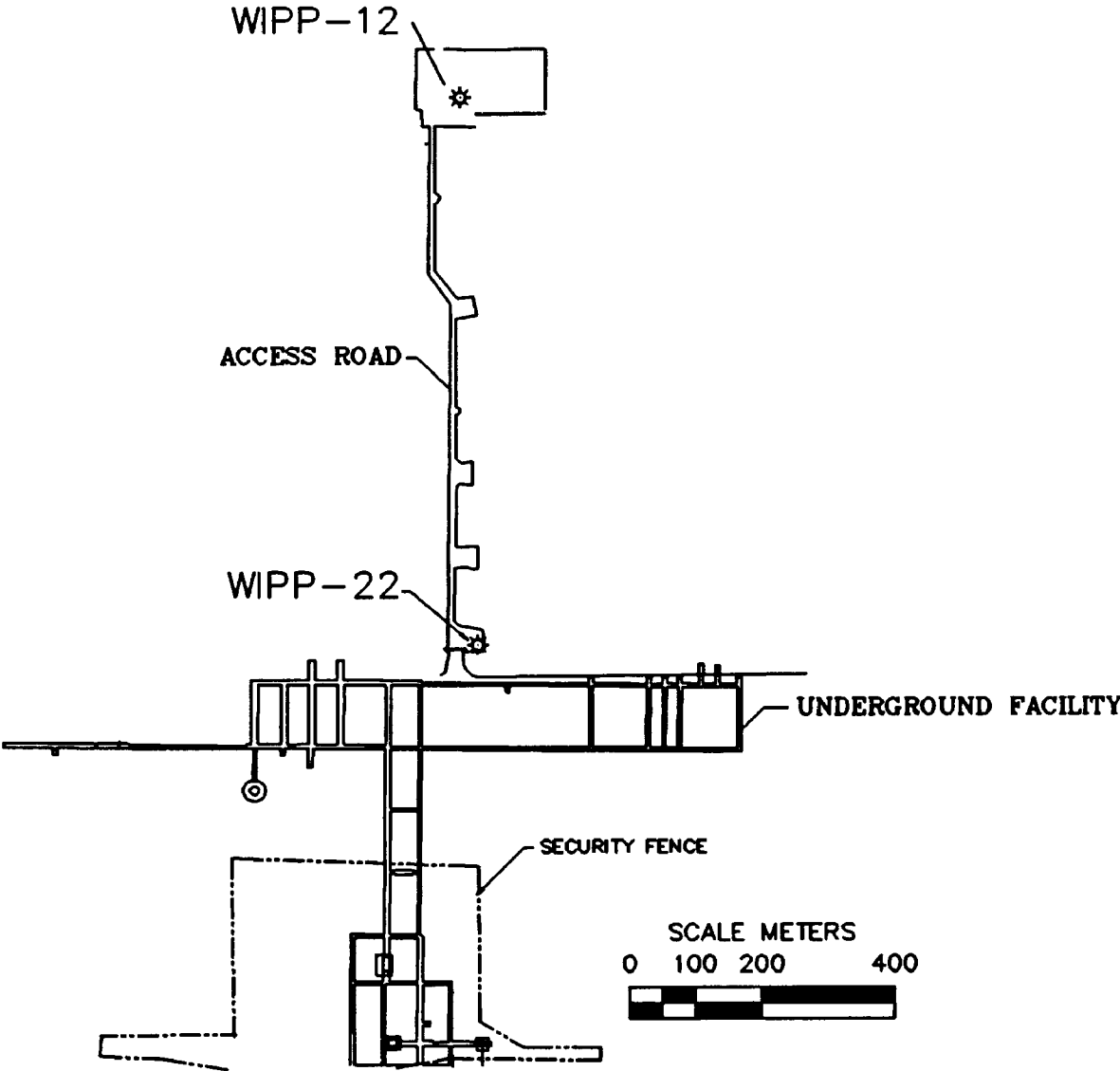


Figure 16 Surface location of WIPP-22 and WIPP-12 boreholes.

Table II Eleven layer model earth conductance and current scaling factors.

Thickness, m	Conductance, mho	Weight Factor	Depth, m
21.61919	0.231517	0.042826	17.40154
30.71046	0.753422	0.139368	43.56636
74.33078	0.176676	0.032681	96.08698
39.02431	0.963818	0.178287	152.7645
9.905238	0.025039	0.004631	177.2293
3.270961	0.10196	0.018861	183.8174
31.61712	0.089334	0.016525	201.2614
16.5226	1.374169	0.254194	225.3313
20.2112	0.156856	0.029015	243.6982
13.09223	1.434263	0.26531	260.3499
127.9465	0.098941	0.018302	330.8693

WIPP-22 Layered Model Cumulative Conductance

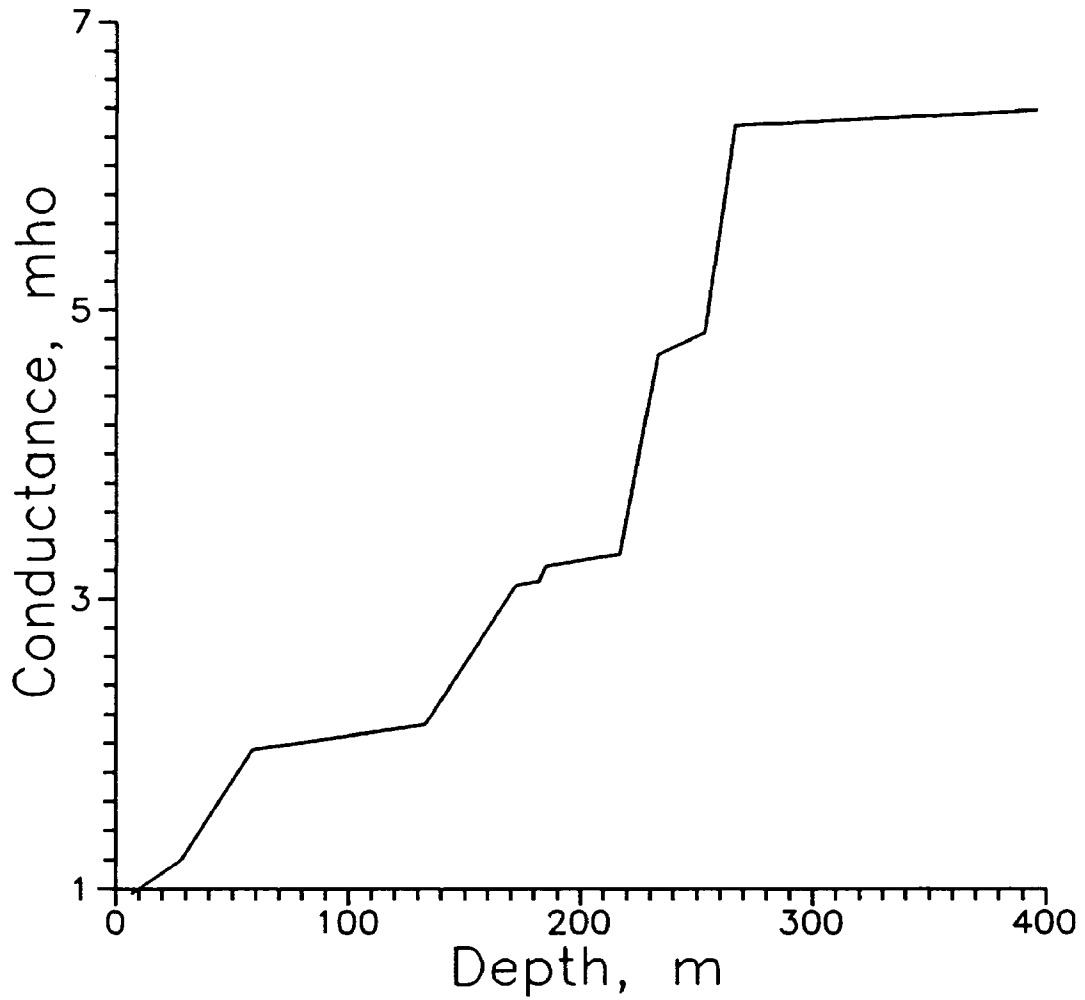


Figure 17 WIPP-22 conductance segments representing eleven layers.

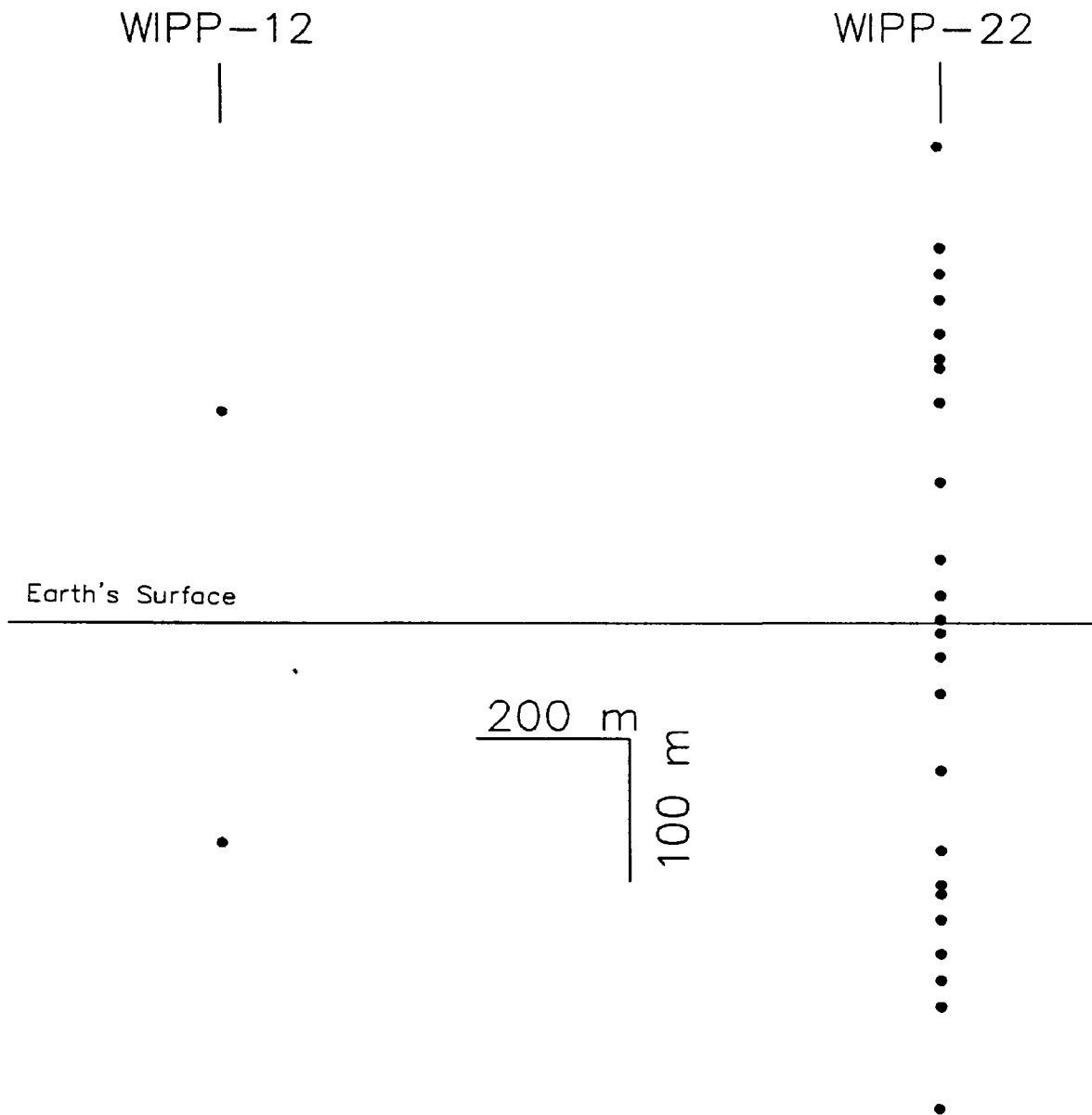


Figure 18 Colinear point sources representing a line source of current at WIPP-22, with a single point source at WIPP-12.

3.3 Modeling of Underground Features.

Underground features that affect the electric field include the resistive cavities of the mine workings, conductive zones due to the presence of water in the salt rock, and resistive bodies such as dissolution voids. These features can be modeled using faceted bodies. In the case of the mine drifts rectangular bodies are used, while lens shaped bodies are used to represent fracture zones and brine pockets.

In order to determine if it is possible to interpret field data using the model, some forward models must be run. Letting a target brine zone be represented by a lens shaped body, the program SPHLENS was used to generate faceted bodies. The body dimensions are the same as for a sphere, but with scaling factors applied in the x, y, and z directions (Figure 19).

Figure 20 shows the synthetic electric field components generated using the DCMODEL program. The profile runs west to east, with a lenticular body flattened in the west-east direction located fifteen meters north of the profile, centered at a depth of 650 meters. Using the same parameters but with the conductive body aligned in the XZ and XY planes, the model response is shown in Figure 21 and Figure 22. The three plots show that a thin conductive zone will have a signal response that is detectable given the geometry of the WIPP site. The orientation of the body will affect the disturbing electric field, possibly making the body undetectable. From the electric field components in Figure 21, the body is oriented so as to be almost undetectable. If random noise were introduced, as exists in the real earth, then it would be impossible to detect such a body. Given this limitation of the method, it should still be possible to interpret field data using the surface charge

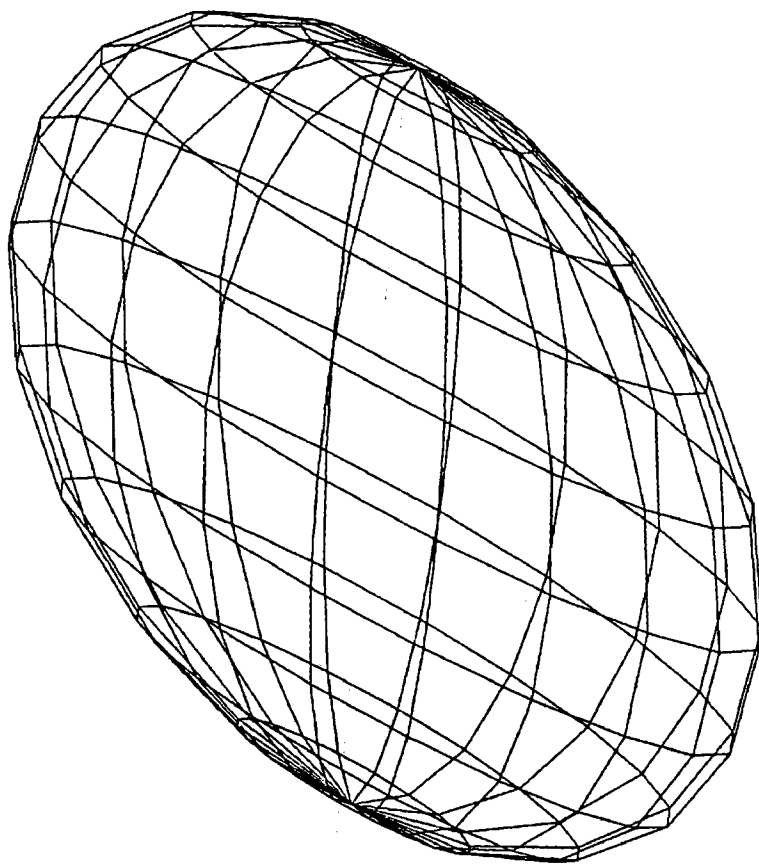


Figure 19 Lens shaped faceted body created using SPHLENS.FOR (200 facets, scale factor $L = 0.2, 1., 1.$).

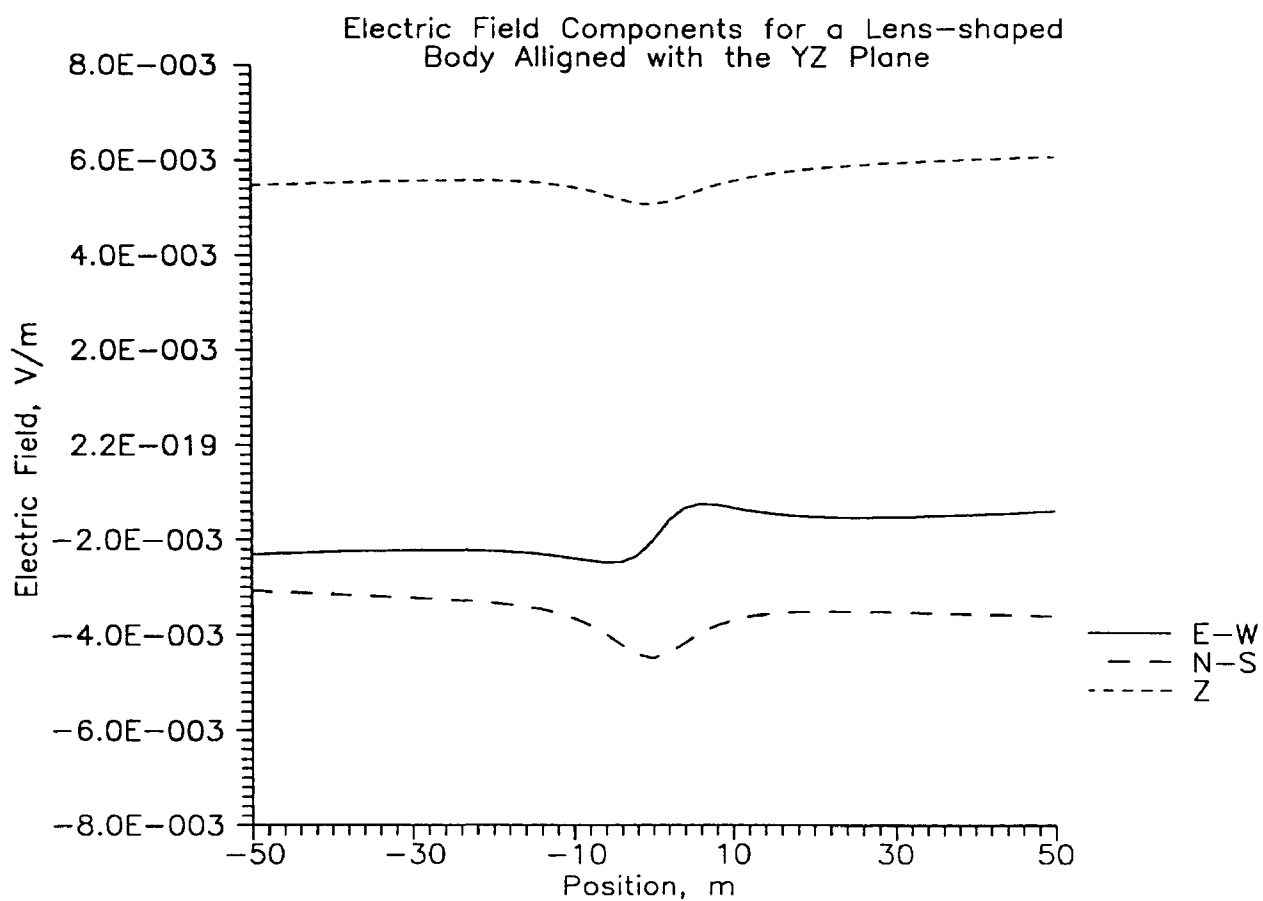


Figure 20 Electric field response of a lens shaped conductive body located fifteen meters north of profile ($R = 10$ m; $L = .2, 1, 1$; and $k = -0.8$).

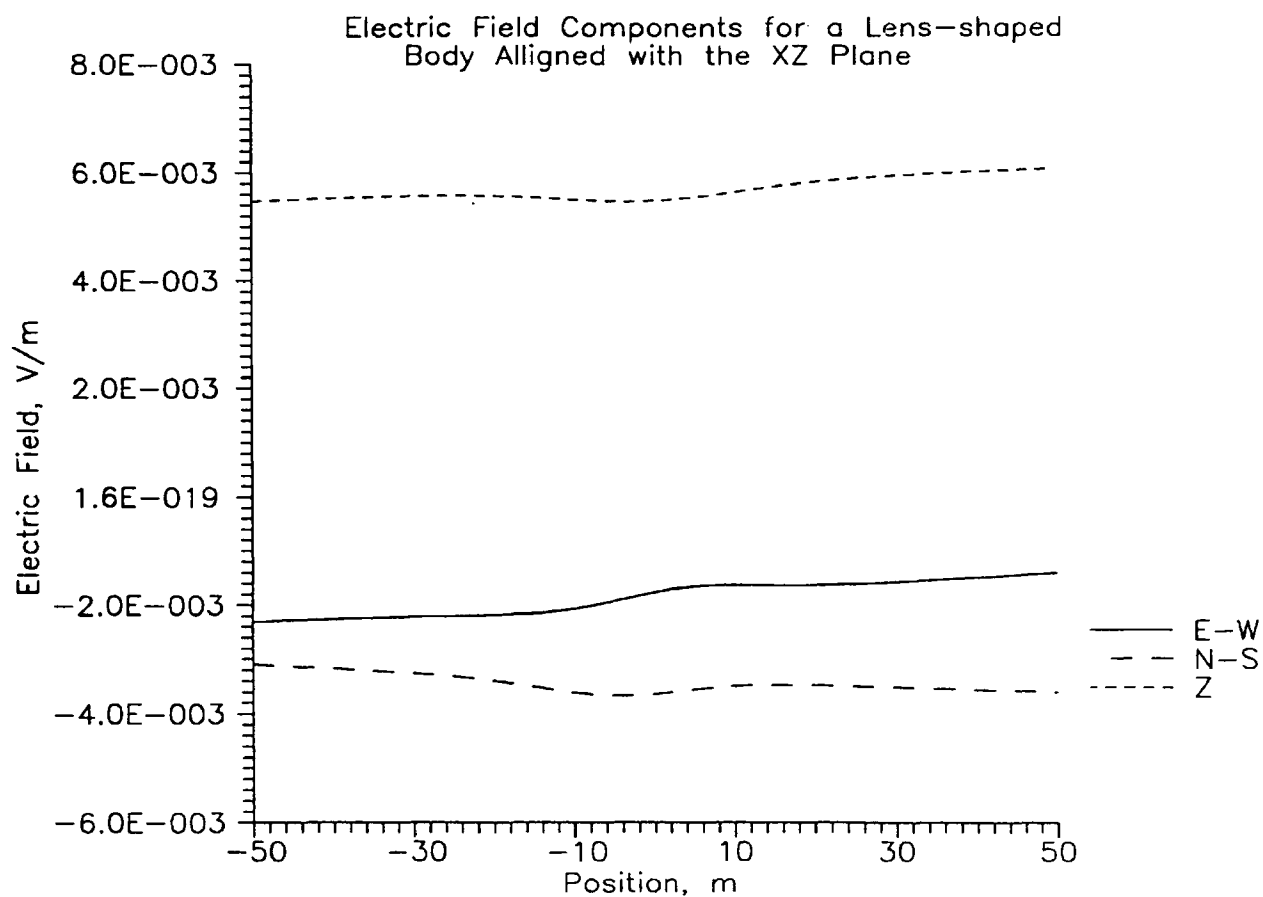


Figure 21 Electric field response of a lens shaped conductive body located fifteen meters north of profile ($R = 10$ m; $L = 1, .2, 1$; and $k = -0.8$).

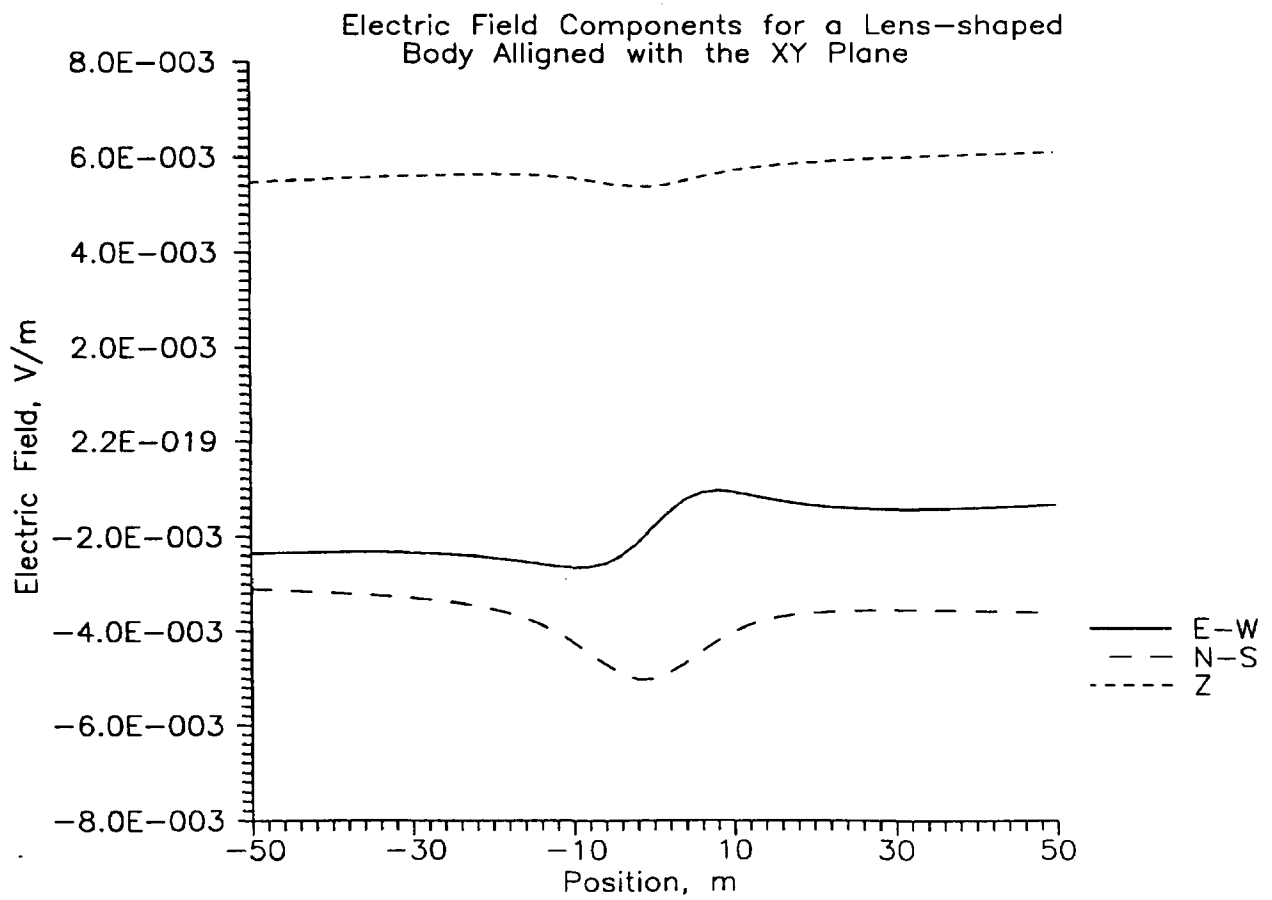


Figure 22 Electric field response of a lens shaped conductive body located fifteen meters north of profile ($R = 10$ m; $L = 1, 1, .2$; and $k = -0.8$).

model. Other simple shaped bodies that could be used to model brine pockets and fracture zones include a thin sheet and a cylindrical body.

Chapter 4

PRESENTATION OF FIELD DATA

4.1 Survey Locations

Four multicomponent DC resistivity surveys were conducted at the WIPP site to map conductive fracture zones. During January, 1989, a survey was performed in the Room G Access drift in the northwest corner of the facility. During that same period, Room 7 of waste storage Panel 1 was surveyed. In addition, surveys were performed in November of 1989 in the Room Q Access and the N300 drift. Survey locations are shown in Figure 23.

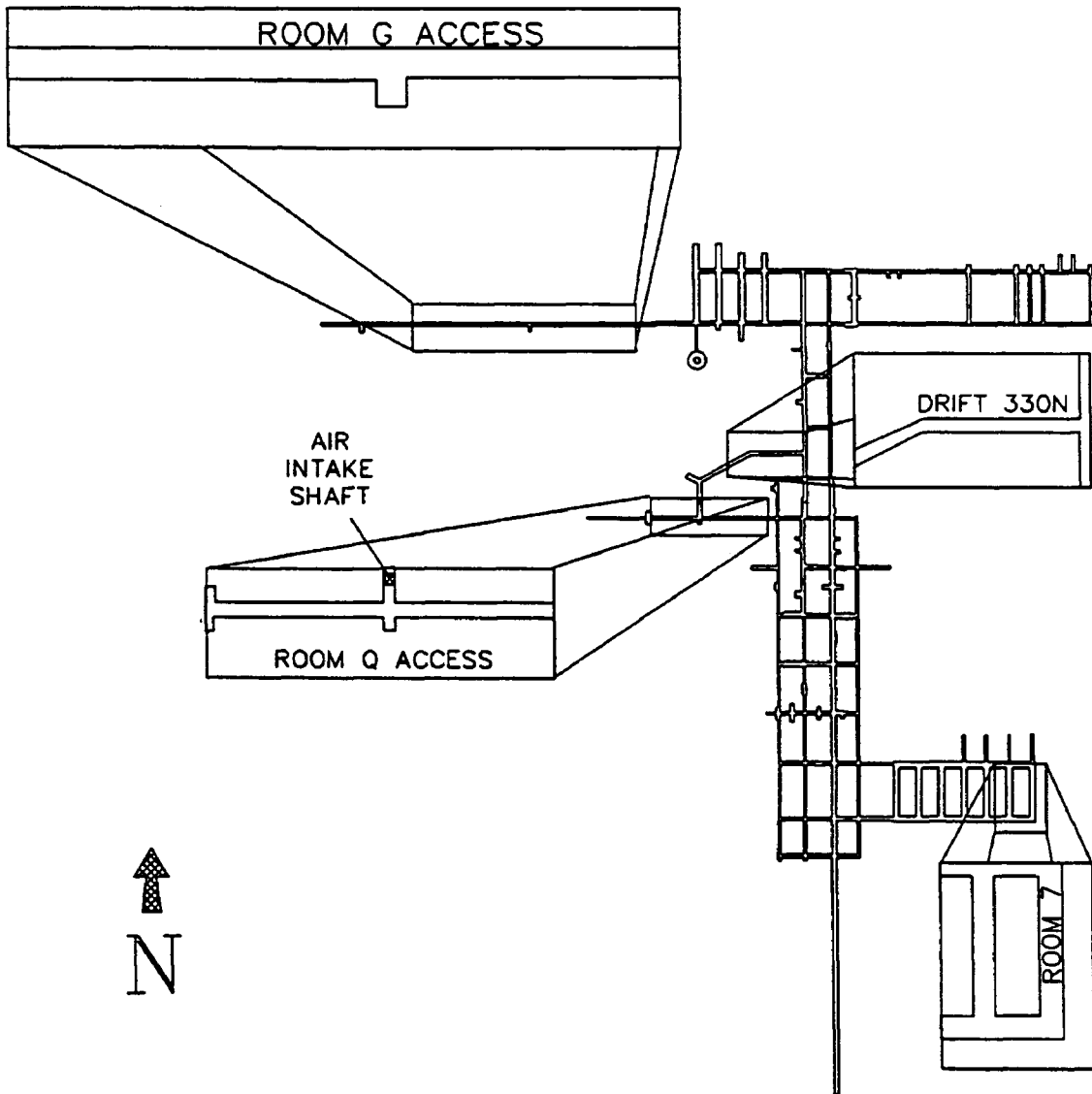


Figure 23 Locations of multicomponent resistivity surveys at WIPP underground facility.

4.2 Room G Access

The survey performed in the Room G Access was sampled at approximately ten foot intervals to map a known region of increased water content. The field data (Appendix B) were processed using the VSWING program and converted to electric field magnitude. Station locations and the electric field data are shown in Figure 24. The region in the middle of the profile exhibits an extremely low response with regards to the rest of the survey. This region of increased conductivity correlates with the existence of hydrous salt formations on the rib of the drift. The hydrous salt formations, which appear similar to small cauliflowers a few centimeters across, are due to the migration of moisture from the rock into the drier air of the drift.

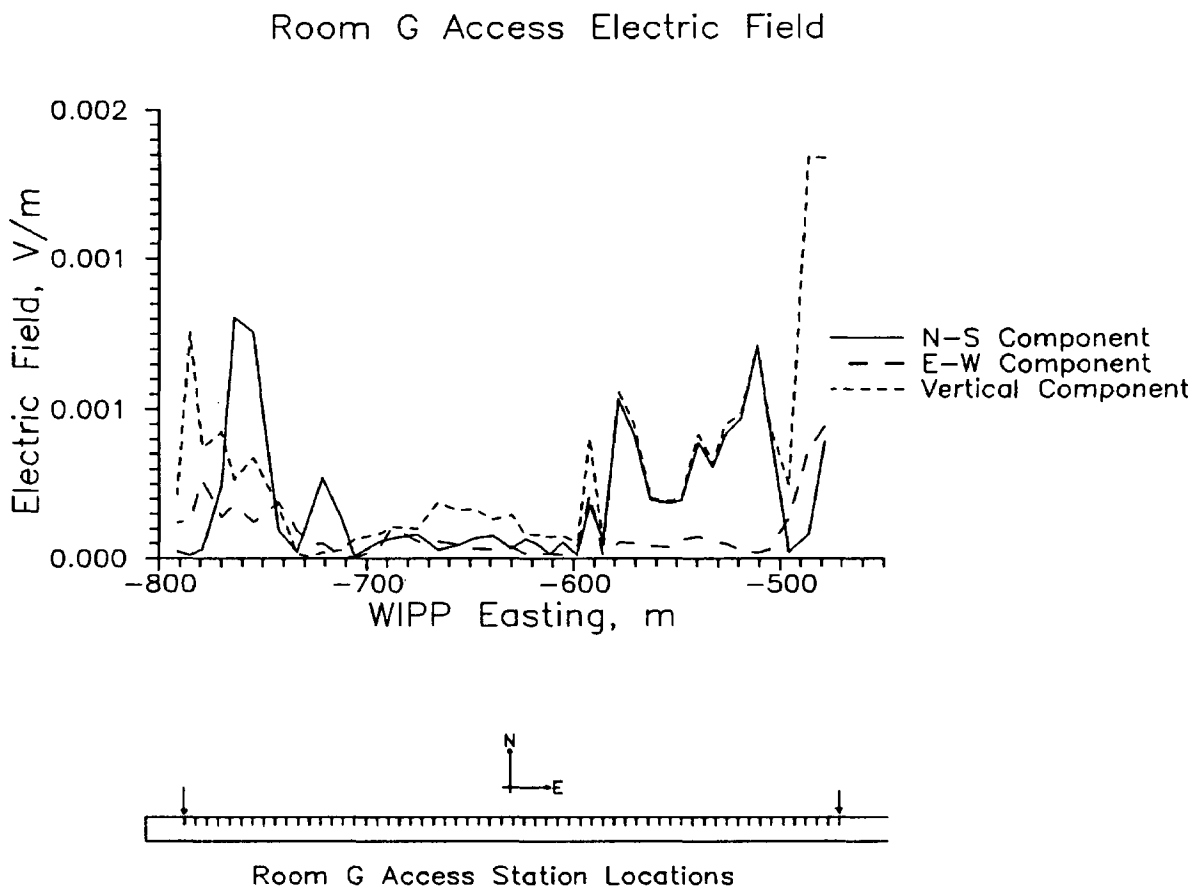


Figure 24 Station locations and electric field data from Room G access multicomponent survey.

4.3 Room 7

Room 7 was surveyed with stations located twenty feet apart. The survey extended around the southeast corner of Room 7 and into the S1950 drift. The electric field data and station locations are shown in Figure 25.

The low value in the electric field at the corner of Room 7 and S1950 drift suggests the presence of a nearby conductive zone, as a conductive body has a lower signal response. Moisture migrates from the salt rock into the drifts, leaving a drier zone near the drift. The dry rind effect at the WIPP site was documented by Pfeifer(1987). Since a corner provides an even greater area for water to migrate through, it is reasonable to assume that a corner should be as dry as the surrounding rock, if not drier. Accordingly, at a corner measurements should show a higher bulk resistivity. In the case of Room 7, the low electric field at the corner suggests an increase in water content nearby. Shortly after the resistivity survey was performed a test hole was drilled at the corner and a higher than normal amount of water was found in the gypsum marker bed some two meters below (D. Borns, personal communication), confirming the presence of increased water content.

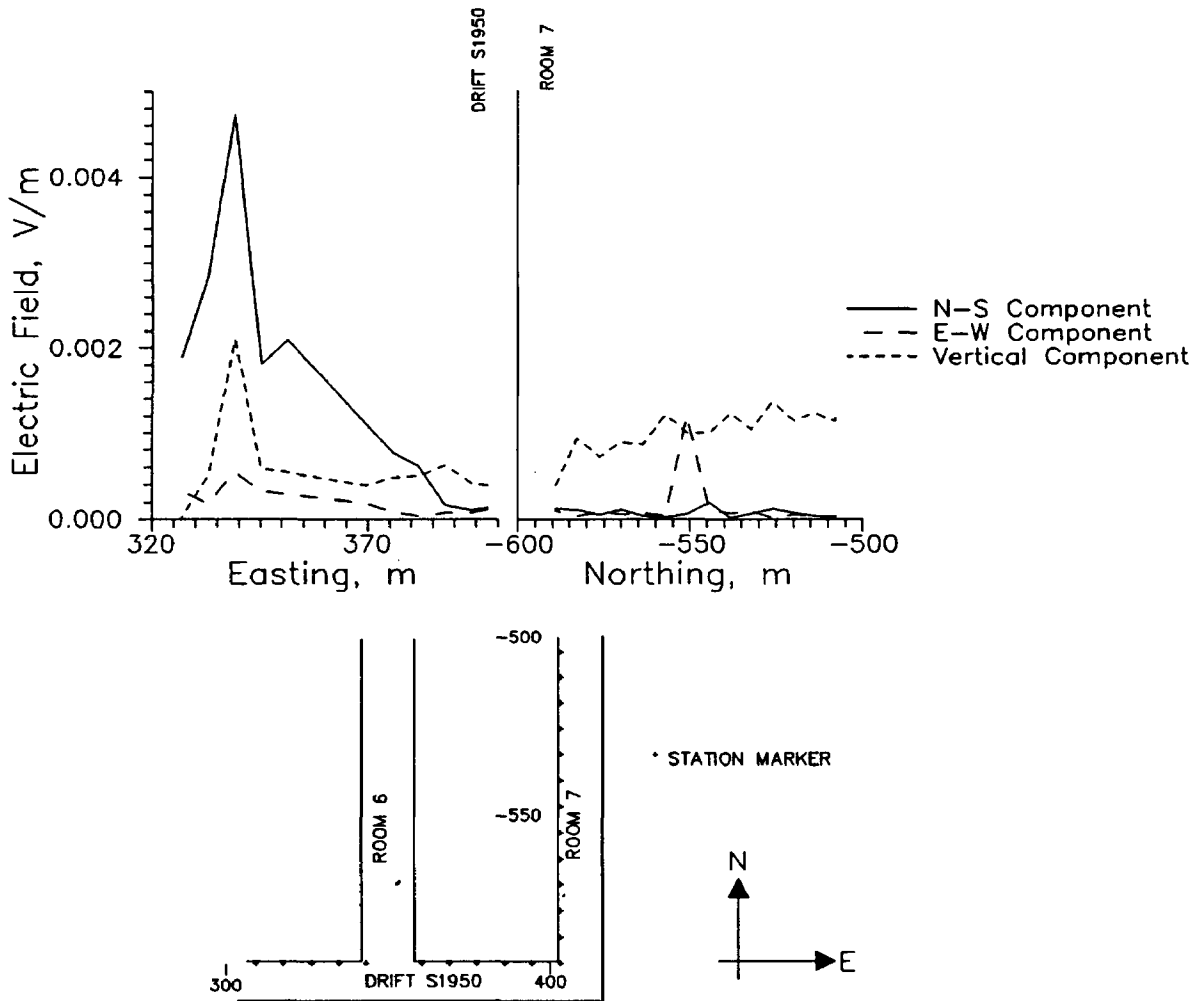


Figure 25 Station locations and electric field data from Room 7.

4.4 Room Q Access

The Room Q Access was surveyed with a station spacing of ten feet. Station locations and the raw data are shown in Figure 26. Two features of note in the survey are the location of the hydrological test probes and the Air Intake Shaft access. The probes were placed in boreholes in the floor of the drift to identify and characterize a suspected brine pocket. The low, broad feature at the east end of the profile suggests a large conductive body. In actuality, the low response is due to water on the surface of the salt rock. Recent drilling in the Air Intake Shaft had released a large amount of water in the drift, which settled at the east end and saturated the rock, making the floor of the drift very conductive and effectively shorting out the electric field.

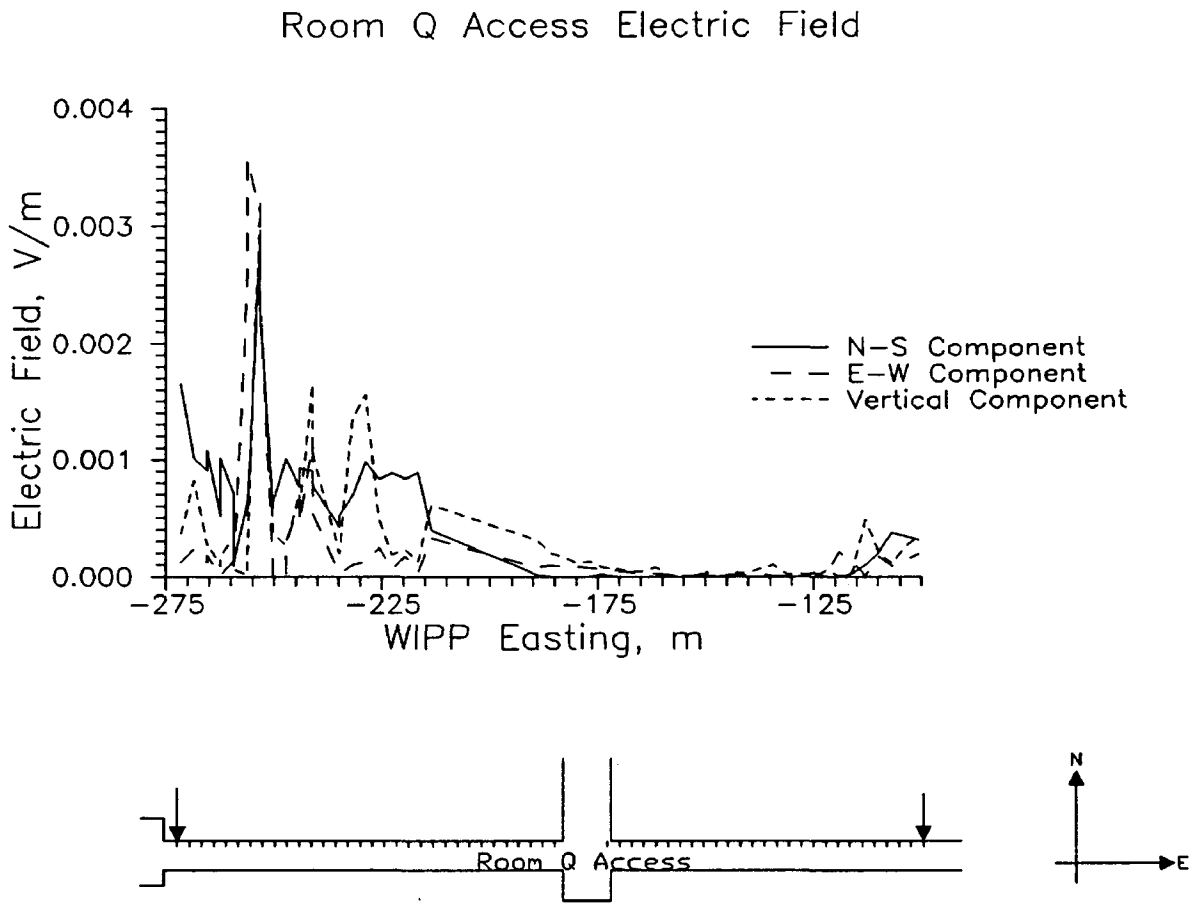


Figure 26 Station locations and electric field data for Room Q Access.

4.5 N300 Drift

The N300 drift was surveyed with stations located at ten foot intervals. The station locations and the electric field data are shown in Figure 27. The vertical component dominates the electric field signal, indicating a near-vertical electric field. However, towards the middle of the profile the vertical component drops in strength and the horizontal components increase. A conductive body would have the effect of pulling the electric field lines into it, increasing the horizontal components and diminishing the vertical component (Figure 28). An initial hypothesis would be that there is a zone of increased water content in the vicinity.

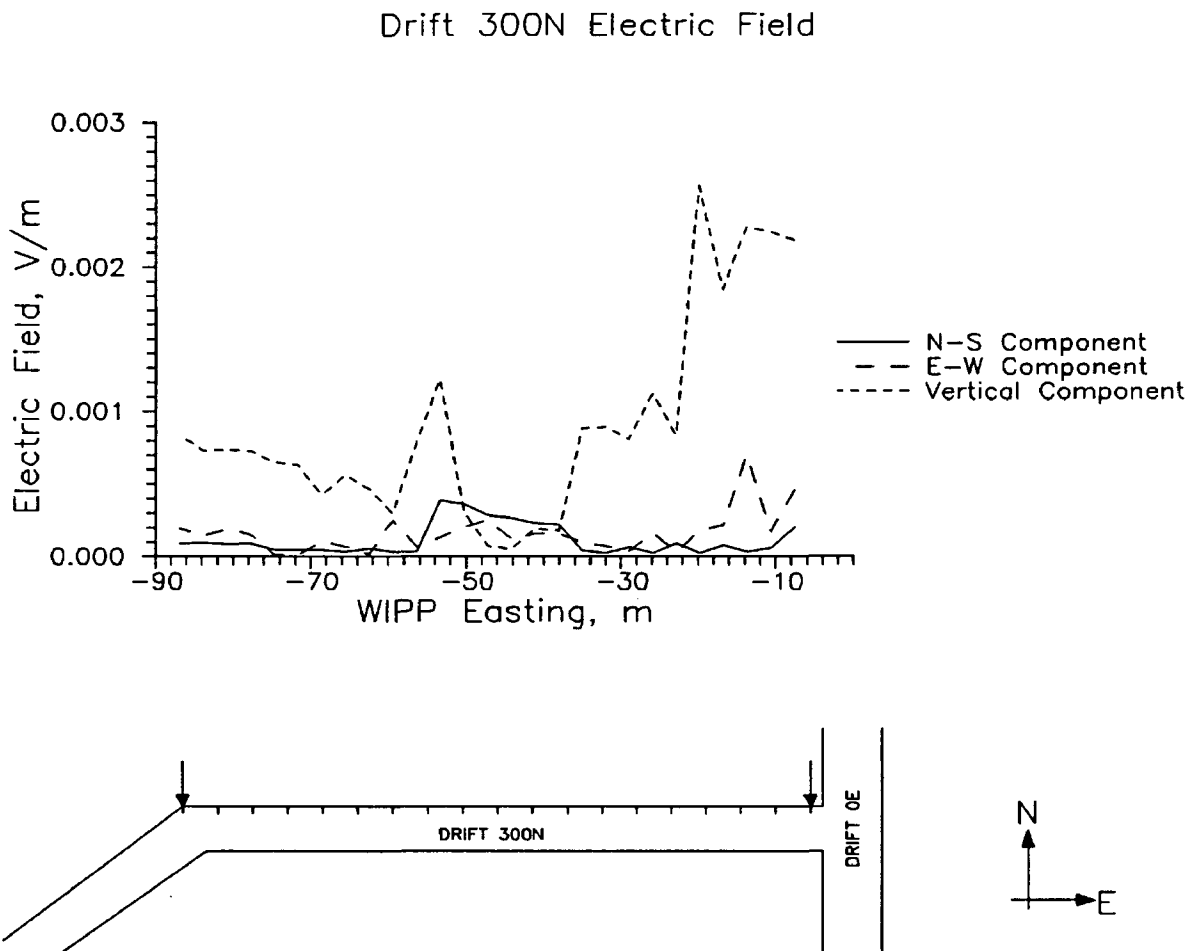


Figure 27 Station locations and electric field data for 300N drift.

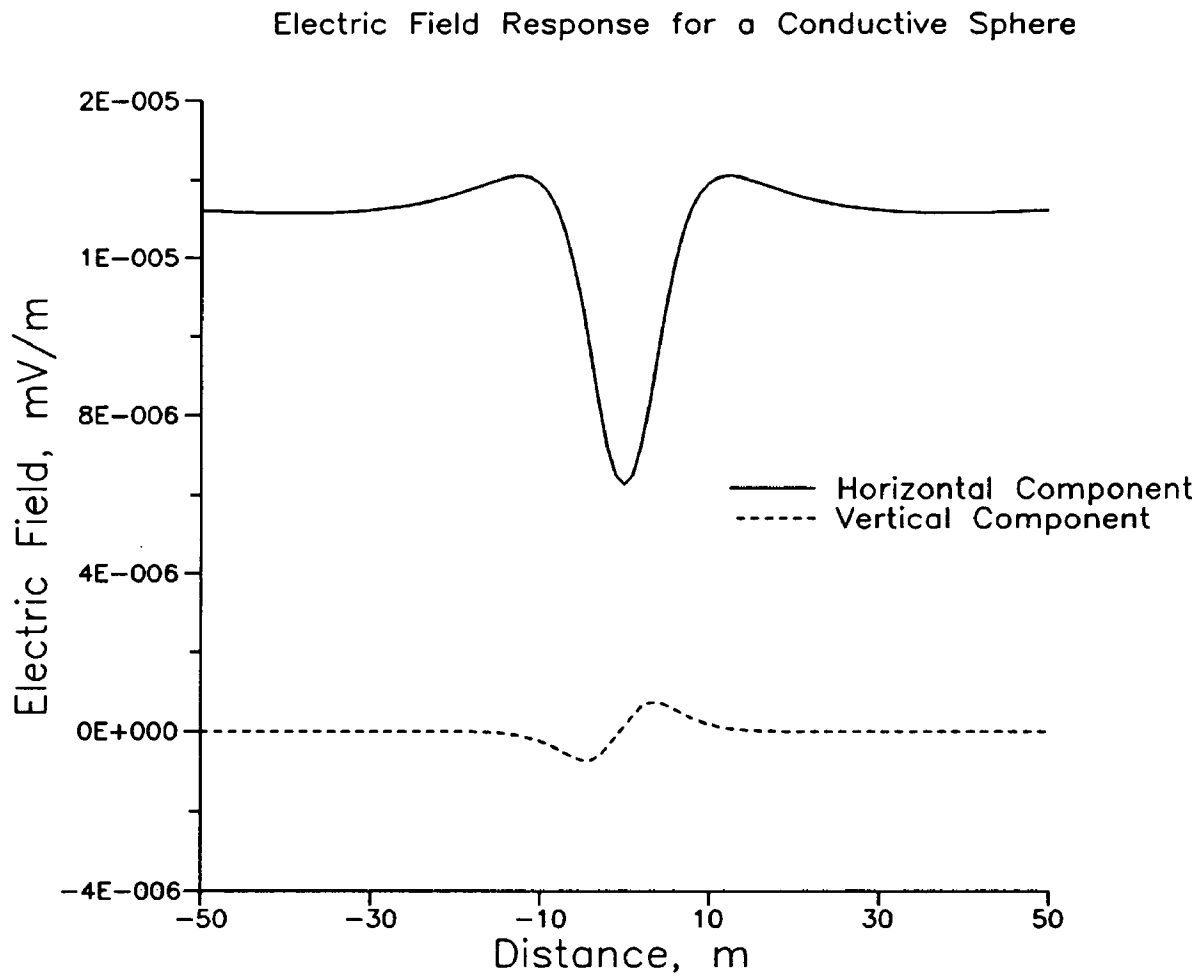


Figure 28 Electric field response of a conductive sphere ($\rho_1=10 \Omega\text{-m}$, $\rho_2=0.01 \Omega\text{-m}$, radius=7 meters, depth=10 meters) generated using DCMODEL.

Chapter 5

MODELING AND INTERPRETATION OF FIELD DATA

5.1 Modeling Results

Inspection of the electric field data reveals very little that can be modeled with simple closed bodies, as noise almost overwhelms the signal. Fortunately, the electric field data from the 300N drift has a signal that displays a feature in the middle region of the survey. Using the configuration and orientation of the 300N drift, models were generated and response curves calculated in order to interpret the observed data. A bipole source was used, with multiple colinear point sources representing the near source electrode.

The first model generated was that of a drift cavity with dimensions similar to the 300N drift. Using MAKE.FOR, a rectangular body was generated and input into the DCMODEL program. Survey stations were modeled parallel to the drift at a distance of five meters from the surface of the faceted body. The surface of the rectangular body was divided into two hundred facets. The disturbing potential is of particular interest, as that is what stands out in an actual survey. The calculated disturbing potential is shown in Figure 29. The effects of an unstable charge distribution are readily seen. The charge distribution on the elongated body did not converge quickly, and would probably diverge if allowed to iterate indefinitely. This effect is likely due to limitations imposed by the assumptions of the modeling method. The use of surface charges on boundary interfaces requires the electric field to be calculated some distance from the surface of the drift. Although field measurements

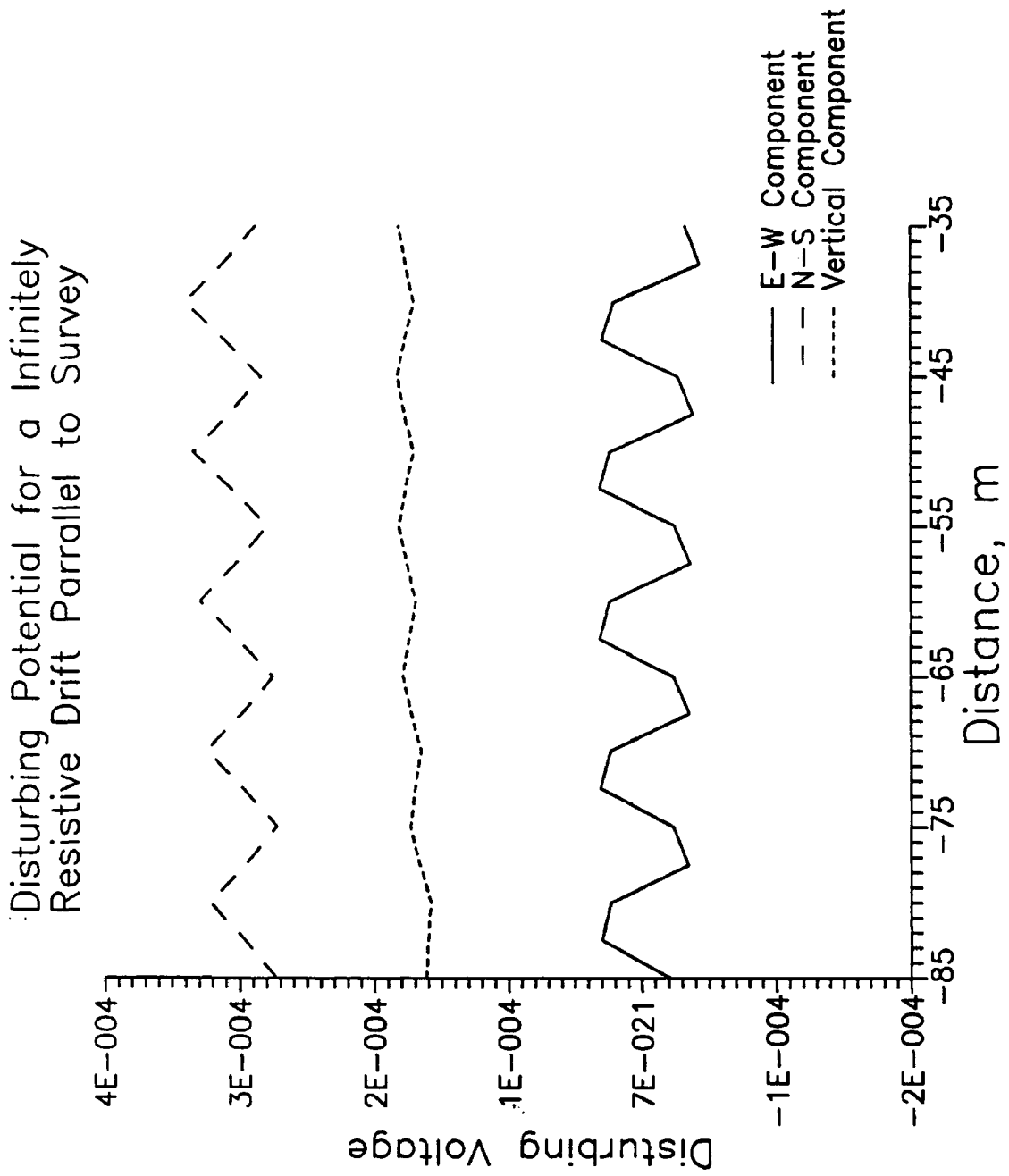


Figure 29 Disturbing potential curves of drift model
(Dimensions: 100,10,10; Location:-55,100,645; grid:10,5,5; k=.9999).

were recorded on the drift faces, it was necessary to assume that drift cavities do not influence the electric field significantly and to continue the modeling with lens shaped bodies.

The data from the 300N drift have a rather distinct signature that allow a qualitative interpretation. However, the information from the acquisition system is handicapped in that the acquisition software is unable to determine the polarity of the voltage. The VSWING program picks the absolute voltage difference, not the relative voltage difference (Appendix B). This only compounds the uniqueness problem, leaving no chance that a model can be generated that will fit the observed data.

With an understanding of the geologic environment and a priori knowledge of the resistivity of the host rock, the forward model can be used to generate response curves that help produce a qualitative interpretation. Model curves were generated using a conductive lens located at various horizons about the drift. Figures 30 through 33 show the responses of a conductive horizontal lens to the north of, above, to the south of, and below the drift. Positive directions are south, west and up. A rule of thumb that can be drawn from the four sets of curves is that the potential is greater towards the conductive body. It becomes obvious when one considers a conductor in an electric field. There is no lateral component of the electric field on the surface of a conductor, only a perpendicular component. The conductor has the effect of drawing electric field lines into it. This is the phenomenon seen in the four response curves.

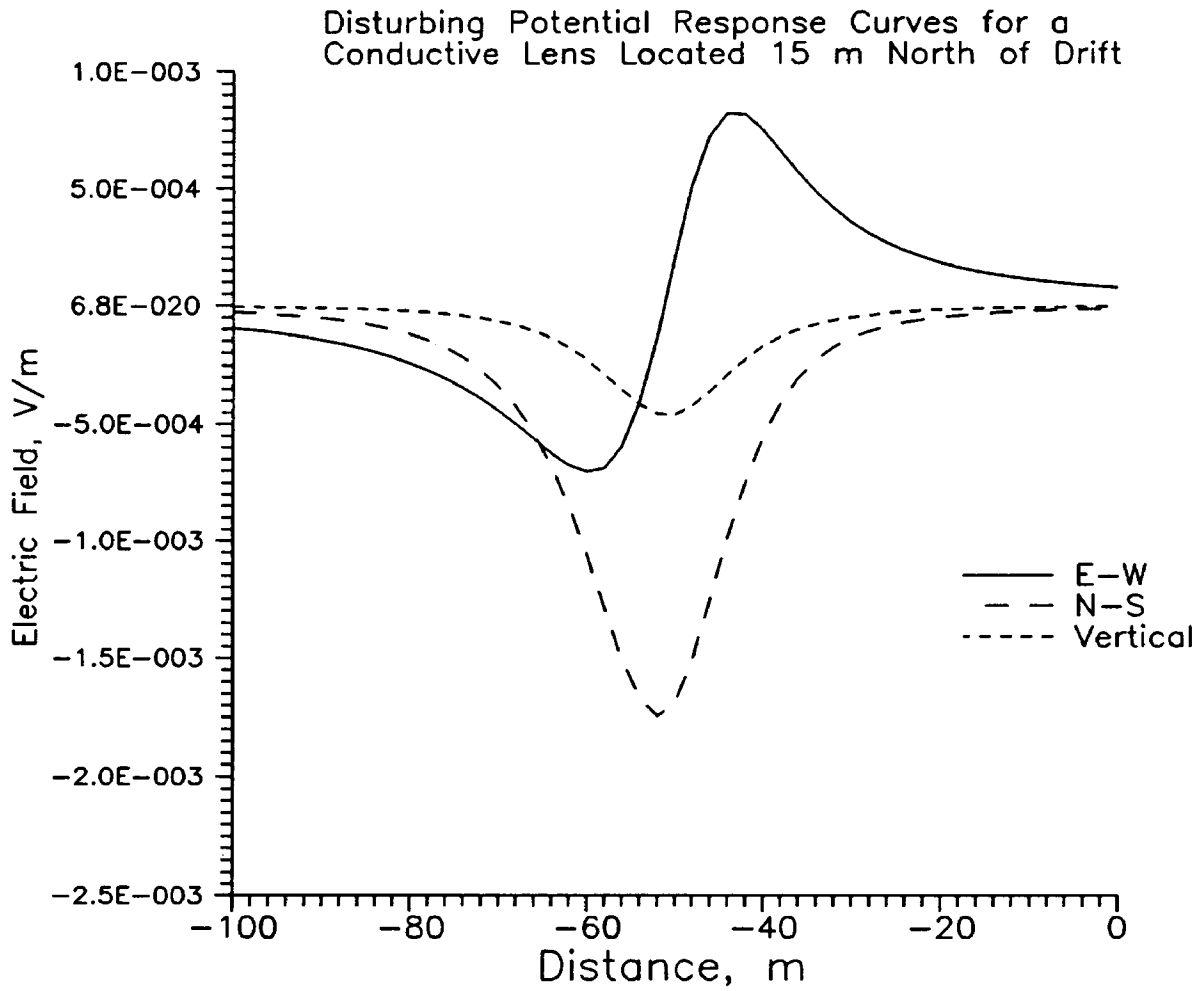


Figure 30 Disturbing potential curves for a conductive lens located 15 m north of drift.

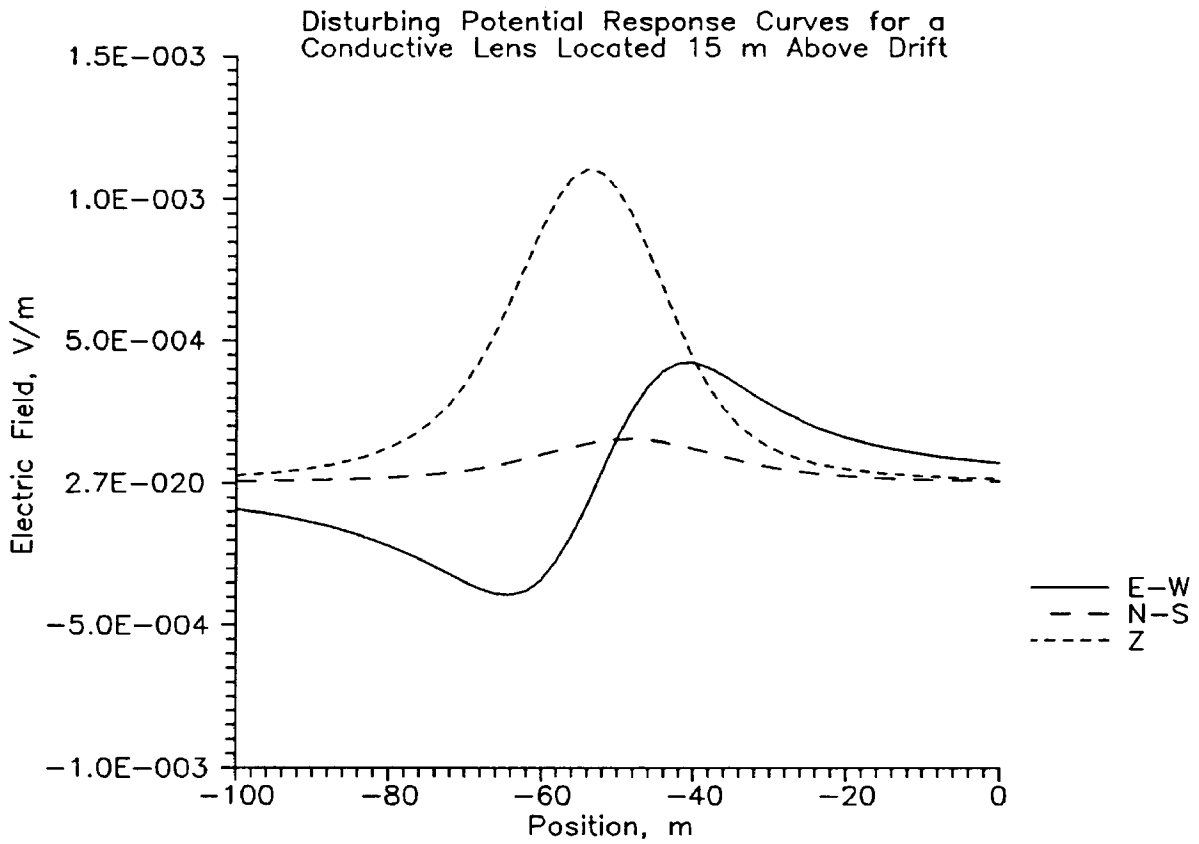


Figure 31 Disturbing potential response curves for a conductive lens located 15 m above the drift.

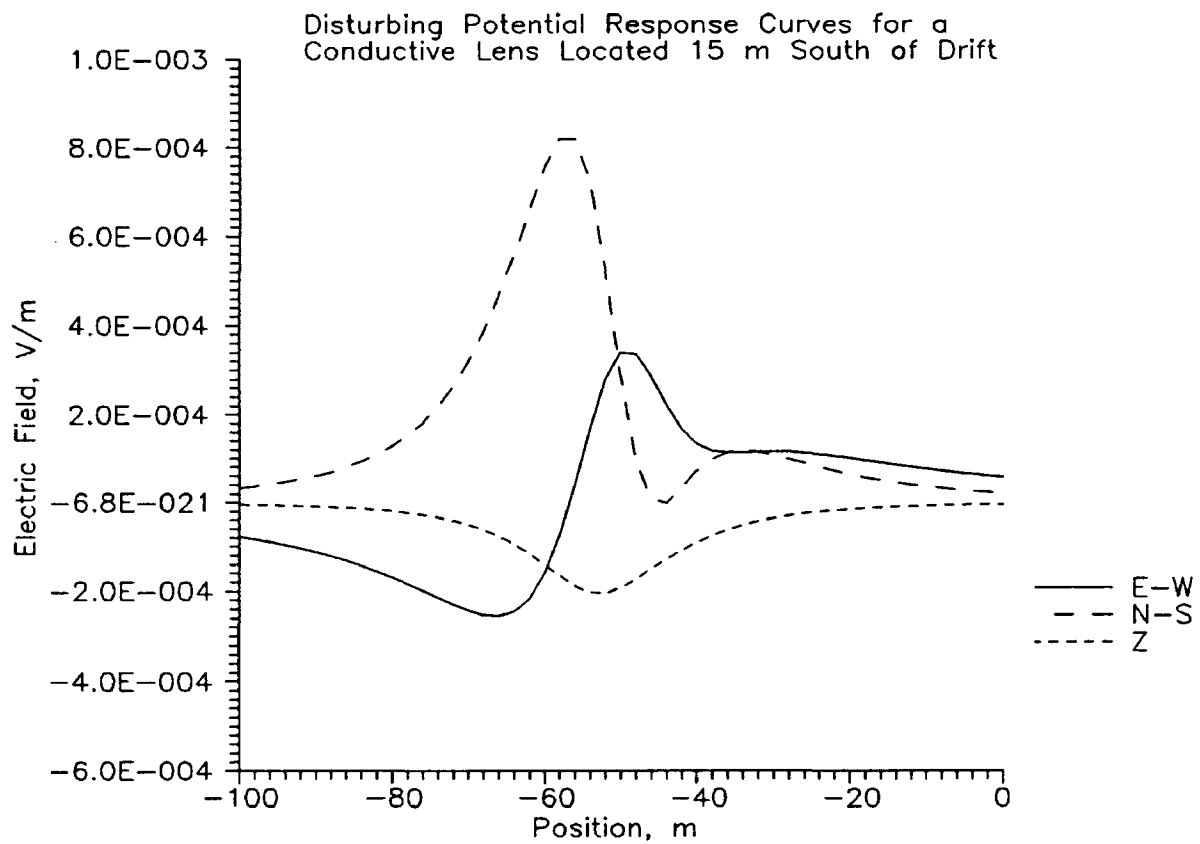


Figure 32 Disturbing potential response curves for a conductive lens located 15 m south of the drift.

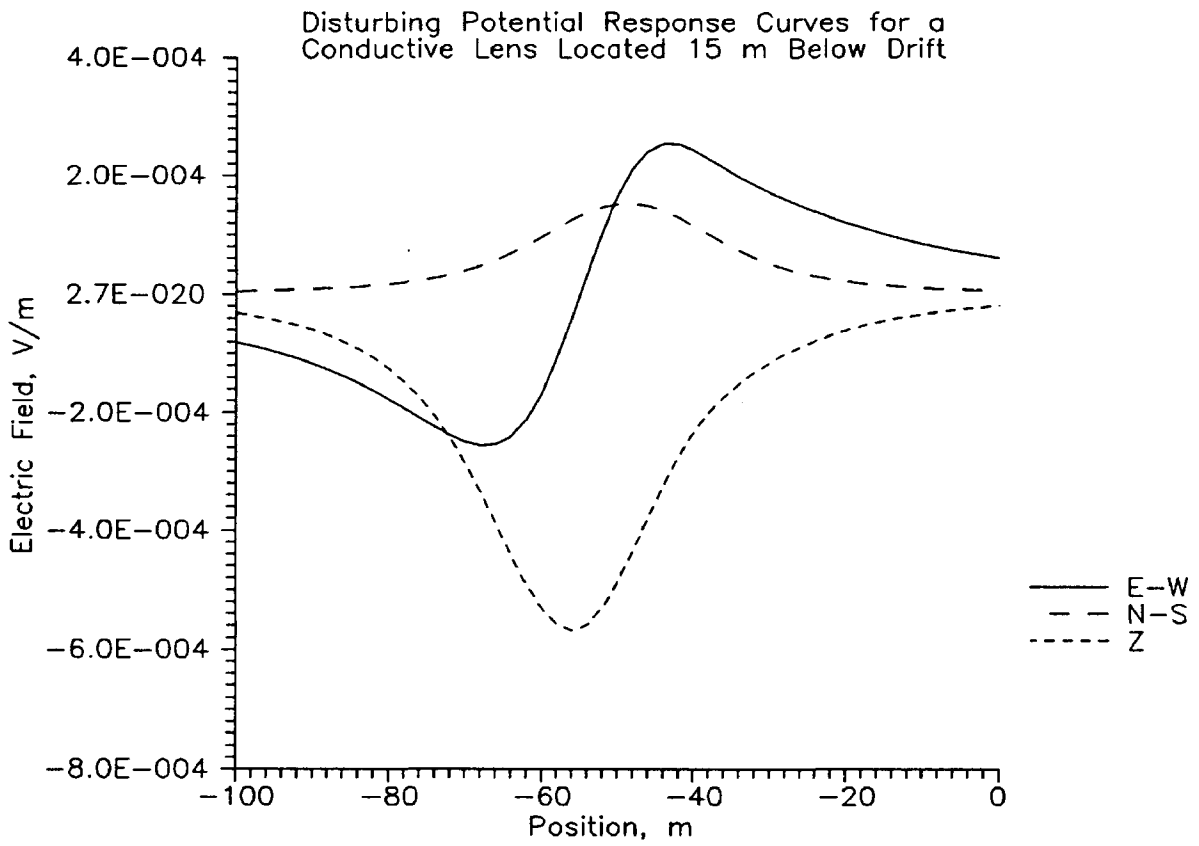


Figure 33 Disturbing potential response curves for a conductive lens located 15 m below the drift.

5.2 Interpretation of Field Data.

Given the limitations of the system, what can be done to interpret the field data? While it may not be possible to uniquely identify the location, shape and resistivity of a structural feature, it should be possible to at least make an estimate as to its dimensions and distance from the drift.

The most important feature to note in the 300N data (Figure 27) is that the vertical component of the electric field is dominant, correlating with the synthetic data from Figure 20. The vertical component in the 300N data dips sharply at approximately -45 meters. The horizontal components appear to increase at the same location, but they could just as easily be negative. Not having polarity information forces us to deal with either case.

The first body to model is a flat-lying conductive lens beneath and to the south of the drift. The vertical component has a promising dip at the right location, but the horizontal components have the wrong sign, as taking the absolute value will result in a dip rather than a peak (Figure 34).

Moving the lens directly beneath the drift smooths out the electric field response considerably. The horizontal components are beginning to look promising. The absolute value of the electric field components yield the curves shown in Figure 35. Although not a unique solution, the model provides a simple structure that could produce the signal seen in the 300N data.

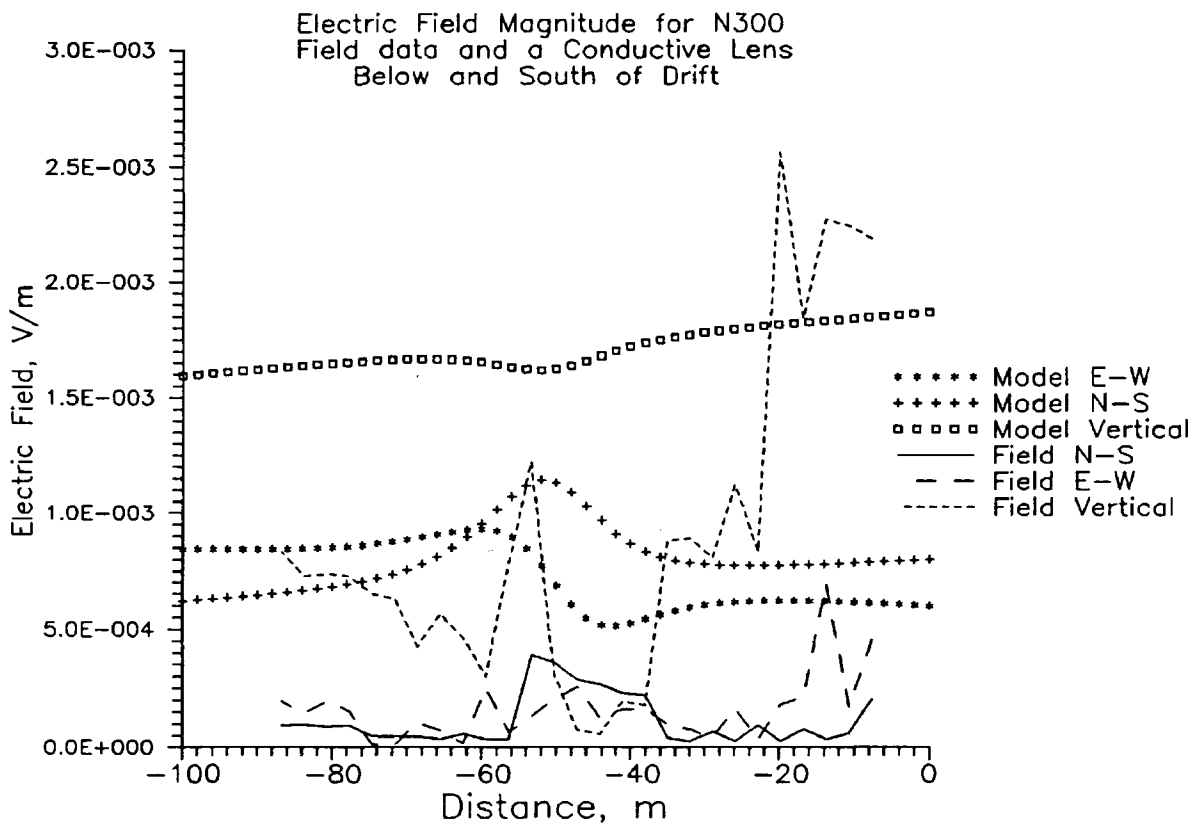


Figure 34 Drift 300N Model: Conductive lens below and to the south of the drift.

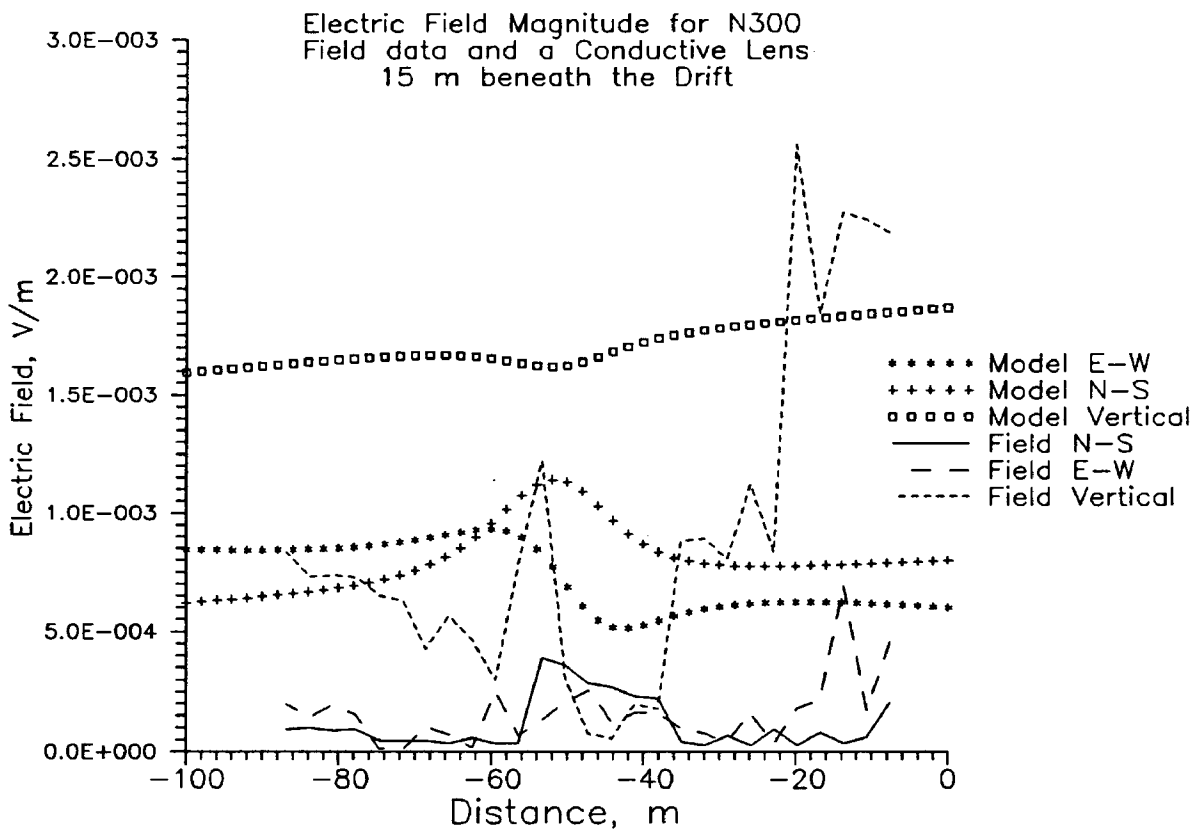


Figure 35 Drift 300N model: Conductive lens located below the drift.

Chapter 6

CONCLUSION

6.1 Success of Boundary Element Method

The results of this research demonstrate that the boundary element method of modelling a DC resistivity response can provide a quick, accurate approximation of the electric field response of a simple model. Modeling the resistivity contrast as a charge distribution on the body surface simplifies model construction to defining the elements composing the boundary of the body.

Furthermore, when modeling the response of a body buried in a half-space the earth-air interface can be accounted for by reflecting current-source images above the plane. The charges on the surface of the body should not have reflected images, as supported by the modeling results. The practical implications of this conclusion affect the computer implementation of the method; memory size and calculation time are reduced.

6.2 Limits of Boundary Element Method

The program can accept any arbitrarily shaped bodies, but it is necessary that these bodies be closed. Therefore, the method should not be used for modeling soundings above a layered half-space extending to infinity.

The method is suitable for conceptualizing a problem. If the electric field response of one or more three-dimensional bodies is desired, the boundary element method will provide a quick view of the response without requiring excessive model

design. If a complex geoelectric model is required to invert field data, finite-element and finite-difference methods may be more accurate. The trade-off lies in the tremendous amount of computation time required to perform three-dimensional finite-element and finite-difference calculations.

6.3 Interpretation of Field Data

A limiting factor in the application of the method to this field example is the use of one closed body in a layered half-space for the geologic model. The field data exhibit real earth signals that defy fitting a simple model. Generating a model with enough bodies to adequately fit the field data is a task suited to an automated inversion program, the complexity of which lies beyond the scope of this thesis.

The interpretation of the field data would be aided greatly if the signal polarity was recorded in addition to the electric field magnitude. The field acquisition system employs a square wave source and records several waveforms. The current processing method of picking the amplitude of the swing removes any polarity information. If there is a reversal in the signal, that information is lost. The use of an asymmetrical source would allow the determination of polarity in the waveform, as would having synchronized clocks in the transmitter and receiver apparatus. Using an asymmetrical source, one where the current is positive for a different duration than it is negative, would require slight modification of the transmitter hardware. On the other hand, using synchronized clocks would require more work modifying the equipment, but could automate the calculation of the voltage swing. Both options merit further investigation.

6.4 Future Work

An aspect of this research that requires further development is the use of the boundary element method in a computer inversion program. The modeling code could be used as a kernel, around which an inversion package could be built. Such a program could find an application in the automated inversion of DC resistivity field data.

As described previously, the field acquisition system in use at CSM needs to be altered in order to record signal polarity. This will provide the information needed to interpret the field data with the boundary element modeling method, and will also aid in the direct interpretation of field data.

REFERENCES

- Alfano, L., 1959, Introduction to the interpretation of resistivity measurements for complicated structural conditions, *Geophysical Prospecting*, vol 7, pp 311-366.
- Andersen, H.T., 1987, Analytic continuation in the interpretation of transient electromagnetic data: PhD Thesis T-3373, Colorado School of Mines.
- Barnett, C.T., 1972, Theoretical modeling of induced polarization effects due to arbitrarily shaped bodies: PhD Thesis, Colorado School of Mines.
- Barrows, L., and Fett, J., 1985, A high-precision gravity survey in the Delaware Basin of Southeastern New Mexico: *Geophysics*, vol 50, no 5, pp 825-833.
- Borns, D.J., and Stormont, J.C., 1988, An Interim Report on Excavation Effect Studies at the Waste Isolation Pilot Plant: The Delineation of the Disturbed Rock Zone, Sandia National Laboratory report SAND87-1375.
- Daniels, J., 1977, Three-dimensional resistivity and induced polarization modeling using buried electrodes, *Geophysics*, vol 42, no 5, pp 1006-1019.
- Dey, A. and Morrison, H.F. 1979, Resistivity modeling for arbitrarily shaped two dimensional structures, *Geophysical Prospecting*, vol 27, pp 106-136.
- Dieter, K., Paterson, N.R., and Grant, F.S., 1969, IP and resistivity type curves for three-dimensional bodies, *Geophysics*, vol 34, pp 614-632.
- Elliot, C.L., 1977, WIPP Site resistivity surveys, Elliot Geophysical Company report.
- Gonzales, M.M., 1989, Compilation and comparison of test-hole location surveys in the vicinity of the Waste Isolation Pilot Plant Site, Sandia National Laboratory report SAND88-1065.
- Keller, G.V. and Frischknecht, F.C. 1966, *Electrical Methods in Geophysical Prospecting*, Pergamon Press Inc., New York.
- Keller, G.V., Skokan, C.K., Andersen, H.T., Pfeifer, M.C., Keller, S.D., and Kim, K.D., 1987, Studies of electrical and electromagnetic methods for characterizing salt properties at the WIPP site, New Mexico: Unpublished Report, Colorado School of Mines.
- Kessels, W., Flentge, I., and Kolditz, H., 1985, DC geoelectric sounding to determine water content in the salt mine ASSE (FRG): *Geophysical Prospecting*: vol 33, no 3, pp 436-446.

- Kolman, B., 1984, *Introductory Linear Algebra with Applications*, Macmillan Publishing Company, New York.
- Matalucci, R.V., 1987, *In situ testing at the Waste Isolation Pilot Plant*, Sandia National Laboratory report SAND87-2382.
- Merkel, R.H., and Alexander, S.S., 1971, Resistivity analysis for models of a sphere in a half-space with buried current sources, *Geophysical Prospecting*, vol 19, pp 640-651.
- Okabe, M., 1981, Boundary element method for the arbitrary inhomogeneities problem in electrical prospecting, *Geophysical Prospecting*, vol 29, pp 39-59.
- Pfeifer, M.C., 1987, *Multicomponent underground DC resistivity study at the Waste Isolation Pilot Plant, Southeast New Mexico: MS thesis T-3372*, Colorado School of Mines.
- Pfeifer, M.C., Borns, D.J., Skokan, C.K., Andersen, H.T., Starett, J., 1989, Geophysical methods to monitor the development of the disturbed rock zone around underground excavation in bedded salt, *SAGEEP 89: Symposium on the Application of Geophysics to Engineering and Environmental Problems*, pp 400-411.
- Pfeifer, M.C., Andersen, H.T., and Skokan, C.K., 1990, Permanent DC- resistivity arrays to monitor the development of a disturbed rock one around underground excavations, *SAGEEP 90*, pp 243-254.
- Scriba, H. 1981 Computation of the electric potential in three-dimensional structures, *Geophysical Prospecting* 29, pp. 790-802.
- Seward, P.D., 1982, *Abridged borehole histories for the Waste Isolation Pilot Plant (WIPP) studies*, Sandia National Laboratory report SAND82-0080.
- Snyder, D.B., 1976, A method for modeling the resistivity and IP response of two-dimensional bodies, *Geophysics*, vol 41, pp 997-1015.
- Starret, J.M., 1989, *A feasibility study for using seismic tomography to monitor the integrity of salt pillars*, MS thesis T-3587: Colorado School of Mines.
- Van Nostrand, R.G. and Cook, K.L., 1966, *Interpretation of Resistivity Data*, USGS Prof.paper 449, Washington D.C., U.S. Government Printing Office.

APPENDIX A-1
DCMODEL.FOR FORTRAN CODE

program dcmode1

C-----
 C A FORTRAN PROGRAM TO APPROXIMATE THE ELECTRIC POTENTIAL ON THE
 C SURFACE DUE TO CHARGE INDUCED BY CURRENT FLOWING FROM THE SURFACE

C THROUGH ONE OR MORE RHOMBOHEDRAL BODIES AT DEPTH.

C

C EARLE M. WILLIAMS, 9/19/88 USING VAX FORTRAN

C last edit, 15 Feb, 1989

C

C 10 APR, 1990 INPUT ARBITRARY FACETED BODY

C

C 01 JUN, 1990 CORRECTED DERIVATIVE, CONVERGES QUICKLY

C

C 13 JUN, 1990 MULTIPLE CURRENT SOURCES AND IMAGES

C

C

C MODEL INPUT FROM FILE 'MODEL.DAT', GENERATED USING

C 'MAKE.FOR' OR 'SPH.FOR'

C THE MAKE PROGRAM GENERATES RECTANGULAR BODIES, WHILE

C THE SPH PROGRAM GENERATES SPHERICAL BODIES. BOTH

C PROGRAMS WRITE FACET DATA TO MODEL.DAT

C-----

C

C

C

C

C COORD(I,J,K,M) IS THE X,Y,Z COORDINATES FOR EVERY FACET

C I=X,Y, OR Z DIRECTION

C J=FACET NUMBER

C

C AB= I VECTOR FROM ORIGIN TO CURRENT SOURCE

C

C RHO0 = RESISTIVITY OF COUNTRY ROCK

C KRHO(J) = RESISTIVITY CONTRAST OF FACET J

C-----

C----- DEFINE VARIABLES AND COMMON BLOCKS -----

C-- DEFINE GLOBAL VARIABLES

INTEGER NUM

REAL COORD(3,2000),DA(2000),NRM(3,2000),KRHO(2000)

```

REAL AB(4,20),ETA,RHO0
REAL CHARGE(2000),CHOLD(2000),DUDN(2000)
INTEGER DIAG,ITER,INUM
COMMON/BODDAT/NUM,COORD,DA,AB,ETA,RHO0,KRHO,
& CHARGE,CHOLD,DUDN,DIAG,ITER,INUM,NRM

```

C--- DEFINE LOCAL VARIABLES

```

REAL FACET(3,4),CROSS(3),CROSS2(3),A(3),B(3),A2(3),B2(3)
REAL AREA,AREA2
CHARACTER*80 COMMENT,INFILE

```

C----- READ IN FACET COORDINATES AND REFLECTION COEFFICIENTS

```

OPEN(3,FILE='MODEL.DAT',STATUS='OLD',ERR=3)
GOTO 8
3 PRINT*, ' ERROR OPENING MODEL.DAT -- ABORTING!!!'
STOP
8 CONTINUE
K=0
10 CONTINUE
READ(3,1,END=15) COMMENT
READ(3,*,END=15) RHO,ICORNER
K=K+1
KRHO(K)=RHO
DO 11 J=1,ICORNER
  DO 9 II=1,3
9 FACET(II,J)=0.
  CONTINUE
  READ(3,*,END=15) (FACET(I,J),I=1,3)
11 CONTINUE
AREA=0.
AREA2=0.

```

C--- CALCULATE CROSS PRODUCT : YIELDS AREA AND NORM

```

DO 12 I=1,3
  A(I)=FACET(I,2)-FACET(I,1)
  B(I)=FACET(I,ICORNER)-FACET(I,1)
  IF(ICORNER.EQ.4) THEN
    A2(I)=FACET(I,4)-FACET(I,3)
    B2(I)=FACET(I,2)-FACET(I,3)
  ENDIF
12 CONTINUE
DO 13 I=1,3
  I2=MOD(I,3)+1
  I3=MOD(I2,3)+1
  CROSS(I)=A(I2)*B(I3)-A(I3)*B(I2)
  AREA=AREA+CROSS(I)*CROSS(I)

```

```

      COORD(I,K)=(FACET(I,1)+FACET(I,2)+FACET(I,3))/3.
      IF(ICORNER.EQ.4) THEN
        CROSS2(I)=A2(I2)*B2(I3)-A2(I3)*B2(I2)
        AREA2=AREA2+CROSS2(I)*CROSS2(I)
        COORD(I,K)=(FACET(I,1)+FACET(I,2)+FACET(I,3)+FACET(I,4))/4.
      ENDIF
13  CONTINUE
      AREA=SQRT(AREA)
      IF(ICORNER.EQ.4) AREA2=SQRT(AREA2)
      DO 14 I=1,3
        NRM(I,K)=CROSS(I)/AREA
14  CONTINUE
      DA(K)=AREA/2.
      IF(ICORNER.EQ.4) DA(K)=DA(K)+AREA2/2.
      AREAT=AREAT+DA(K)
      IF(K.GT.2000) THEN
        PRINT*, ' TOO MANY FACETS IN DATA FILE!! --- ABORTING!!'
        STOP
      ENDIF
      GOTO 10
15  CONTINUE
      CLOSE(3)
      NUM = K
      WRITE(*,3003) NUM
      WRITE(*,3004) AREAT
3003  FORMAT(3X,14,' FACETS READ FROM INPUT FILE')
3004  FORMAT(' TOTAL AREA = ',F8.2)

C----- INPUT USER SPECIFIED VARIABLES
20  PRINT*, ' INPUT FILENAME (TYPE "END" OR "^Z" TO QUIT)? : '
      READ(*,1,END=1100) INFILE
      IF(INFILE.EQ.'END'.OR.INFILE.EQ.'end') GOTO 1100
      OPEN(1,FILE=INFILE,STATUS='OLD',ERR=1000)
      READ(1,1) COMMENT
      READ(1,*) RHO0
      READ(1,1) COMMENT
      READ(1,*) DIAG
      READ(1,1) COMMENT
      READ(1,*) ITER,eta

1  FORMAT(A80)
2  FORMAT(A6)

      if(diag.gt.2) then
        do 16 ifc=1,NUM

```



```

      else
        R2=R2+(M(I)-COORD(I,L))**2
      endif
90    CONTINUE
      IF(R1.EQ.0.) GOTO 300
      R1=SQRT(R1)
      r2=SQRT(r2)
      UM=CHARGE(L)*(1./R1+1./r2)*DA(L)
      U=U+UM
300 CONTINUE
      U=U/4./PI
      RETURN
      END

```

```

C-----
C----- CALCULATE FIRST ORDER CHARGE DISTRIBUTION -----

```

SUBROUTINE FIRST

```

C--- DEFINE GLOBAL VARIABLES
      INTEGER NUM
      REAL COORD(3,2000),DA(2000),NRM(3,2000),KRHO(2000)
      REAL AB(4,20),ETA,RHO0
      REAL CHARGE(2000),CHOLD(2000),DUDN(2000)
      INTEGER DIAG,ITER,INUM
      COMMON/BODDAT/NUM,COORD,DA,AB,ETA,RHO0,KRHO,
      & CHARGE,CHOLD,DUDN,DIAG,ITER,INUM,NRM

C--- DEFINE LOCAL VARIABLES
      REAL RSQ,RSQI,B,BI,C,CI,DOT,DOTI

C-- CALCULATE THE VALUE OF PI
      PI=ACOS(-1.)

C--- DU/DN USES CONSTANTS RHO0 AND PI
      CONST=RHO0/PI/4.

C--- LOOP FOR EACH FACET
      DO 200 I=1,NUM
C--- CALCULATE DU/DN
C          DOT PRODUCT OF AB AND NORMAL
C          DU/DN =----- * CONST
C                   /  2      2      2 \ 3/2

```

```

C          \ X + Y + Z /
C
C
C--- USE CURRENT SOURCES AND CURRENT SOURCE IMAGES
  DO 25 ICUR=1,INUM
    DOT=0.
    DOTI=0.
    RSQ=0.
    RSQI=0.
    DO 20 ISUM=1,3
      B=AB(ISUM,ICUR)-COORD(ISUM,I)
      IF(ISUM.EQ.3) THEN
        BI=-AB(ISUM,ICUR)-COORD(ISUM,I)
      ELSE
        BI=B
      ENDIF
      C=B*NRM(ISUM,I)
      CI=BI*NRM(ISUM,I)
      RSQ=RSQ+B*B
      RSQI=RSQI+BI*BI
      DOT=DOT+C
      DOTI=DOTI+CI
20    CONTINUE
      RSQ=(SQRT(RSQ)**3)
      RSQI=(SQRT(RSQI)**3)
      DUDN(I)=DUDN(I)+CONST*(DOT/RSQ+DOTI/RSQI)*AB(4,ICUR)
25    CONTINUE
      CHARGE(I)=DUDN(I)*KRHO(I)*2.
      CHOLD(I)=CHARGE(I)
200  CONTINUE
      RETURN
      END

```

```

C-----
C-----NORMAL POTENTIAL CALCULATION -----
      SUBROUTINE NORMAL(M,K,U)

```

```

C--- DEFINE GLOBAL VARIABLES
      INTEGER NUM
      REAL COORD(3,2000),DA(2000),NRM(3,2000),KRHO(2000)
      REAL AB(4,20),ETA,RHO0
      REAL CHARGE(2000),CHOLD(2000),DUDN(2000)
      INTEGER DIAG,ITER,INUM

```

```
COMMON/BODDAT/NUM,COORD,DA,AB,ETA,RHO0,KRHO,
& CHARGE,CHOLD,DUDN,DIAG,ITER,INUM,NRM
```

```
C--- DEFINE LOCAL VARIABLES
```

```
REAL M(3),U,AM,AMI,PI
INTEGER K
```

```
PI=ACOS(-1.)
```

```
C--- CALCULATE NORMAL POTENTIAL DUE TO CURRENT SOURCES
```

```
am=0.
```

```
AMI=0.
```

```
do 300 ix=1,3
```

```
am=am+(AB(ix,K)-m(ix))**2
```

```
IF(IX.EQ.3) THEN
```

```
AMI=AMI+(-AB(IX,K)-M(IX))**2
```

```
ELSE
```

```
AMI=AMI+(AB(IX,K)-M(IX))**2
```

```
ENDIF
```

```
300 continue
```

```
am=SQRT(am)
```

```
AMI=SQRT(AMI)
```

```
U=RHO0/pi/4.*AB(4,K)*(1./AM+1./AMI)
```

```
RETURN
```

```
END
```

```
C-----
```

```
C----- SECOND ORDER APPX. -----
```

```
SUBROUTINE SECOND
```

```
C--- DEFINE GLOBAL VARIABLES
```

```
INTEGER NUM
```

```
REAL COORD(3,2000),DA(2000),NRM(3,2000),KRHO(2000)
```

```
REAL AB(4,20),ETA,RHO0
```

```
REAL CHARGE(2000),CHOLD(2000),DUDN(2000)
```

```
INTEGER DIAG,ITER,INUM
```

```
COMMON/BODDAT/NUM,COORD,DA,AB,ETA,RHO0,KRHO,
& CHARGE,CHOLD,DUDN,DIAG,ITER,INUM,NRM
```

```
C--- DEFINE LOCAL VARIABLES
```

```
REAL PI,B,DOT,RSQ,DERIV,QI
```

```
PI=ACOS(-1.)
```

```
C--- LOOP FOR EACH FACET
```

```
DO 300 I=1,NUM
```

```
C----- FOR EACH ELEMENT, SUM THE EFFECTS OF CHARGES ON ALL OTHER ELEMENTS
```

```

      QI=0.
      DO 150 J=1,NUM
        IF(J.EQ.I) GOTO 150
C--- AND CALCULATE SCALAR SUM OF DISTANCE COMPONENTS TO FIT INTO
C--- THE FORMULA:
C   DV/DN = -DOTPROD(V,N)/(X**2 + Y**2 + Z**2)**3/2
C
C--- WHERE V IS THE VECTOR FROM Qi TO Qj
C
      DOT=0.
      DO 101 IS=1,3
        B=COORD(IS,J)-COORD(IS,I)
        DOT=DOT+NRM(IS,I)*B
        RSQ=RSQ+B*B
101    CONTINUE
      RSQ=(SQRT(RSQ)**3)
C--- CALCULATE DERIV OF DISTANCE
      IF (RSQ.GT.0.) THEN
        DERIV=DOT/RSQ
        QI=QI+CHOLD(J)*DA(J)*DERIV
      ELSE
        WRITE(10,*) ' SECOND DISTANCE OF ZERO ',I,J
        WRITE(10,*) (COORD(II,J),II=1,3)
      ENDIF
      RSQ=0.
150    CONTINUE
      CHARGE(I)=(DUDN(I)+QI/4./PI)*KRHO(I)*2.
      CHOLD(I)=CHARGE(I)
300    CONTINUE
      RETURN
      END

```

```

C-----
C----- IMAGE THE BODY AND NOTE INTERACTIVE EFFECTS -----
      SUBROUTINE IMAGE

```

```

C--- DEFINE GLOBAL VARIABLES
      INTEGER NUM
      REAL COORD(3,2000),DA(2000),NRM(3,2000),KRHO(2000)
      REAL AB(4,20),ETA,RHO0
      REAL CHARGE(2000),CHOLD(2000),DUDN(2000)
      INTEGER DIAG,ITER,INUM
      COMMON/BODDAT/NUM,COORD,DA,AB,ETA,RHO0,KRHO,
& CHARGE,CHOLD,DUDN,DIAG,ITER,INUM,NRM

```

```
C--- DEFINE LOCAL VARIABLES
      REAL PI,B,DOT,RSQ,DERIV
```

```
      PI=ACOS(-1.)
```

```
C--- LOOP FOR EACH FACET
      DO 300 I=1,NUM
```

```
C----- FOR EACH ELEMENT, SUM THE EFFECTS OF CHARGES ON ALL OTHER ELEMENTS
```

```
      QI=0.
```

```
      DO 150 J=1,NUM
```

```
        IF(J.EQ.I) GOTO 150
```

```
C--- AND CALCULATE SCALAR SUM OF DISTANCE COMPONENTS TO FIT INTO
C--- THE FORMULA:
```

```
C   DV/DN = -DOTPROD(V,N)/(X**2 + Y**2 + Z**2)**3/2
```

```
C
```

```
C--- WHERE V IS THE VECTOR FROM Qi TO Qj
```

```
C
```

```
      DOT=0.
```

```
      RSQ=0.
```

```
      DO 101 IS=1,3
```

```
        B=COORD(IS,J)-COORD(IS,I)
```

```
        IF(IS.EQ.3) B=-COORD(IS,J)-COORD(IS,I)
```

```
        DOT=DOT+NRM(IS,I)*B
```

```
        RSQ=RSQ+B*B
```

```
101    CONTINUE
```

```
C--- CALCULATE DERIV OF DISTANCE
```

```
      IF (RSQ.NE.0.) THEN
```

```
        RSQ=SQRT(RSQ)**3
```

```
        DERIV=DOT/RSQ
```

```
        QI=QI-CHOLD(J)*DA(J)*DERIV
```

```
      ELSE
```

```
        WRITE(10,*) ' SECOND DISTANCE OF ZERO ',I,J
```

```
        WRITE(10,*) (COORD(II,J),II=1,3)
```

```
      ENDIF
```

```
150    CONTINUE
```

```
      CHARGE(I)=(DUDN(I)+QI/4./PI)*KRHO(I)*2.
```

```
      CHOLD(I)=CHARGE(I)
```

```
300    CONTINUE
```

```
      RETURN
```

```
      END
```

```
C----- BIPOLE-DIPOLE SURVEY -----
      SUBROUTINE TEST
```

C--- DEFINE GLOBAL VARIABLES

```

INTEGER NUM
REAL COORD(3,2000),DA(2000),NRM(3,2000),KRHO(2000)
REAL AB(4,20),ETA,RHO0
REAL CHARGE(2000),CHOLD(2000),DUDN(2000)
INTEGER DIAG,ITER,INUM
COMMON/BODDAT/NUM,COORD,DA,AB,ETA,RHO0,KRHO,
& CHARGE,CHOLD,DUDN,DIAG,ITER,INUM,NRM

```

C--- DEFINE LOCAL VARIABLES

```

character*20 appout,potout
REAL M1M2(3,2),DEL(3),DELTA,D,C,DIPOLE,INORTH,CURAMP
REAL MX(3),MY(3),MZ(3)
CHARACTER*80 COMMENT
REAL M(3),U1,UN,UD,UX,UY,UZ,AMX,AMY,AMZ
REAL UMX,UMY,UMZ,UDX,UDY,UDZ,AM,RHOX,RHOY,RHOZ

```

1 format(A80)

C--- READ IN VARIABLES NEEDED FOR POLE-POLE MODEL (same as for dipole-dipole)

```

      READ(1,1) COMMENT
      READ(1,*) INUM
      READ(1,1) COMMENT
      DO 2 J=1,INUM
      READ(1,*) (AB(I,J),I=1,4)
2     CONTINUE
      READ(1,1) COMMENT
      READ(1,*) (M1M2(I,1),I=1,3)
      READ(1,1) COMMENT
      READ(1,*) (M1M2(I,2),I=1,3)
      READ(1,1) COMMENT
      READ(1,*) DIPOLE
      READ(1,1) COMMENT
      READ(1,*) INORTH
      READ(1,1) COMMENT
      READ(1,*) CURAMP
      READ(1,1) COMMENT
      READ(1,*) ISTATION
      read(1,1) appout
      read(1,1) potout
      open(2,file='NORMAL.DAT',status='UNKNOWN')
      open(3,file='DISTURB.DAT',status='UNKNOWN')
      open(20,file=potout,status='UNKNOWN')
      open(21,file=appout,status='UNKNOWN')

```

```

PI=ACOS(-1.)
DO 40 J=1,3
  DEL(J)=(M1M2(J,2)-M1M2(J,1))/FLOAT(ISTATION)
40 CONTINUE

```

```

CALL FIRST

```

C--- CALCULATE SECOND ORDER CHARGE DISTRIBUTION BY ADDING INTERACTIVE
C--- TERMS TO FIRST ORDER APPROXIMATION

```

do 10 jb=1,num
  ch=charge(jb)*da(JB)
  if(ch.gt.0.) then
    chpls=chpls+ch
  else
    chneg=chneg+ch
  endif
10 CONTINUE
C=CHPLS+CHNEG
WRITE(*,1000) chpls,c
CHPLS=0.
CHNEG=0.
5 CONTINUE
  if(iter2.gt.ITER) then
    print*, ' Number of iterations exceeds user defined maximum.'
    print*, ' ... Ceasing iterations and continuing execution!'
    print*, ' '
    goto 6
  endif
CALL SECOND
C CALL IMAGE
do 24 jb=1,num
  ch=charge(jb)*da(JB)
  if(ch.gt.0.) then
    chpls=chpls+ch
  else
    chneg=chneg+ch
  endif
24 continue
D=CHPLS+CHNEG
chpls=0.
chneg=0.
ITER2=ITER2+1
IF(ABS(C).EQ.0.) GOTO 6
DELTA=(D-C)/ABS(C)

```

```

    PERCENT=DELTA*100.
    WRITE(*,25) ITER2,PERCENT,d
25  FORMAT(' Iteration',I3,'; ',F9.2,'% change in net charge ',e11.3)
C--- QUIT IF NONCONVERGING, END ITERATIONS IF CHANGE SMALL
    if(iter2.gt.30) then
        print*,' Nonconverging charge ditribution!! -- Aborting...'
        stop
    endif
    if (ABS(DELTA).lt.eta) goto 6
    C=D
    goto 5
6   CONTINUE

    if(diag.gt.2) then
        id=id+1
        do 16 ifc=1,NUM
            if (coord(3,ifc).gt.0.) then
                write(18,*) (coord(ij,ifc),ij=1,2),charge(ifc)
            endif
16   continue
        endif

    print*,' Calling Potential'

C---- Calculate potential by summing up over charge elements
    DO 150 ILOOP=0,ISTATION
        DO 90 ICOUNT = 1,3
            M(ICOUNT) = M1M2(ICOUNT,1)+(ILOOP*DEL(ICOUNT))
90   continue
        DO 92 II=1,3
            MX(II)=M(II)
            MY(II)=M(II)
            MZ(II)=M(II)
92   CONTINUE

C----- ASSIGN COORDINATES FOR DIPOLE ELECTRODES
    MX(1)=MX(1)+INORTH*DIPOLE
    MY(2)=MY(2)+INORTH*DIPOLE
    MZ(3)=MZ(3)-DIPOLE

C----- CALCULATE NORMAL POTENTIAL DUE TO CURRENT SOURCE
C----- USE CURRENT SOURCES AND IMAGES WITH EQUATIONS FOR WHOLE SPACE

```

```

DO 99 II=1,INUM
  CALL NORMAL(M,II,UM)
  CALL NORMAL(MX,II,UMX)
  CALL NORMAL(MY,II,UMY)
  CALL NORMAL(MZ,II,UMZ)
  UX0=UX0+UMX-UM
  UY0=UY0+UMY-UM
  UZ0=UZ0+UMZ-UM
  UM=0.
  UMX=0.
  UMY=0.
  UMZ=0.
DO 95 IS=1,3
  AM=AM+(M(IS)-AB(IS,II))**2
  AMX=AMX+(MX(IS)-AB(IS,II))**2
  AMY=AMY+(MY(IS)-AB(IS,II))**2
  AMZ=AMZ+(MZ(IS)-AB(IS,II))**2
C----- ASSIGN COORDINATES FOR IMAGE SOURCES
  IF(IS.NE.3) THEN
    AMIM=AMIM+(M(IS)-AB(IS,II))**2
    AMXIM=AMXIM+(MX(IS)-AB(IS,II))**2
    AMYIM=AMYIM+(MY(IS)-AB(IS,II))**2
    AMZIM=AMZIM+(MZ(IS)-AB(IS,II))**2
  ELSE
    AMIM=AMIM+(M(IS)+AB(IS,II))**2
    AMXIM=AMXIM+(MX(IS)+AB(IS,II))**2
    AMYIM=AMYIM+(MY(IS)+AB(IS,II))**2
    AMZIM=AMZIM+(MZ(IS)+AB(IS,II))**2
  ENDIF
95 CONTINUE
  AM=SQRT(AM)
  AMX=SQRT(AMX)
  AMY=SQRT(AMY)
  AMZ=SQRT(AMZ)
  AMIM=SQRT(AMIM)
  AMXIM=SQRT(AMXIM)
  AMYIM=SQRT(AMYIM)
  AMZIM=SQRT(AMZIM)
  ALPHAX=ALPHAX+AB(4,II)/AMX-AB(4,II)/AM
  ALPHAY=ALPHAY+AB(4,II)/AMY-AB(4,II)/AM
  ALPHAZ=ALPHAZ+AB(4,II)/AMZ-AB(4,II)/AM
  ALXIM=ALXIM+AB(4,II)/AMXIM-AB(4,II)/AMIM
  ALYIM=ALYIM+AB(4,II)/AMYIM-AB(4,II)/AMIM
  ALZIM=ALZIM+AB(4,II)/AMZIM-AB(4,II)/AMIM
  AM=0.

```

```
    AMX=0.
    AMY=0.
    AMZ=0.
      AMIM=0.
      AMXIM=0.
      AMYIM=0.
      AMZIM=0.
99  CONTINUE

C----- CALCULATE DISTURBING POTENTIAL
      CALL DISTURB(M,U1)
      CALL DISTURB(MX,UDX)
      CALL DISTURB(MY,UDY)
      CALL DISTURB(MZ,UDZ)
      UXD=UDX-U1
      UYD=UDY-U1
      UZD=UDZ-U1

C----- CALCULATE TOTAL POTENTIAL AND APPARENT RESISTIVITY
      UX=(UX0+UXD)
      UY=(UY0+UYD)
      UZ=(UZ0+UZD)
      WRITE(2,1003) (M(I),I=1,3),UX0*CURAMP,UY0*CURAMP,UZ0*CURAMP
      WRITE(3,1003) (M(I),I=1,3),UXD*CURAMP,UYD*CURAMP,UZD*CURAMP
      WRITE(20,1003) (M(I),I=1,3),UX*CURAMP,UY*CURAMP,UZ*CURAMP
      RHOX=UX*PI*(1./ALPHAX+1./ALXIM)
      RHOY=UY*PI*(1./ALPHAY+1./ALYIM)
      RHOZ=UZ*PI*(1./ALPHAZ+1./ALZIM)
      WRITE(21,1002) (M(I),I=1,3),RHOX,RHOY,RHOZ

C---- ZERO OUT VARIABLES
      ALPHAX=0.
      ALPHAY=0.
      ALPHAZ=0.
      ALXIM=0.
      ALYIM=0.
      ALZIM=0.
      U1=0.
      UDX=0.
      UDY=0.
      UDZ=0.
      UX=0.
      UY=0.
      UZ=0.
      UX0=0.
```

```
      UY0=0.  
      UZ0=0.  
150  CONTINUE  
      RETURN  
  
1000  FORMAT(' Total positive charge: ',e9.3,'; net charge: ',  
      & e9.3)  
1002  format(2x,f8.2,2(' ',f10.2),3(' ',f12.6))  
1003  format(2x,f8.2,2(' ',f10.2),3(' ',e12.4))  
      END
```

APPENDIX A-2
SPHLENS.FOR PROGRAM CODE

program splens

```

C-----
C
C   a program to generate a data file containing model information
C   for a sphere
C   to be used in the MODEL dc resistivity modeling program
C
C   With a modification to make lens shaped bodies 8/28/90
C-----
C
C
C
REAL TRANSLAT(3),radius,scale(3)
REAL KRHO
real facet(3,4,2000)
integer lats,longs, diag,icorner(2000)
CHARACTER*80 COMMENT,INFILE

C----- INPUT USER SPECIFIED VARIABLES
10 PRINT*, ' INPUT FILENAME (TYPE "END" OR "^Z" TO QUIT)? : '
   READ(*,1,END=1100) INFILE
   IF(INFILE.EQ.'END'.OR.INFILE.EQ.'end') GOTO 1100
   OPEN(1,FILE=INFILE,STATUS='OLD',ERR=1000)
   READ(1,1) COMMENT
   READ(1,*) radius, lats, longs
   READ(1,1) COMMENT
   READ(1,*) (scale(i),i=1,3)
   READ(1,1) COMMENT
   READ(1,*) (TRANSLAT(I),I=1,3)
   READ(1,1) COMMENT
   READ(1,*) kRHO
   READ(1,1) COMMENT
   read(1,*) diag

1 FORMAT(A80)

OPEN(15,FILE='MODEL.DAT',STATUS='UNKNOWN')
OPEN(16,FILE='POLAR.DAT',STATUS='UNKNOWN')
OPEN(13,FILE='facets.dxf',STATUS='UNKNOWN')

pi=acos(-1.)
dphi=2.*pi/(float(longs))

```

```
dtheta=pi/(float(lats))
```

```
c---- assign coordinates of facets first in polar coordinates
```

```
do 200 ith=1,lats
  theta2=theta2+dtheta
  ic=4
  if (ith.eq.1.or.ith.eq.lats) ic=3
  phi2=0.
  phi1=0.
  do 100 iph=1,longs
    phi2=phi2+dphi
    ielem=ielem+1
    icorner(ielem)=ic
    if(ith.eq.1) then
      i3=i3+1
      facet(2,1,ielem)=theta2
      facet(2,2,ielem)=theta2
      facet(2,3,ielem)=0.
      facet(3,1,ielem)=phi1
      facet(3,2,ielem)=phi2
      facet(3,3,ielem)=0.
    elseif(ith.eq.lats) then
      i3=i3+1
      facet(2,1,ielem)=pi
      facet(2,2,ielem)=theta1
      facet(2,3,ielem)=theta1
      facet(3,1,ielem)=0.
      facet(3,2,ielem)=phi1
      facet(3,3,ielem)=phi2
    else
      facet(2,1,ielem)=theta2
      facet(2,2,ielem)=theta2
      facet(2,3,ielem)=theta1
      facet(2,4,ielem)=theta1
      facet(3,1,ielem)=phi1
      facet(3,2,ielem)=phi2
      facet(3,3,ielem)=phi2
      facet(3,4,ielem)=phi1
    endif
  enddo
  PHI1=PHI2
100 continue
  THETA1=THETA2
200 continue
print*, ' Number of elements : ',ielem
print*, ' Number of three-point elements: ',i3
```

C----- WRITE POLAR FACETS TO A DATA FILE

```

WRITE(16,'(2X)')
DO 220 k=1,ielem
  WRITE(16,2004) KRHO,icorner(k)
  do 210 j=1,icorner(k)
    FACET(1,J,K)=RADIUS
    write(16,2000) (facet(i,j,k),I=1,3)
210   continue
  WRITE(16,2002)
220  CONTINUE

```

C--- convert polar to cartesian coordinates

```

do 250 k=1,ielem
  do 240 j=1,icorner(k)
    a=radius*sin(facet(2,j,k))
    x=a*cos(facet(3,j,k))
    y=a*sin(facet(3,j,k))
    z=radius*cos(facet(2,j,k))
    facet(1,j,k)=x
    facet(2,j,k)=y
    facet(3,j,k)=z
240   continue
250   continue

```

c---- SCALE COORDINATES BY EACH AXIS DIRECTION: SCALE(I)

```

DO 310 K=1,IELEM
  DO 305 J=1,ICORNER(K)
    DO 300 I=1,3
      FACET(I,J,K)=FACET(I,J,K)*SCALE(I)
300   CONTINUE
305   CONTINUE
310  CONTINUE

```

c--- TRANSLATE FACETS TO FINAL POSITION

```

DO 350 K=1,ielem
  DO 330 J=1,icorner(k)
    DO 320 I=1,3
      FACET(I,J,K)=FACET(I,J,K)+TRANSLAT(i)
320   CONTINUE
330   CONTINUE
350  CONTINUE

```

C----- WRITE FACETS TO A DXF FILE

```

do 600 k=1,ielem
  write(13,21)
  do 500 j=1,4
    jj=j
    if(j.eq.4) then
      if(icorner(k).eq.3) jj = 1
    endif
    do 400 i=1,3
      inum=i*10 + j-1
      write(13,20) inum,facet(i,jj,k)
400    continue
500    continue
  write(13,22)
600  CONTINUE

```

C----- WRITE XYZ FACETS TO A DATA FILE

```

WRITE(15,'(2X)')
DO 900 k=1,ielem
  WRITE(15,2004) KRHO,icorner(k)
  do 800 j=1,icorner(k)
    write(15,2000) (facet(i,j,k),I=1,3)
800    continue
  WRITE(15,2002)
900  CONTINUE

```

```

GOTO 10
1000 PRINT*,' ERROR OPENING INPUT FILE -- PROGRAM ABORTING '
GOTO 1200
1100 PRINT*,' NORMAL END OF PROGRAM '
1200 STOP

```

```

20  format(1x,i4,/,f8.3)
21  format(' 3DFACE'/' 8'/' 0')
22  format(' 0')
2000 FORMAT(F12.4,',',F12.4,',',F12.4)
2002 FORMAT(1X)
2004 FORMAT(F12.4,2x,i2)

```

END

APPENDIX A-3

VSWING.C PROGRAM CODE

```
/*      VSWING.C data retrieval and voltage swing calculation program
      companion for VGET.C
*/

#include <stdio.h>
#include <stdlib.h>
#include <math.h>
#include <string.h>
#include <time.h>
#include <ctype.h>
#include <graph.h>
#include <cxlwin.h>
#include <cxlkey.h>
#include <cxlvid.h>
#include <cxlstr.h>

static int *savescrn,crow,ccol;
float vdat[1024][4]; /* real value component data */
int idat[4096]; /* integer component data array */
float a;
char *ans[] = {"No","Yes",NULL};
char header[80];
int igain;
int ascii;
float freq; /* sampling frequency, Hz */
float gain; /* total system gain */
float ext_gain = 1;
float cal[4] = {0.95, 1.45, 1.0, 1.};
float max = 5; /* maximum voltage on A/D board */
float min = -5; /* minimum voltage on A/D board */
int num; /* number of samples */
float swing[4]; /* components of voltage swing */
int channels; /* number of acquisition channels */
int file_open = 0;

static void add_shadow(void);
void ask_quit(void);
void del_files(void);
void directory();
void dos_shell(void);
int get_line(int line_pos, char far *image, int old);
void go(void);
void init_program();
void main_menu(void);
```

```

void normal_end(void);
void period();
static void pre_menu1(void);
void putpixel(int ia, int ib, int ic, int id);
void save_files(void);
void select_bin();
void select_asc();
void v_swing(int first, int wavelength);
void win_message(char string[80], int time);

main()
{
    init_program();
    main_menu();
}

void win_message(char string[80], int time)
{
    if(!wopen(9,24,13,57,0,LCYAN|_BROWN,WHITE|_BLACK)) exit(0);
    add_shadow();
    wputs(string);
    waitkeyt(time);
    wclose();
}

void period()
{
    ;
}

void main_menu(void)
{
    hidecur();
    wsetesc(0);
    wopen(0,0,22,75,3,WHITE|_RED,WHITE|_BLACK);
    wtitle("[ VSWING Main Menu ]",TCENTER,WHITE|_BLACK);
    wmessage("[ F6:Go F9:DOS F10:Quit ]",1,25,WHITE|_BLACK);
    whline(1,1,76,0,WHITE);

    /* define and process the main menu */
    wmenubeg(1,1,1,75,5,WHITE|_BLACK,WHITE|_BLACK,NULL);
    wmenuitem(0,2,"Go [F6] ", 'G',1,0,go,0x4000,0);
    wmenuitem(0,18,"Period" , 'P',2,0,period,0,0);
}

```

```

wmenuitem(0,34,"Files  ", 'F',3,M_HASPD,NULL,0,0);
wmenubeg(2,33,8,49,0,WHITE|_BLACK,WHITE|_BLACK,NULL);
wmenuitem(0,0,"Save   ", 'S',30,0,save_files,0,0);
wmenuitem(1,0,"get Bin  ", 'B',31,0,select_bin,0,0);
wmenuitem(2,0,"get Ascii ", 'A',32,0,select_asc,0,0);
wmenuitem(3,0,"Directory ", 'D',33,0,directory,0,0);
wmenuitem(4,0,"dOs [F9]", 'O',34,0,dos_shell,0x4300,0);
wmenuend(30,M_PD|M_SAVE,16,1,WHITE|_BLACK,WHITE|_BLACK,0,BLACK|_LGREY);
wmenuitem(0,50,"Quit [F10]", 'Q',4,0,ask_quit,0x4400,0);
wmenuend(1,M_HORZ,16,1,WHITE|_BLACK,WHITE|_BLACK,0,BLACK|_LGREY);
wmenuget();
}

```

```

static void add_shadow(void)
{
    wshadow(LGREY|_BLACK);
}

```

```

void putpixel(int ix, int iy, int ic, int id)
{
    long x,y,lx,ly,lc;
    float fd;

    fd = id;
    lx = ix;
    ly = iy;
    lc = ic;
    x = (lx * 640) / fd;
    y = (200 * ly / 3) + (200 * lc / 12288);
    _setpixel(x,y);
}

```

```

void normal_end()
{
    wcloseall();
    showcur();
    exit(0);
}

```

```

static void pre_menu1(void)
{
    hidecur();
    add_shadow();
}

```

```

}
```

```

void ask_quit(void)
```

```

{
    char ch;

    if(!wopen(9,26,13,56,0,LCYAN|_BROWN,WHITE|_BLACK)) exit(0);
    add_shadow();
    wputs("\n Quit VGET3, are you sure? N\b");
    clearkeys();
    showcur();
    ch=wgetchf("YyNn",'N');
    hidecur();
    if(toupper(ch)=='Y') normal_end();
    else wclose();
}

```

```

void directory()
```

```

{

wpickfile(10,10,20,65,0,LCYAN|_RED,WHITE|_BLACK,BLACK|_LGREY,1,"*.*",add_shadow);
}

```

```

void select_bin()
```

```

{
    int i,j;
    FILE *binfile;
    char *file_name, str[81], header[81];

```

```

    wsetesc(1);

```

```

if((file_name=wpickfile(10,10,20,65,0,LCYAN|_RED,WHITE|_BLACK,BLACK|_LGREY,1,"*.*",add_shadow)) == NULL)

```

```

{
    printf(str,"\n Error opening file %s",file_name);
    win_message(str,50);
    if(!wopen(10,10,14,70,0,LCYAN|_BROWN,WHITE|_BLACK)) exit(0);
    wprintf("\n Enter name of binary file : ");
    wgets(file_name);
    wclose();
}

```

```

wsetesc(0);

```

```

if ((binfile = fopen(file_name, "rb")) != NULL)
{
if(!wopen(10,10,18,70,0,LCYAN|_BROWN,WHITE|_BLACK)) exit(0);
wprintf("\n Reading from file %s ",file_name);
fgets(header,80,binfile);
wprintf("\n %s",header);
waitkeyt(200);
fgets(str,80,binfile);
wprintf("%s",str);
waitkeyt(200);
wclear();
sscanf(str, "%f %d %d %f %f %d %f", &freq, &num, &channels, &max, &min, &igain, &gain);
wprintf(" %.1f %d %d %.1f %.1f %d %.1f", freq, num, channels, max, min, igain, gain);
waitkeyt(100);
fread(idat, sizeof(int), 4096, binfile);
fclose(binfile);
wclear();
wprintf("\n idat[12] = %d", idat[12]);
waitkeyt(40);
wclose();
file_open = 1;
ascii = 0;
}
}

```

```

void select_asc()

```

```

{
int i,j;
FILE *ascfile;
char *file_name, str[60], datastr[81], format[30];

for(i = 0; i < (num * 3); i++)
{
idat[i] = 0;
}
wsetesc(1);

```

```

if((file_name=wpickfile(10,10,20,65,0,WHITE|_BLACK,WHITE|_BLACK,BLACK|_LGREY,1,"*. *
",add_shadow)) == NULL)
{
printf(str, "/n Error opening file %s", file_name);
win_message(str, 50);
if(!wopen(10,10,14,70,0,LCYAN|_BROWN,WHITE|_BLACK)) exit(0);
wprintf("\n Enter name of ascii file : ");

```

```

    wgets(file_name);
    wclose();
}
wsetesc(0);
if ((ascfile = fopen(file_name,"r")) != NULL)
{
    if(!wopen(10,10,15,70,0,LCYAN|_BROWN,WHITE|_BLACK)) exit(0);
    wprintf(" Reading from file %s\n",file_name);
    fgets(header,78,ascfile);
    wprintf(" %s",header);
    i = j = 0;
    fgets(datastr,80,ascfile);
    channels = sscanf(datastr," %f %f %f %f %f %f %f %f\n",&vdat[0][0],
        &vdat[0][1],&vdat[0][2],&vdat[0][3]);
    wprintf("\n Number of columns = %d\n Number of rows   =",channels);
    while(!feof(ascfile))
    {
        i++;
        wgotoxy(3,21);
        wprintf(" %d ",i);
        fgets(datastr,80,ascfile);
        sscanf(datastr," %f %f %f %f\n",&vdat[i][0],
            &vdat[i][1],&vdat[i][2],&vdat[i][3]);
    }
    num = i;
    fclose(ascfile);
    wclose();
    file_open = 1;
}
else
{
    win_message("Error opening ASCII file",50);
}
ascii = 1;
}

```

```

void go()
{
    int free, i, j, k, l, status, value = 0;
    float scale, temp;
    char str[40];
    char far *image1, *image2;
    unsigned short line_style;
    FILE *idatfile;
}

```

```

int x_position, y_position, first_step, second_step, wave, pos;
int vhigh, vlow;
float vmean[4];
float vmax[4] = {0.,0.,0.,0.}, vmin[4] = {0.,0.,0.,0.}, vscale = 0.;

if(file_open)
{
    scale = (max - min)/4096;
    if (!ascii)
    {
        for(i = 0; i < num; i++)
        {
            for(j = 0; j < channels; j++)
                vdat[i][j] = ((idat[channels*i+j] * scale) + min) / (gain);
        }
    }
    else
    {
        for(j = 0; j < channels; j++)
        {
            vmax[j] = vdat[0][j];
            vmin[j] = vdat[0][j];
        }
        for(i = 1; i < num; i++)
        {
            for(j = 0; j < channels; j++)
            {
                if(vdat[i][j] > vmax[j]) vmax[j] = vdat[i][j];
                if(vdat[i][j] < vmin[j]) vmin[j] = vdat[i][j];
            }
        }
        vhigh = vlow = 0;
        for(j = 0; j < channels; j++)
            vmean[j] = vmin[j] + (vmax[j] - vmin[j])/2;
        for(j = 1; j < channels; j++)
            if((vmax[j]-vmin[j]) > (vmax[j-1]-vmin[j-1])) vhigh = j;
        vscale = (vmax[vhigh] - vmin[vhigh]) * 1.2;
        if(!wopen(10,10,16,70,0,LCYAN|_BROWN,WHITE|_BLACK)) exit(0);
        for(j = 0; j < channels; j++)
            wprintf(" %f %f %f\n",vmin[j],vmean[j],vmax[j]);
        wprintf(" %f\n",vscale);
        waitkey(200);
        wclose();
        for(i = 0; i < num; i++)
        {

```

```

    for(j = 0; j < channels; j++)
    {
        temp = (vdat[i][j]-vmean[j]) / vscale;
        idat[i*channels+j] = (temp * 4096) + 2048;
    }
}
clearkeys();
readcur(&crow,&ccol);
savescrn = ssave();
if((status = _setvideomode(_HRESBW)) != 0)
{
    _setcolor(15);
    line_style = _getlinestyle();
    _setlinestyle(0xFF00);
    _moveto(0,0);
    _lineto(0,199);
    _getimage(0,0,0,199,image1);
    _getimage(0,0,0,199,image2);
    _setlinestyle(line_style);
    _moveto(0,0);
    _lineto(639,0);
    _lineto(639,199);
    _lineto(0,199);
    _lineto(0,0);
    for(j=1; j < channels; j++)
    {
        _moveto(0,j*199/channels);
        _lineto(639,j*199/channels);
    }
    for(i = 0; i < num && kbhit() == 0; i++)
    {
        for(j = 0; j < channels; j++)
        {
            putpixel(i, j, idat[channels*i+j], num);
        }
    }
    _setttextposition(25,30);
    _outtext("Select first step");
    _putimage(0, 0, image1, _GXOR);
    pos = 0;
    x_position = get_line(pos, image1, 0);
    first_step = x_position;
    _setttextposition(25,30);
    _outtext("Select second step");
}

```

```

    pos = x_position;
    x_position = get_line(pos, image2, 1);
    second_step = x_position;
    if(kbhit() == 0) waitkey();
}
clearkeys();
_setvideomode(_DEFAULTMODE);
srestore(savescrn);
gotoxy_(crow,ccol);
hidecur();
temp = num;
temp /= 640.0;
wave = (second_step - first_step) * temp;
first_step *= temp;
if(!wopen(10,10,16,70,0,LCYAN|_BROWN,WHITE|_BLACK)) exit(0);
wprintf(" First = %d, wave = %d",first_step,wave);
waitkeyt(100);
v_swing(first_step,wave);
wprintf(" Swing components : \n ");
for(j = 0; j < channels; j++) wprintf(" %f",swing[j]);
waitkeyt(200);
wclose();
}
else
    win_message("\n A file must be selected first!",50);
}

```

```

int get_line(int line_pos, char far *image, int old)
{
    unsigned int key;
    int numhits, original;
    char string[20];

    original = line_pos;
    numhits = 0;
    do
    {
        key = getxch();
        if(key == 0x4B00 && line_pos > 0) /* left arrow */
        {
            _putimage(line_pos,0,image,_GXOR);
            line_pos--;
            _putimage(line_pos,0,image,_GXOR);
            if((line_pos + 1) == original && old)
                _putimage(line_pos+1,0,image,_GXOR);
        }
    }
}

```

```

    }
    if(key == 0x0F00 && line_pos > 7) /* left arrow */
    {
        _putimage(line_pos,0,image,_GXOR);
        line_pos -= 8;
        _putimage(line_pos,0,image,_GXOR);
        if((line_pos + 8) == original && old)
            _putimage(line_pos+8,0,image,_GXOR);
    }
    if(key == 0x4D00 && line_pos < 639) /* right arrow */
    {
        _putimage(line_pos,0,image,_GXOR);
        line_pos++;
        _putimage(line_pos,0,image,_GXOR);
        if((line_pos - 1) == original && old)
            _putimage(line_pos-1,0,image,_GXOR);
    }
    if(key == 0x0F09 && line_pos < 632) /* left arrow */
    {
        _putimage(line_pos,0,image,_GXOR);
        line_pos += 8;
        _putimage(line_pos,0,image,_GXOR);
        if((line_pos - 8) == original && old)
            _putimage(line_pos-8,0,image,_GXOR);
    }
    numhits++;
} while(key != 0x1C0D);
return(line_pos);
}

```

```

void v_swing(int first, int wavelength)
{
    FILE *swingfile;
    int l, m, n, o, drift, istep, sign;
    float va[4], vb[4], d, stepave[4][10], temp, fo, diff, step_len, ll;
    float ave[4], vsum[4], tsum[4], vtsum[4], vsum[4], ttsum[4], fnum;

    fnum = num;
    if(!wopen(10,10,18,70,0,LCYAN|_BROWN,WHITE|_BLACK)) exit(0);
    wprintf("\n Remove drift? ");
    drift = wselstr(1,17,WHITE|_BLACK,ans);
    if ((swingfile = fopen("vswing.out","w")) == NULL)
        win_message("Error opening SWING.OUT ",50);
}

```

```

wclear();
for(m = 0; m < channels; m++)
{
ave[m] = swing[m] = va[m] = vb[m] = 0;
vsum[m] = tsum[m] = vtsum[m] = vvsum[m] = ttsum[m] = 0;
for(l = 0; l < 10; l++)
stepave[m][l] = 0.0;
if(drift)
{
for(l = 0; l < num; l++)
{
vsum[m] += vdat[l][m];
tsum[m] += l;
vtsum[m] += (vdat[l][m]*l);
vvsum[m] += (vdat[l][m]*vdat[l][m]);
ttsum[m] += (l * l);
}
d = (num * ttsum[m]) - (tsum[m] * tsum[m]);
va[m] = ((num * vtsum[m]) - (vsum[m] * tsum[m]))/d;
vb[m] = (vsum[m] - (va[m] * tsum[m]))/fnum;
}
for (l = 0; l < num; l++)
{
if(drift) vdat[l][m] -= (va[m] * l + vb[m]);
ave[m] += vdat[l][m];
}
ave[m] /= fnum;
ll = 0;
o = 0;
for(l = 0; l < (first - 5); l++)
stepave[m][0] += vdat[l][m];
ll += 1.0;
stepave[m][0] /= ll;
l = first + 1;
while(l < num)
{
temp = stepave[m][o];
wprintf(" %ft",temp);
o++;
step_len = 0.0;
for(n = 5; n < (wavelength - 5) && (l + n) < num; n++)
{
stepave[m][o] += vdat[l+n][m];
step_len += 1.0;;
}
}

```

```

    stepave[m][o] /= step_len;
    diff = (stepave[m][o] - temp);
    wprintf(" %f, %f : ",diff,step_len);
    if(stepave[m][o] < ave[m])
        diff *= -1;
    swing[m] += diff;
    l += wavelength;
    };
    wprintf("\n");
    fo = o;
    swing[m] /= fo;
    }
    wprintf("\n Number of steps: %d",o);
    waitkey(500);
    wclose();
    }

```

```
void save_files()
```

```

{
    int i,j;
    FILE *binfile, *updatefile;
    char file_time[9], file_name[40], temp[5], str[40], update_name[40];

    if(!wopen(10,15,14,65,0,LCYAN|_BROWN,WHITE|_BLACK)) exit(0);
    showcur();
    wprintf("\n Enter name of update file : ");
    wget(update_name);
    hidecur();
    wprintf(" Updating VSWING file %s",update_name);
    updatefile = fopen(update_name,"a");
    fprintf(updatefile,"%s %f, %f, %f\n",file_name,swing[0],swing[1],
        swing[2]);
    fclose(updatefile);
    wclose();
}

```

```
void dos_shell()
```

```

{
    int *scrn2;
    showcur();
    if((scrn2=ssave())==NULL) exit(0);
    clrscr(LGREY|_BLACK);
    printf("Type EXIT to return....\n");
    system("COMMAND");
}

```

```
    srestore(scrn2);
    hidecur();
}

void init_program()
{
    char string[81];
    FILE *infile;

    videoinit();
    hidecur();
    clrscrn();
    if ((infile = fopen("vswing.scr","r")) != NULL)
    {
        while( fgets(string,80,infile) != NULL) fputs(string,stdout);
        fclose(infile);
        waitkeyt(60);
        clrscrn();
    }
}

/* program end */
```

APPENDIX B
MULTICOMPONENT RESISTIVITY SURVEY DATA

ROOM G ACCESS

Position (m)			E magnitude (V/m)			
x	y	z	x	y	z	total
-478.104	341.2998	653	0.000393	0.000443	0.001338	0.000074
-486.029	341.2998	653	0.000084	0.000366	0.001344	0.000071
-495.782	341.2998	653	0.000022	0.000134	0.000244	0.000077
-504.926	341.2998	653	0.000440	0.000031	0.000457	0.000072
-511.022	341.2998	653	0.000711	0.00002	0.000712	0.000086
-518.642	341.2998	653	0.000469	0.000024	0.000485	0.000066
-526.262	341.2998	653	0.000418	0.000050	0.000451	0.000077
-532.358	341.2998	653	0.000305	0.000053	0.000316	0.000065
-539.369	341.2998	653	0.000389	0.000074	0.000415	0.000098
-547.598	341.2998	653	0.000193	0.000064	0.000205	0.000076
-553.694	341.2998	653	0.000186	0.000037	0.000191	0.000055
-562.838	341.2998	653	0.000195	0.000042	0.000202	0.000057
-570.458	341.2998	653	0.000410	0.000049	0.000446	0.000046
-578.078	341.2998	653	0.000531	0.000053	0.000560	0.000059
-585.698	341.2998	653	0.000061	0.000010	0.000032	0.000070
-592.099	341.2998	653	0.000180	0.000218	0.000406	0.000017
-598.195	341.2998	653	0.000010	0.000036	0.000053	0.000065
-605.510	341.2998	653	0.000053	0.000013	0.000075	0.000093
-611.606	341.2998	653	0.000014	0.000015	0.000072	0.000075
-617.702	341.2998	653	0.000047	0.000016	0.000078	0.000092
-623.798	341.2998	653	0.000065	0.000016	0.000080	0.000105
-629.894	341.2998	653	0.000033	0.000037	0.000146	0.000155
-639.038	341.2998	653	0.000076	0.000030	0.00013	0.000153
-648.182	341.2998	653	0.000068	0.000032	0.000166	0.000183
-656.107	341.2998	653	0.000042	0.000046	0.000162	0.000174
-665.556	341.2998	653	0.000028	0.000057	0.000186	0.000197
-675.614	341.2998	653	0.000079	0.000056	0.000099	0.000139
-687.806	341.2998	653	0.000066	0.000104	0.000106	0.000163
-693.902	341.2998	653	0.000056	0.000033	0.000082	0.000105
-706.094	341.2998	653	0.000008	0.000002	0.000064	0.000064
-712.190	341.2998	653	0.000134	0.000009	0.000028	0.000137
-721.334	341.2998	653	0.000268	0.000049	0.000019	0.000274
-727.430	341.2998	653	0.000144	0.000046	0.000008	0.000151
-733.526	341.2998	653	0.000022	0.000091	0.000013	0.000095
-742.670	341.2998	653	0.000093	0.000188	0.000172	0.000271
-754.862	341.2998	653	0.000755	0.000121	0.000338	0.000836
-764.006	341.2998	653	0.000804	0.000179	0.000265	0.000865
-770.102	341.2998	653	0.000244	0.000139	0.000424	0.000509
-779.246	341.2998	653	0.000033	0.000260	0.000373	0.000456
-785.342	341.2998	653	0.000010	0.000130	0.000755	0.000766
-791.438	341.2998	653	0.000024	0.000118	0.000214	0.000246

-791.438 341.2998

653

0.000024 0.000118 0.000214 0.000246

ROOM 7

Position (m)			E magnitude (V/m)			
x	y	z	x	y	z	total
397.5608	-507.822	653	0.000053	0.000052	0.001190	0.001192
397.5608	-507.822	653	0.000050	0.000016	0.001146	0.001147
397.5608	-513.918	653	0.000055	0.000058	0.001242	0.001245
397.5608	-520.014	653	0.000088	0.000069	0.001156	0.001161
397.5608	-526.110	653	0.000133	0.000035	0.001374	0.001381
397.5608	-532.206	653	0.000079	0.000108	0.001052	0.001060
397.5608	-538.302	653	0.000032	0.000087	0.001239	0.001242
397.5608	-544.398	653	0.000212	0.000124	0.001014	0.001043
397.5608	-550.799	653	0.000076	0.001206	0.001014	0.001578
397.5608	-557.199	653	0.000040	0.000055	0.001223	0.001225
397.5608	-563.600	653	0.000055	0.000084	0.000880	0.000886
397.5608	-570.001	653	0.000131	0.000075	0.000902	0.000915
397.5608	-576.402	653	0.000071	0.000100	0.000737	0.000747
397.5608	-582.803	653	0.000131	0.000052	0.000947	0.000957
397.5608	-589.203	653	0.000134	0.000113	0.000391	0.000429
397.5608	-589.203	653	0.000134	0.000113	0.000391	0.000429
393.9032	-589.203	653	0.000106	0.000078	0.000415	0.000435
387.8072	-589.203	653	0.000169	0.000076	0.000624	0.000651
381.7112	-589.203	653	0.000611	0.000034	0.000498	0.000789
375.6152	-589.203	653	0.000769	0.000089	0.000483	0.000913
369.5192	-589.203	653	0.001110	0.000184	0.000393	0.001192
351.2312	-589.203	653	0.002093	0.000289	0.000544	0.002182
345.1352	-589.203	653	0.001814	0.000321	0.000583	0.001932
339.0392	-589.203	653	0.004724	0.000546	0.002098	0.005198
332.9432	-589.203	653	0.002836	0.000184	0.000502	0.002887
326.8472	-589.203	653	0.001887	0.000313	0.000025	0.001913

ROOM Q ACCESS

Position (m)			E magnitude (V/m)			
x	y	z	x	y	z	total
-271.526	-26.5684	653	0.001654	0.000117	0.000360	0.001697
-268.476	-26.5684	653	0.001009	0.000233	0.000818	0.001320
-265.426	-26.5684	653	0.000906	0.00012	0.000265	0.000952
-262.376	-26.5684	653	0.000515	0.000004	0.000086	0.000522
-259.326	-26.5684	653	0.000703	0.000128	0.000325	0.000785
-256.276	-26.5684	653	0.000517	0.003562	0.000064	0.003600
-253.226	-26.5684	653	0.002898	0.003103	0.003188	0.005309
-250.176	-26.5684	653	0.00059	0.000020	0.000361	0.000691
-247.126	-26.5684	653	0.001011	0.000297	0.000287	0.001092
-244.076	-26.5684	653	0.000759	0.000628	0.000706	0.001212
-241.026	-26.5684	653	0.000897	0.001138	0.001651	0.002197
-234.926	-26.5684	653	0.000422	0.000033	0.000205	0.000470
-265.426	-26.5684	653	0.001075	0.000178	0.000283	0.001126
-262.376	-26.5684	653	0.001010	0.000007	0.000168	0.001024
-259.326	-26.5684	653	0.000115	0.000027	0.000063	0.000134
-256.276	-26.5684	653	0.000629	0.002418	0.000014	0.002498
-253.226	-26.5684	653	0.002293	0.002437	0.002415	0.004127
-250.176	-26.5684	653	0.000630	0.000078	0.000363	0.000731
-247.126	-26.5684	653	0.001004	0.000024	0.000265	0.001038
-244.076	-26.5684	653	0.000928	0.000451	0.000564	0.001176
-241.026	-26.5684	653	0.000773	0.000536	0.001052	0.001411
-234.926	-26.5684	653	0.000517	0.000027	0.000196	0.000554
-231.876	-26.5684	653	0.000680	0.000101	0.001341	0.001507
-228.826	-26.5684	653	0.000978	0.000122	0.001557	0.001843
-225.776	-26.5684	653	0.000831	0.000246	0.000488	0.000995
-222.726	-26.5684	653	0.000883	0.000056	0.000188	0.000904
-219.676	-26.5684	653	0.000836	0.000173	0.000230	0.000884
-216.626	-26.5684	653	0.000888	0.000038	0.000126	0.000898
-213.576	-26.5684	653	0.000393	0.000328	0.00061	0.000796
-189.176	-26.5684	653	0.000016	0.000078	0.000310	0.000320
-186.126	-26.5684	653	0.000003	0.000093	0.000203	0.000223
-183.076	-26.5684	653	0.000002	0.000087	0.000169	0.000190
-180.026	-26.5684	653	0.000004	0.000088	0.000115	0.000145
-176.976	-26.5684	653	0.000003	0.000073	0.000131	0.000150
-173.926	-26.5684	653	0.000022	0.000063	0.000079	0.000104
-170.876	-26.5684	653	0.000004	0.000053	0.000070	0.000088
-167.826	-26.5684	653	0.000000	0.000038	0.000044	0.000058
-164.776	-26.5684	653	0.000001	0.000029	0.000046	0.000054
-161.726	-26.5684	653	0.000002	0.000030	0.000079	0.000085
-158.676	-26.5684	653	0.000012	0.00002	0.000016	0.000028
-158.676	-26.5684	653	0.000006	0.000017	0.000013	0.000022

-155.626	-26.5684	653	0.000000	0.000014	0.000011	0.000018
-152.576	-26.5684	653	0.000000	0.000013	0.000005	0.000014
-149.526	-26.5684	653	0.000006	0.000034	0.000013	0.000037
-146.476	-26.5684	653	0.000001	0.000016	0.000002	0.000016
-143.426	-26.5684	653	0.000003	0.000016	0.000037	0.000040
-140.376	-26.5684	653	0.000002	0.000019	0.000033	0.000039
-137.326	-26.5684	653	0.000001	0.000021	0.000068	0.000071
-134.276	-26.5684	653	0	0.000014	0.000103	0.000103
-131.226	-26.5684	653	0.000000	0.000005	0.000022	0.000022
-128.176	-26.5684	653	0.000000	0.000006	0.000032	0.000032
-125.126	-26.5684	653	0.000036	0.000000	0.000002	0.000036
-122.076	-26.5684	653	0.000000	0.000002	0.000054	0.000054
-119.026	-26.5684	653	0.000004	0.000210	0.000007	0.000210
-115.976	-26.5684	653	0.000027	0.000130	0.000033	0.000137
-112.926	-26.5684	653	0.000100	0.000007	0.000483	0.000494
-109.876	-26.5684	653	0.000208	0.000174	0.000203	0.000339
-106.826	-26.5684	653	0.000373	0.000089	0.000109	0.000399
-103.776	-26.5684	653	0.000345	0.000146	0.00026	0.000456
-100.726	-26.5684	653	0.00031	0.000197	0.000345	0.000504

DRIFT 300N

Position (m)			E magnitude (V/m)			
x	y	z	x	y	z	total
-7.62	96.9264	653	0.000203	0.000456	0.002185	0.002241
-10.668	96.9264	653	0.000061	0.000171	0.002242	0.002249
-13.716	96.9264	653	0.000034	0.000693	0.002271	0.002375
-16.764	96.9264	653	0.000078	0.000218	0.00184	0.001854
-19.812	96.9264	653	0.000026	0.000180	0.002558	0.002565
-22.86	96.9264	653	0.000092	0.000032	0.000833	0.000839
-25.908	96.9264	653	0.000027	0.000161	0.001121	0.001133
-28.956	96.9264	653	0.000064	0.000038	0.000805	0.000808
-32.004	96.9264	653	0.000027	0.000076	0.000891	0.000894
-35.052	96.9264	653	0.000041	0.000096	0.000882	0.000888
-38.1	96.9264	653	0.000222	0.000161	0.000178	0.000327
-41.148	96.9264	653	0.000231	0.000161	0.000195	0.000343
-44.196	96.9264	653	0.000268	0.000123	0.000054	0.000300
-47.244	96.9264	653	0.000286	0.000256	0.000074	0.000391
-50.292	96.9264	653	0.000360	0.000205	0.000307	0.000516
-53.34	96.9264	653	0.000390	0.000133	0.001221	0.001289
-56.388	96.9264	653	0.000035	0.000066	0.000782	0.000785
-59.436	96.9264	653	0.000035	0.000250	0.000299	0.000392
-62.484	96.9264	653	0.000056	0.000017	0.000464	0.000468
-65.532	96.9264	653	0.000034	0.000071	0.000565	0.000570
-68.58	96.9264	653	0.000047	0.000104	0.000427	0.000442
-71.628	96.9264	653	0.000045	0.000011	0.00063	0.000631
-74.676	96.9264	653	0.000047	0.000012	0.000650	0.000652
-77.724	96.9264	653	0.000093	0.000152	0.000728	0.000750
-80.772	96.9264	653	0.000087	0.000194	0.000738	0.000768
-83.82	96.9264	653	0.000097	0.000143	0.000729	0.000749
-86.868	96.9264	653	0.000092	0.000198	0.000834	0.000862

APPENDIX C
DATA ACQUISITION SYSTEM

DATA ACQUISITION SYSTEM

Bipole-Dipole DC Resistivity Method

At the WIPP site two cased boreholes are used as source electrodes. The electrodes are situated 1.3 kilometers apart, creating an electrical bipole field. In addition, the well casing acts as a vertical line source of current in the earth, compared to the traditional point source on the surface. The receiving electrodes are located underground with a separation of two meters. A common ground electrode is placed at the station location and three other electrodes are placed orthogonally two meters from ground.

Current Sources

The boreholes were used as electrodes in order to get the current to penetrate the Salado formation. A three-phase, 27 kW generator supplied 220 VAC. The voltage was regulated using a switching box to provide a DC current that switched polarity every four seconds. The resulting current signal, an alternating square wave with a peak-to-peak amplitude of 100 amperes, is shown in Figure C-1.

Receiver System

Non-polarizing porous pots containing copper electrodes in a copper sulfate solution were used as electrodes to observe the potential underground. The input from each of the reference electrodes was fed to the input of an isolated, differential, three-channel amplifier. The input from the reference, or ground, electrode was fed to the ground input of the amplifier (Figure C-2).

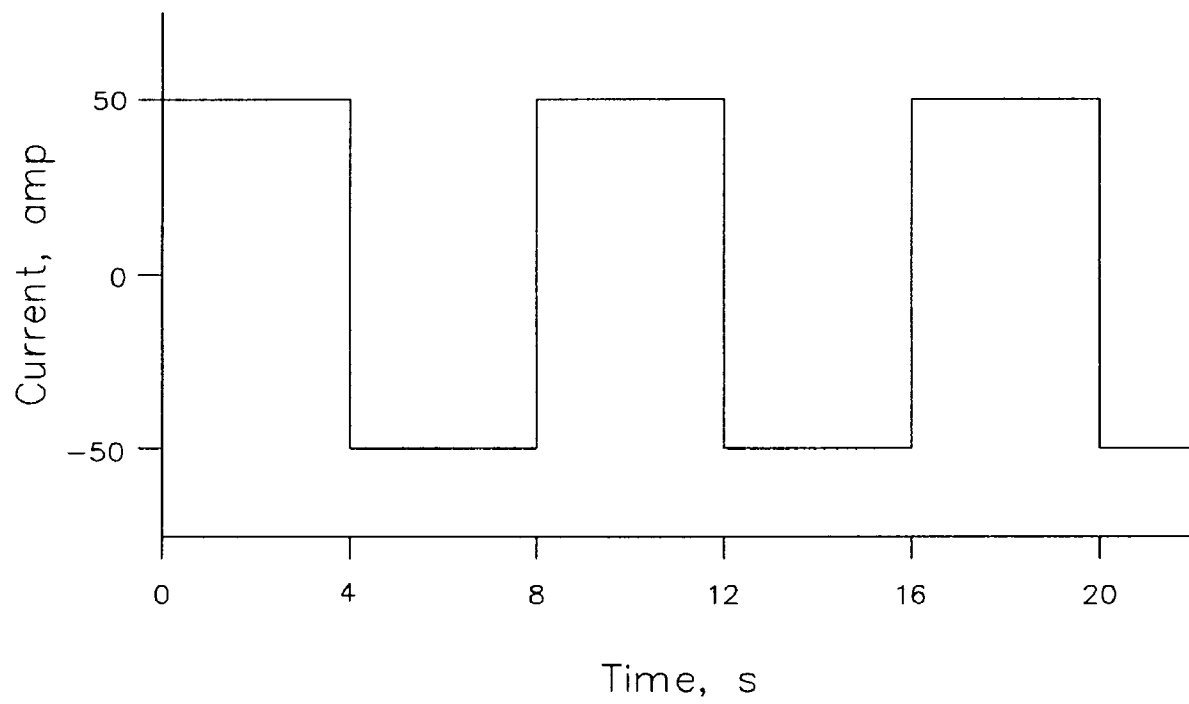


Figure C-1 Current source with a period of eight seconds.

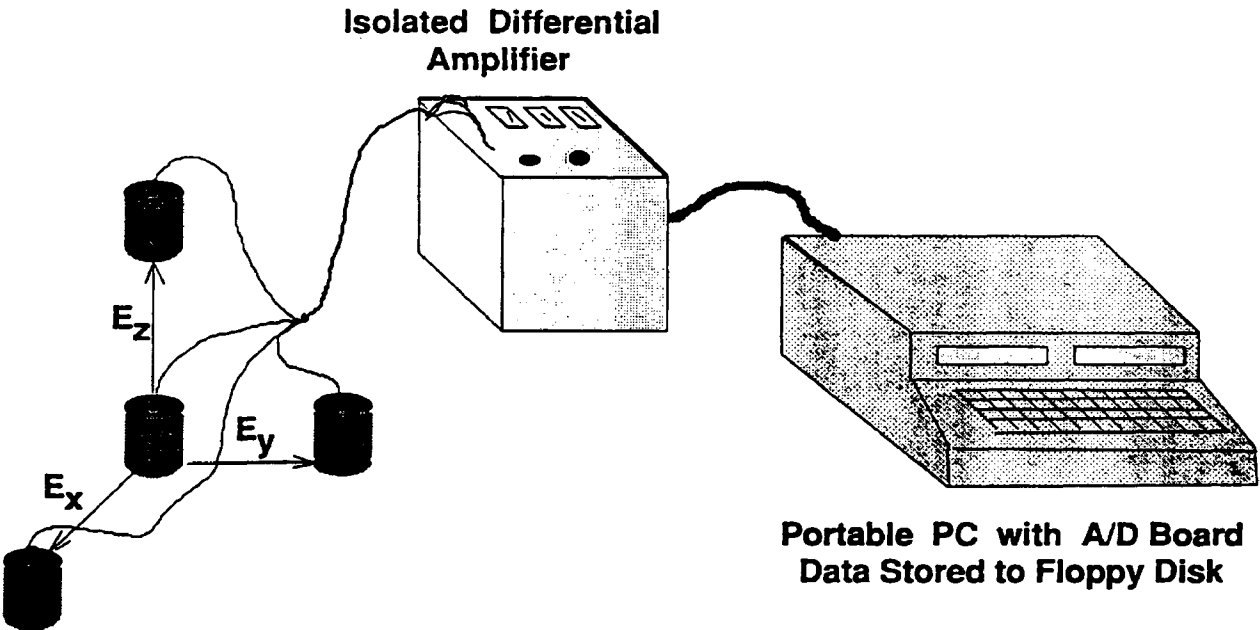


Figure C-2 Diagram of acquisition system measuring three orthogonal components of electric field.

Output from the amplifier is fed to an analog-to-digital (A/D) board mounted in a PC-compatible computer. The A/D board has 12 bit resolution, an input range of 20 volts, and an internal three bit binary gain. Software was written in the C programming language to implement a library of routines available to control the A/D board. The program VGETC samples the input voltage of the three channels at frequencies of 1 to 100 Hz. The data are printed to screen, and then stored to floppy disk. A schematic of the acquisition system is shown in Figure C-3.

Determination of Electric Field Strength

A typical data record contains 1024 data points for each of the three components. A sampling rate of 50 Hz was used in order to have several waveforms in the record yet keep the sampling time to a minimum. A plot of a sample record is shown in Figure C-4. The acquisition program internal and external gain, then stores the resulting value. Several stations worth of data could be stored to a single floppy disk and brought to the surface for processing.

After a survey was completed, the program VSWING was used to pick the value of the recorded voltage swing. The waveform provides the voltage for both a positive and negative current. The program VSWING calculates the mean value for each segment of the waveform. The difference between successive segments in the waveform yields twice the current for a non-alternating current, and automatically removes any spurious background potential. With a dipole spacing of two meters, the mean value of the electric field magnitude is given by

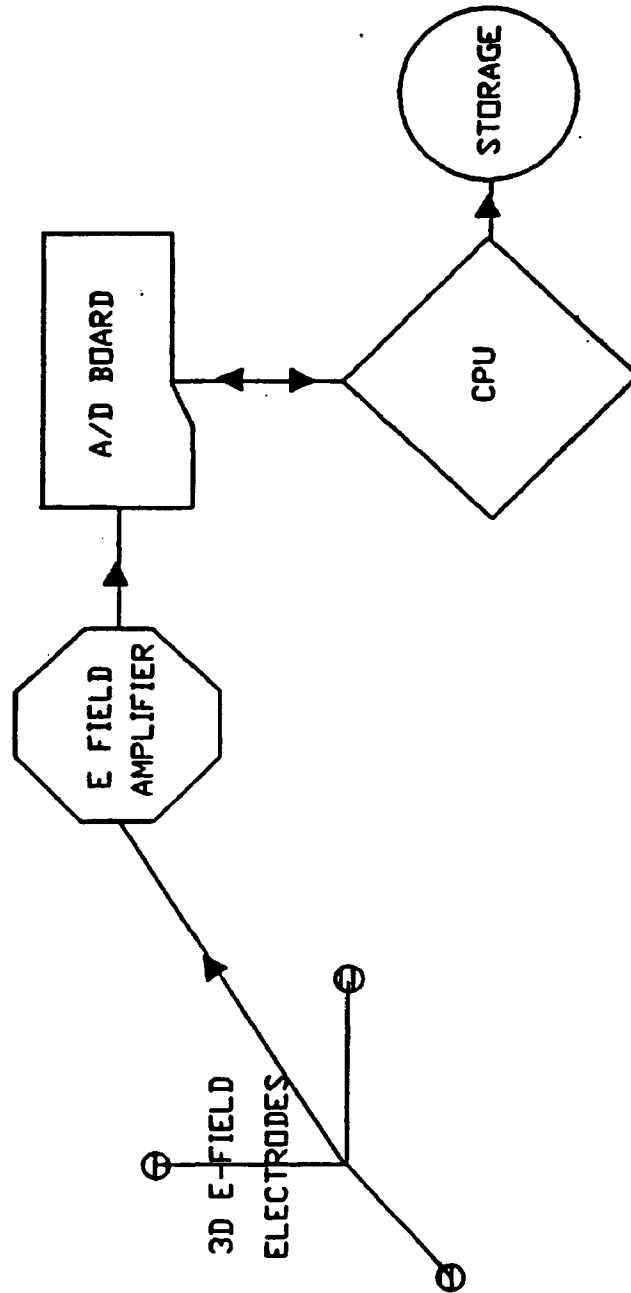


Figure C-3 Schematic diagram of acquisition system.

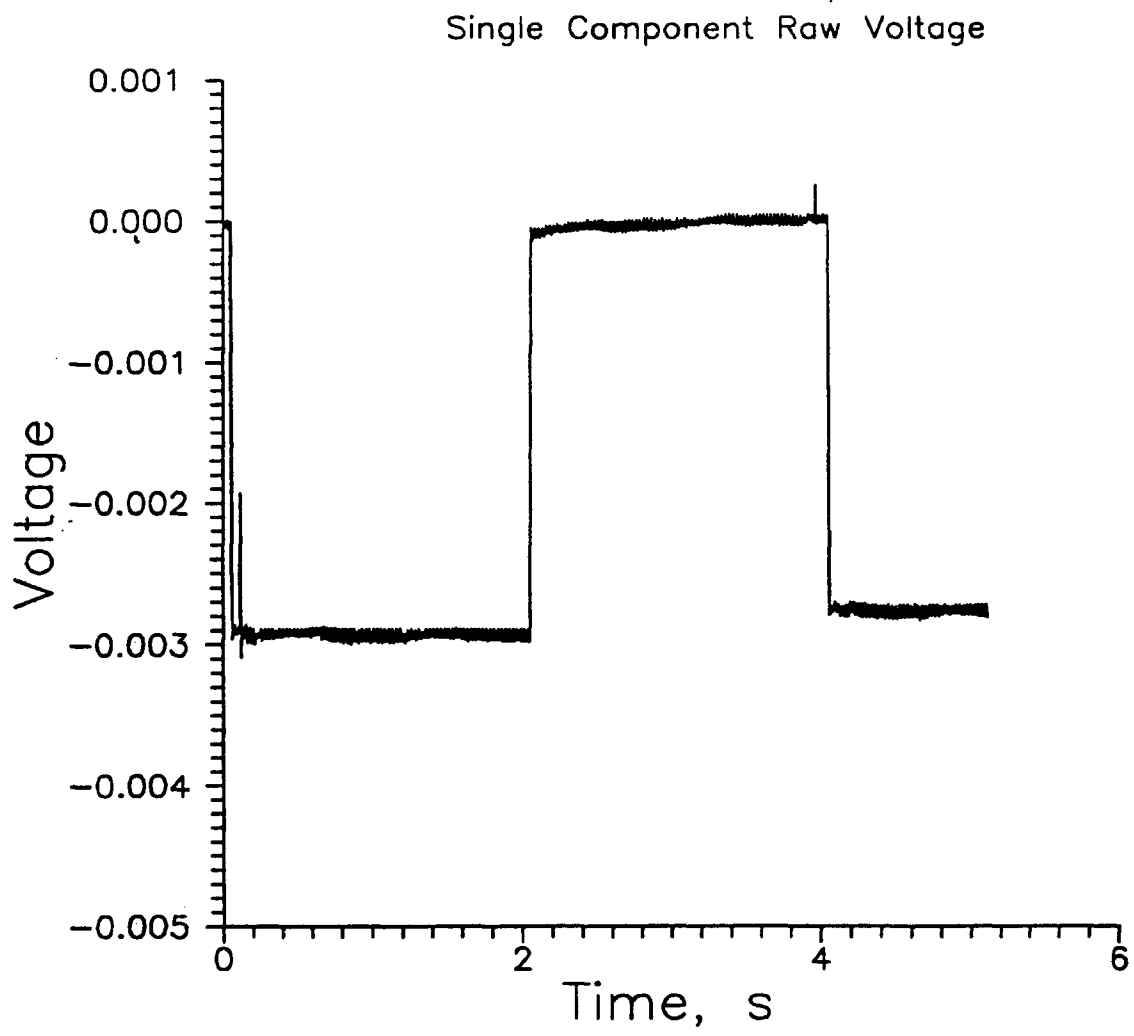


Figure C-4 Sample data record from receiver acquisition system.

$$|E| = \frac{|\Delta U|}{2} .$$